A GLOBAL THREE-DIMENSIONAL MODEL OF THE CIRCULATION AND CHEMISTRY OF LONG-LIVED ATMOSPHERIC SPECIES

BY

AMRAM GOLOMBEK
M.Sc. Technion
(1968)

SUBMITTED TO THE DEPARTMENT OF METEOROLOGY AND PHYSICAL OCEANOGRAPHY IN PARTIAL FULFILLMENT OF THE REQUIREMENTS FOR THE DEGREE OF DOCTOR OF PHILOSOPHY IN METEOROLOGY

at the

MASSACHUSETTS INSTITUTE OF TECHNOLOGY

July 1982

© Massachusetts Institute of Technology

Signature Redacted

Signature of Author _____
Department of Meteorology and Physical Oceanography July 19, 1982

Signature Redacted

Certified by _____
Ronald G. Prinn, Thesis Supervisor

Signature Redacted

Accepted by _____
Ronald G. Prinn, Chairman, Department Committee

Archives

MASSACHUSETTS INSTITUTE OF TECHNOLOGY

JUL 19 1982

LIBRARIES

A Global Three-dimensional Model of the Circulation and Chemistry of Long-lived Atmospheric Species

by

Amram Golombek

Submitted to the Department of Meteorology and Physical Oceacography on July , 1982 in partial fulfillment of the requirements for the Degree of Doctor of Philosophy in Meteorology

ABSTRACT

A unique, efficient, low resolution spectral model for studying the circulation, photochemistry and chemistry of some long-lived atmospheric species was developed.

The model was successfully validated by studying the circulation and photochemistry of the two fluorocarbons $CFCl_3$, CF_2Cl_2, carbontetrachloride (CCl_4) and nitrous oxide (N_2O) and by comparing the results to atmospheric measurements of these species.

The model was further used in studying the circulation, photochemistry and chemistry of methylchloroform (CH_3CCl_3) and by comparison to surface measurements of this compound, an OH free radical tropospheric distribution was recommended.

Global trends and lifetimes of all five species were calculated. The current atmospheric lifetimes of $CFCl_3$, CF_2Cl_2, CH_3CCl_3, CCl_4 and N_2O were found to be 78, 232, 12, 49 and 185 years respectively. Using decreased O_2 absorption cross-sections in the Herzberg continuum as suggested by recent work, a current $CFCl_3$ atmospheric lifetime of only 45 years is obtained. Model runs were pursued for at least 30 months of integration, and the integration time needed for each species was 8 seconds per one calendar day on a CDC 7600 computer.

Thesis Supervisor: Dr. Ronald G. Prinn

Title: Professor of Meteorology.

TO MY WIFE

ORA

Acknowledgements

I would like to thank my advisor, Dr. Ronald Prinn for his valuable assistance and advice and numerous helpful discussions.

I would also like to thank Liz Manzi who typed the manuscript and Isabelle Kole who drafted the figures.

My stay in MIT was made possible by a Grant from the Israeli Government. This thesis was supported in part by NASA Grant NSG-2010 to MIT.

CONTENTS

1. Introduction..... 13

2. Method 25

2.1.1 The mathematical model..... 25

2.1.2 The MIT/GIT ozone mathematical model.....

2.2 Initialization, input data, and boundary conditions..... 51

2.2.1 Two-dimensional initial profile..... 51

2.2.2 Anthropogenic source..... 57

2.2.3 Photochemical dissociation..... 70

2.2.4 Reaction of CH_3CCl_3 with OH radicals..... 77

2.2.5 Reactions with $O(^1D)$..... 80

2.2.6 Oceanic sink..... 80

2.2.7 Other sinks..... 87

2.2.8 Boundary conditions..... 88

3. Results..... 88

3.1 Generl reasults..... 88

3.1.1 Numerical stability and convergence..... 88

3.1.2 Model diagnostic parameters..... 89

3.2 Results for the fluorocarbons $CFCl_3$ and CF_2Cl_2 90

3.3 Results for CCl_4 and N_2O.....112

3.4 Discussion of the results for $CFCl_3$, CF_2Cl_2, CCl_4 and N_2O.....132

3.5 Results for CH_3CCl_3.....141

3.6 Oceanic sink.....172

3.7 Sensitivity of results to O_2 Herzberg continuum cross-sections.....173

4. General summary and conclusions.....183

4.1 Global averages.....183

4.2 Seasonal averages.....186

4.3 Atmospheric lifetimes.....189

4.4 Accomplishments of the thesis.....191

5. References.....194

List of Tables

Table 1: General characteristics of the tracers..... 16
Table 2: The model horizontal grid points..... 26
Table 3: The model vertical levels..... 27
Table 4: Conversion factors and constants..... 41
Table 5: ALE stations locations..... 52
Table 6: July 1978 surface tracers mixing ratios..... 53
Table 7: Initial vertical profiles..... 58
Table 8: Tracers release to the atmosphere, 1951-1982 62
Table 9: Anthropogenic surface source distribution... 65-66
Table 10: Area and mass of each grid point..... 68
Table 11: Tracers absorption cross-sections..... 72-74
Table 12: Photodissociation rates and photochemical lifetimes..... 75-76
Table 13: Experimental values for k_{OH}..... 78
Table 14: MIT/GIT model stratospheric OH distribution 79
Table 15: Reaction rate constants of $O(^1D)$..... 81
Table 16: Oceanic sink constants..... 85
Table 17: Surface trends of $CFC\ell_3$ and $CF_2C\ell_2$.....102
Table 18: Surface trends of $CC\ell_4$ and N_2O.....125
Table 19: Material balance for $CFC\ell_3$ in the lower Southern hemisphere troposphere.....138
Table 20: Contributions to the mixing ratio prediction equation of $CFC\ell_3$.....140
Table 21: Surface trends of $CH_3CC\ell_3$.....155
Table 22: Initial $CH_3CC\ell_3$ surface distribution, RUN F 160
Table 23: Lifetime of $CH_3CC\ell_3$ and tropospheric OH number density.....169
Table 24: Tropospheric OH radical concentrations.....170
Table 25: Correction in J values.....174
Table 26: Updated mixing ratios at 33 Km.....176
Table 27: Updated lifetimes and correlation factors...178
Table 28: Updated $CFC\ell_3$ lifetimes and trends.....182
Table 29: Global trends.....185
Table 30: Tracers mixing ratios, Winter 1980/81.....187
Table 31: Summarized results.....190

List of Figures

Figure 1: The model zonal winds..... 45
Figure 2: The model temperature field..... 46
Figure 3: The model meridional circulation..... 47
Figure 4: The model predicted ozone distributions.... 48-50
Figure 5: Initial tracers latitudinal distribution, July 1978..... 54-56
Figure 6: Initial vertical profiles..... 59-61
Figure 7: Number density $O(^1D)$ vertical profile..... 82
Figure 8: Lifetime trends of $CFCl_3$ and CF_2Cl_2..... 91-92
Figure 9: Column destruction of $CFCl_3$ and CF_2Cl_2..... 95
Figure 10: Monthly-mean surface trends of $CFCl_3$ and CF_2Cl_2..... 97-101
Figure 11: Vertical profiles of $CFCl_3$ and CF_2Cl_2.....107-109
Figure 12: Latitudinal $CFCl_3$ and CF_2Cl_2 surface distribution.....110-111
Figure 13: Latitude-altitude $CFCl_3$ distribution.....113
Figure 14: Latitude-altitude CF_2Cl_2 distribution.....114
Figure 15: Latitude-longtitude $CFCl_3$ surface distribution.....115
Figure 16: Latitude-longtitude CF_2Cl_2 surface distribution.....116
Figure 17: The source weighting factor distribution of $CFCl_3$.....117
Figure 18: Lifetime trends of CCl_4 and N_2O.....118
Figure 19: Monthly-mean surface trends of CCl_4 and N_2O 120-124
Figure 20: Vertical profiles of N_2O.....127-129
Figure 21: Latitudinal CCl_4 and N_2O surface distribution.....130-131
Figure 22: Latitude-altitude CCl_4 distribution.....133

Figure 23: Latitude-altitude N_2O distribution.....134
Figure 24: Latitude-longtitude surface CCl_4 distribution.....135
Figure 25: Monthly-mean surface trends of CH_3CCl_3 RUN A.....143-147
Figure 26: The OH radical tropospheric distribution, RUN B.....148-149
Figure 27: Monthly-mean surface trends of CH_3CCl_3, RUN B and RUN F.....150-154
Figure 28: The OH radical tropospheric distribution, RUN E.....157-158
Figure 29: Lifetime trend of CH_3CCl_3.....162
Figure 30: Latitudinal CH_3CCl_3 surface distribution..163-165
Figure 31: Latitude-altitude CH_3CCl_3 distribution....166
Figure 32: Latitude-longtitude CH_3CCl_3 surface distribution.....168
Figure 33: Surface trend and η correlation.....180
Figure 34: Updated $CFCl_3$ vertical profile.....181

List of Symbols

a	earth's radius
A, B	constants in the second order reaction rate formula, constants in the linear fit formula
Δc	concentration gradient across the exchange layer between atmosphere and ocean
C_p	specific heat at constant pressure for dry air
f	Coriolis parameter
F	friction term
g	gravitational acceleration
h	Planck's constant
H	Henry's constant
H_o, H_m	scale heights
I	incident solar radiation
J	photodissociation integral
J	Jacobian
k	Boltzman constant
$\hat{k}$	unit vector in the vertical direction
k_d	surface drag coefficient
k_m, K_d	eddy diffusion coefficients
k_i	second order rate constants
L, N_ℓ	truncation indices in the spherical harmonics series
m	mixing ratio
M	molecular weight
n	number density
n_m	number density for dry air
N	column number density
NLAT, NLONG	indices of latitude and longtitude in the grid form
p	pressure
P	non-dimensional pressure
pptv	mixing ratio units $1:10^{-12}$ by volume
ppbv	mixing ratio units $1:10^{-9}$ by volume

q	local heating rate per unit mass
q'	deviation of local heating rate from its horizontal average
R	universal gas constant for dry air
s	the area represented by a surface grid point
Δt	integration time step
T, $\overline{T}$, T'	absolute temperature, its horizontal average, the deviation from the horizontal average
T_s	temperature in the standard atmosphere
T_o	average model atmospheric temperature
u, v	components of horizontal wind (eastward and northward)
$\vec{V}$	horizontal wind vector
w	weight of column of air
W	non-dimensional vertical velocity
x, y, z	cartezian coordinates in the eastward, northward and upward directions
X	see χ
Z	non-dimensional vertical coordinate
α	absorption cross-section
δ	horizontal divergence of $\vec{V}$
ζ	vertical component of relative vorticity
χ	horizontal velocity potential ($\chi = \frac{\partial X}{\partial P}$)
κ	$\frac{R}{C_p}$
λ	longtitude
Λ	wavelength
ν	frequency of electromagnetic radiation
φ	zenith angle
ϕ	latitude
Π	Legendre polynomial

ρ	density
ξ	exponent describing radiation decrease due to column absorption
η	parameter in the trend formula correlation
ψ	stream function
Ω	Earth's rotation
L	operator equal to ∇^{-2}

1. INTRODUCTION

This thesis describes an efficient three-dimensional spectral model for the circulation and chemistry of long-lived chemical pollutants in the troposphere and lower stratosphere. This model uses precalculated three-dimensional spectral fields of vorticities, vertical velocities and ozone mixing ratios, and predicts the mixing ratios of the various long-lived chemical tracers as a function of time.

The predictions of this model for five particular tracers are compared with available global measurements of the horizontal, vertical, and temporal distribution of these tracers. In general, agreement between predicted and observed variables is good, but there are disagreements for certain of the species studied which are critically analyzed.

The need for an efficient global circulation model for studies of tropospheric chemistry have become apparent as our knowledge of the accumulation and chemical consequences of a number of anthropogenic pollutants has burgeoned in the last few years. The problem with existing global tracer circulation models is that the computer time required for the purely dynamical portions of the calculations firstly prevents the incorporation of significant amounts of chemistry into these models and secondly prevents the running of these models over time scales of several years or longer.

One conventional way of circumventing the computational problems of three-dimensional chemical models has been to develop two-dimensional models. However, such models must

make dubious assumptions about the simulation of atmospheric eddy transports and are of limited use in understanding the available detailed three-dimensional data on tracer species.

The approach taken in this thesis has been to explore the use of a three-dimensional model with horizontal resolution significantly less than that typical in tropospheric general circulation models. While this assumption can be criticized on dynamical grounds, the rationale has been that this assumption is far less dubious then those used in two-dimensional models and that the lower resolution three-dimensional model can be regarded as a "parametrized" model which can be adequately tested and validated by comparison with observations.

The five tracers chosen for the detailed predictions using this model are those measured by the Atmospheric Lifetime Experiment (Prinn *et al.*, 1982a). The five chemicals are $CFC\ell_3$, $CF_2C\ell_2$, $CC\ell_4$, N_2O and $CH_3CC\ell_3$ and were chosen because extensive measurements of these compounds are available not only from the Atmospheric Lifetime Experiment (ALE) itself but also from other ground based, aircraft, and balloon experiments over a several-year time period.

The halocarbons $CFC\ell_3$, $CF_2C\ell_2$, $CC\ell_4$ and $CH_3CC\ell_3$ are almost exclusively anthropogenic pollutants which are released mainly in the Northern hemisphere. Nitrous oxide has both natural and anthropogenic sources, and is released both from land and ocean surfaces. The latitudinal surface distribution of the N_2O source is apparently almost homogeneous, while the sources of the four halocarbons are much more prevalent in

the Northern hemisphere, with the $CH_3CC\ell_3$ source having the steepest gradient between hemispheres. Some general characteristics of the five species we are modelling are provided in Table 1. Methyl-chloroform ($CH_3\ CC\ell_3$) has also the current largest increase rate, $CFC\ell_3$, $CF_2C\ell_2$ and $CC\ell_4$ follow, while N_2O is currently increasing very slowly. All tracers except $CH_3CC\ell_3$, appear to have mainly a photochemical sink--namely destruction by short uv radiation in the stratosphere (and also to a lesser extent by their reaction with $O(^1D)$ radicals in the stratosphere). The principal known sink of $CH_3CC\ell_3$ is its reaction with OH free radicals in the equatorial troposphere. One of the important results of our model study is the prediction of lifetime values for these tracers, based on their presently known sinks and sources. Thus for $CFC\ell_3$, $CF_2C\ell_2$, $CC\ell_4$ and N_2O we compute a lifetime based on photodissociation removal only, while for $CH_3CC\ell_3$ we calculate the lifetime based both on its photodissociation and its reaction with OH radicals. In our study of $CH_3CC\ell_3$ we also compute the appropriate tropospheric OH radical distribution in the model which allows the best agreement between observed and model $CH_3CC\ell_3$ concentrations.

The accumulation and circulation of the chemicals which we have chosen to study, have considerable importance in the chemistry of the global atmosphere. General concern about the increasing burden of all five of these chemicals in the atmosphere, is based on their possible effect on the ozone layer--as suggested by Molina and Rowland (1974a, 1974b), Crutzen

Table 1 : General Characteristics of the Tracers.

Tracer	Source	Strength	Burden NH	Burden SH	Trend	Lifetime (yrs)	Sinks
$CFCl_3$	A	270	190	170	6	10-∞	UV
CF_2Cl_2	A	400	300	270	6	20-∞	UV
CCl_4	A	100	135	130	2	-	UV
N_2O	N,A	15000	302	301	0.2	150-175	UV
CH_3CCl_3	A	510	165-180	120	9	3-11	OH, UV
Refer.	1-5	5	5	5	1	1,5	5

Source: A - Anthropogenic, N - Natural.

Source Strength: Current Source Strength (10^9 gm yr^{-1}).

Burden: Current Tropospheric Burden

$CFCl_3$, CF_2Cl_2, CCl_4, CH_3CCl_3 (pptv)

N_2O (ppbv).

Trend: Observed Current Trend (percent per year).

Lifetime: Estimated Lifetime, Recently Published (years).

Sinks: Main identified Sinks.

UV - Photodissociation by Short Wave Solar Radiation in the Stratosphere

OH - Scavenging by OH free Radicals in the Troposphere and Stratosphere.

References: 1 - Prinn et al. (1982a)

2 - Cunnold et al. (1982a, 1982b)

3 - Simmonds et al.(1982)

4 - Levy et al. (1979)

5 - WMO (1981).

(1974), McElroy *et al.* (1976), and McConnell and Schiff (1978). These pollutants during the course of their stratospheric photodissociation, produce either chlorine or nitrogen oxides which can catalytically destroy ozone. Furthermore, these pollutants have strong infra-red absorption bands in the window regions of the atmosphere, so that their increased burden is able to amplify the overall atmospheric greenhouse effect, and contribute in this way to climate changes (Ramanathan, 1975; Wang *et al.*, 1976).

An important part of the calculations which predict future ozone depletions, is a knowledge of the lifetimes of $CFC\ell_3$, $CF_2C\ell_2$, $CC\ell_4$, $CH_3CC\ell_3$ and N_2O, and it is for this reason that we will explicitly compute atmospheric lifetimes in our model.

Before 1977 the best estimates for the photodissociation lifetime of $CFC\ell_3$ were 30-100 years based on one-dimensional models (Rowland and Molina, 1976; Pack *et al.*, 1977; NAS 1979). However, it was also pointed out that a lifetime as short as 10-15 years was not inconsistent with observations when one considered the variability and accuracy of the data (Sze and Wu, 1976; Jesson *et al.* 1977; Cunnold *et al.* 1978). The only two-dimensional model calculations done so far for the steady-state lifetime of $CFC\ell_3$ (Sze and Ko, 1981) have resulted in a value of 65 years. One-dimensional models predict a photochemical lifetime for $CF_2C\ell_2$ of 40-250 years (NAS, 1979) and there are no published results from two-dimensional models for this compound. There are no one- or multi-dimensional

model estimates for the photochemical lifetime of $CC\ell_4$ of which we are aware. The current best model estimates for the photodissociation lifetime of N_2O are 175, 150 and 159 years as given by the three-dimensional study of Johnson *et al.* (1979), the three-dimensional study of Levy *et al.* (1979) and the two-dimensional study of Sze and Ko (1981), respectively.

Estimates of the globally-averaged atmospheric lifetime of $CH_3CC\ell_3$ have varied considerably over the past few years. For example, zero- of one-dimensional calculations were published by Yung *et al.* (1975), Cox *et al.* (1976), Singh (1977a), Crutzen and Fishman (1977), McConnel and Schiff (1978), Rasmussen and Khalil (1981), Makide and Rowland (1981), who estimated lifetime values of 3, 1.1, 7.2 $\pm$ 1.2, 6-10.7, 8, 6-10, 6.9 $\pm$ 1.2 years respectively. Using two-dimensional box models, Lovelock (1977), Neely and Plonka (1978), Singh (1977b), Chang and Penner (1978), Singh *et al.* (1979), and Logan *et al.* (1981) calculated $CH_3CC\ell_3$ lifetime values of 5-10, 3.3 $\pm$ 0.7, 8.3, 11.3, 8-10 and 5 years respectively. Using two-dimensional grid models, Derwent and Eggleton (1978, 1981) computed $CH_3CC\ell_3$ lifetime values of 5.4 and 3.6-6 years respectively. These different $CH_3CC\ell_3$ lifetime estimates have been obtained by specifying either the concentrations of OH radicals, or by considering the global mass balance between $CH_3CC\ell_3$ sources and sinks, or by combining both approaches. Lifetime estimates vary due to these different basic approaches, due to different estimates of tropospheric OH radicals concentrations, and their reaction rate with $CH_3CC\ell_3$, and due to

uncertainties in the anthropogenic emissions, concentrations and trends of $CH_3CC\ell_3$, and due to differences in the structure and details of the atmospheric models involved in each calculation. Except for N_2O, no previous three-dimensional calculations exist for the lifetimes of the five tracers involved in our study.

The accumulation, circulation, and lifetime of $CH_3CC\ell_3$ is important not only for predictions concerning the ozone layer, but for the prediction of tropospheric OH concentrations.

Since the early seventies, when Levy (1971, 1972), first predicted the presence of OH in the troposphere, it has become apparent that OH is playing a major role in tropospheric chemistry. It is the crucial reactant in certain chemical reactions, which scavenge many natural and anthropogenic compounds from the atmosphere. To name a few reactions:

$$OH + CO \rightarrow CO_2 + H$$

$$OH + CH_4 \rightarrow CH_3 + H_2O$$

$$OH + H_2S \rightarrow H_2O + HS$$

$$OH + SO_2 \rightarrow HSO_3$$

$$OH + NO_2 + M \rightarrow HNO_3 + M$$

$$OH + OCS \rightarrow CO_2 + HS$$

$$OH + CS_2 \rightarrow OCS + HS$$

$$OH + O_3 \rightarrow HO_2 + O_2$$

$$OH + RH + M \rightarrow H_2O + R + M$$

$$OH + CH_iC\ell_j F_k \rightarrow H_2O + CH_{i-1} C\ell_j F_k$$

$$OH + CH_iBr_j \rightarrow H_2O + CH_{i-1} Br_j$$

Because the hydroxyl radical (OH) serves as an oxidizer to many reduced gases emitted at the surface of the earth, it is a major driving force in the biogeochemical cycling of many elements. It is also a coupling agent between the basic chemical cycles of hydrogen, oxygen, nitrogen, chlorine and sulfur in the atmosphere. Finally, it also rapidly attacks the bonded hydrogen atoms in many acids, hydrocarbons (saturated and unsaturated) and halocarbons. Over the past few years OH has become recognized as an important member of almost every major atmospheric chemistry problem and is now a key factor in solving these problems, with all the impact these problems have on our daily and future life. To name a few examples:

- OH removal of CH_4 and NH_3 affects the greenhouse effect created by these chemicals (Wang *et al.* (1976)

- OH reaction with natural and anthropogenic pollutants, helps clean the air of major and minor pollutants with a wide range of hazardous impacts on our health including eye and lung irritants and carcinogens (e.g., H_2S, SO_2, polycyclic aromatic hydrocarbons, CO)

- OH reaction with $CH_3CC\ell_3$ limits the latter's influence on ozone -- the more $CH_3CC\ell_3$ is destroyed in tropospheric levels by OH radicals, the less ozone will be depleted in stratospheric levels. The same hydrogen removal reaction occurs also in the tropospheric scavenging by OH radicals of the hydrogen containing fluorocarbons: $CHC\ell_2F$,

$CHCl F_2$, and other halocarbons: $CHCl_3$, CH_2Cl_2, CH_2ClCH_2Cl, $CHClCCl_2$, CH_3Br, CH_2BrCH_2Br, CH_3I

- OH participation in the nitrogen and chlorine cycles has an important effect on the destruction rate of stratospheric ozone by NO and Cl
- OH incorporation in the natural and anthropogenic nitrogen and sulfur cycles, helps convert NO_2 and SO_2 to HNO_3 and H_2SO_4, thus directly affecting the acidity of rain.

This major role of OH in atmospheric chemistry, has created a concentrated effort to establish its concentration in the troposphere and stratosphere as accurately as possible. Not only is an accurate measurement of the instantaneous distribution of OH radicals needed, but also a trend analysis of this field is necessary, since OH average global concentration may decrease as more pollutants (e.g., CO) are released to our atmosphere, thus using up more and more OH radicals.

The most natural path of research would be to detect and measure directly the OH radical in the atmosphere. The abundance of middle and upper stratospheric OH radicals has been measured using a few experimental techniques: (a) Solar flux induced resonance fluorescence observed by a rocket-borne spectrometer, Anderson (1971a, 1971b), which provides a local concentration measurement by determining the change in total column emission rate as a function of altitude; (b) Balloon-borne in-situ molecular resonance fluorescence using

a plasma discharge resonance lamp to induce fluorescence. The fluorescence chamber is lowered through the stratosphere on a parachute to control the altitude and velocity of the probe (Anderson; 1976, 1980); (c) Ground-based high resolution solar absorption by an interferometer which resolves a single rotational line in the (0-0) band of OH at 309nm. The total column density of terrestrial OH between the instrument and the sun is observed, dominated by the altitude interval 25-65km (Burnett, 1976, 1977; Burnett and Burnett, 1981); and finally, (d) Balloon-borne laser induced detection and ranging (LIDAR) in which a pulsed laser system coupled to a telescope is used to observe the backscattered fluorescence from OH. The laser is turned to the (1-0) band of the A-X transition at 282nm and the fluorescence at 309nm (the 0-0 band) is observed as a function of time following the laser pulse (Heaps and McGee, 1981). Generally there is a good agreement among these techniques, and the OH profile between 30-70km is reasonably well established.

In the troposphere and lower stratosphere (15-30km) the situation is different. Measurements of OH in the troposhere are difficult, inaccurate, and show a large variability. The passive optical absorption technique (Penner *et al.*, 1976), is still not yet fully developed as argued by Killinger and Wang (1977). The isotope tracing technique of Campbell *et al.* (1979) still suffers from calibration and systematic errors. The laser-induced fluorescence method of Wang and Davis (1974a, 1974b), and Davis *et al.* (1976) is still marred by a

multitude of interferences (Hanabusa *et al.*, 1977; Wang *et al.*, 1981). Much effort is now being put into these measurements in the GAMETAG sampling program (Davis, 1980).

All these experimental difficulties and interferences result in direct OH tropospheric measurements which suffers from large standard deviations. Added to these experimental difficulties, is the fact that OH tropospheric concentrations apparently show a rapid space and time variability, making it difficult to assess a globally-averaged OH free radical concentration based on direct tropospheric measurements.

In order to avoid the difficulties associated with the direct determination of OH in the atmosphere, Lovelock (1977), suggested the use of $CH_3CC\ell_3$ as an indirect probe for determining the OH distribution in the troposphere. As we mentioned earlier, the main recognized sink for $CH_3CC\ell_3$ in the troposphere is its reaction with OH free radicals. Thus if global measurements of $CH_3CC\ell_3$ are available, and we take into account its known source distribution from industrial areas over the globe and its stratospheric loss by uv photodissociation, the only unknown needed to evaluate the $CH_3CC\ell_3$ atmospheric mass balance is the OH atmospheric distribution. Following Lovelock's idea, this same technique was tried by Crutzen and Fishman (1977), Singh (1977a, 1977b), Neely and Plonka (1978), Derwent and Eggleton (1981), and by Logan *et al.* (1981).

Another indirect method involves a study of the CO budget. Here one studies the CO reaction with OH radicals

as the principal sink (Logan *et al.*, 1981; Volz *et al.*, 1981). The Volz *et al.* (1981) study for example suggested an average tropospheric OH concentration of 6.5×10^5 molecules cm^{-3}, using a two-dimensional model. Most recently, Pinto *et al.* (1981), found a value of 7×10^5 molecules cm^{-3} using a three-dimensional general circulation model, apparently in good agreement. However, when all the direct and indirect methods for determining OH are studied, it is apparent that there is a considerable disagreement and/or uncertainty as to the global distribution and concentration of tropospheric OH radicals (e.g., Allam *et al.*, 1981; Chameides and Tan, 1981; Logan *et al.* 1981; Seiler and Fishman, 1981; Volz *et al.*, 1981; Turco *et al.*, 1981).

An important result from this thesis is therefore the first three-dimensional study of the use of $CH_3CC\ell_3$ as an indirect probe for determining atmospheric OH concentrations. The results which are obtained are in fact in good agreement with the indirect method using CO (Volz *et al.*,1981).

In Chapter 2 of the thesis we will describe the three-dimensional model developed and used in the chemical studies. All the input data used for initialization of the intergrations will also be presented in this chapter.

In Chapter 3 we will show the results of the model integrations for all five species, and we will discuss these results including a comparison with existing measurements from various sources. In Chapter 4 we will draw and summarize the

general conclusions from our model runs and describe the specific new achievements of this thesis.

2. METHOD

2.1.1 The mathematical model uses the same general techniques for tracer transport and chemistry as were used by Cunnold *et al.* (1975, 1980) in their dynamical-chemical spectral model for ozone. Our coordinate system uses in the horizontal, longtitude λ (positive eastward) and latitude ϕ. Dependence on λ, ϕ in the horizontal is represented in spherical harmonics (except for non-linear chemical reaction terms which are evaluated in 240 grid points: 15 latitudes (NLAT) and (16 longitudes (NLONG), Table 2). In the vertical the model uses p defined as $P = \frac{p}{1000mb}$, where p is the pressure in (mb), and $Z = -\ell nP$. Levels in the vertical are equally spaced in increments ΔZ equivalent to $\sim$3km. There are 26 levels from the surface to about 70km (Table 3), where Z changes from $Z=0$ at the surface, to $\sim Z=10.1$ at the top. Using the hydrostatic relation, $dp=-\rho g dz$ and the equation of state for dry air, $p=\rho RT$, we get $dZ=\frac{g}{RT}\,dz$. Equally chosen increments $\Delta Z = 0.406$, correspond to almost equal increments in height of 2.9Km. For an average temperature $T_o = 239°k$ we can define an average scale height, $H_o = \frac{RT_o}{g} \simeq 7km$.

The input dynamical parameters (vorticities, vertical velocities) are in quasi-geostrophic balance, following the

Table 2 : The Model Horizontal Grid Points.

NLAT	Latitude (degrees)
1	80.5°N
2	69 °N
3	57.5°N
4	46 °N
5	34.5°N
6	23 °N
7	11.5°N
8	0°
9	11.5°S
10	23 °S
11	34.5°S
12	46 °S
13	57.5°S
14	69 °S
15	80.5°S

NLONG	Longtitude (degrees)
1	0°
2	22.5°E
3	45 °E
4	67.5°E
5	90 °E
6	112.5°E
7	135 °E
8	157.5°E
9	180 °E
10	157.5°W
11	135 °W
12	112.5°W
13	90 °W
14	67.5°W
15	45 °W
16	22.5°W

Table 3 : The Model Vertical Levels.

Level	Z	p (mb)	z (Km)	$\overline{T}$ (^{o}K)
1	10.14	0.04	71.6	211
2	9.73	0.06	69.0	219
3	9.33	0.09	66.3	226.5
4	8.92	0.13	63.5	234
5	8.52	0.20	60.6	241.5
6	8.11	0.30	57.6	249.5
7	7.70	0.45	54.5	258.5
8	7.30	0.68	51.4	267
9	6.89	1.01	48.2	267.5
10	6.49	1.52	45.0	261.5
11	6.08	2.28	41.9	245.5
12	5.68	3.43	38.8	248.5
13	5.27	5.14	35.9	242.5
14	4.87	7.71	33.0	237
15	4.46	11.6	30.2	231
16	4.06	17.3	27.5	225
17	3.65	26.0	24.8	219.5
18	3.24	39.0	22.2	214.5
19	2.84	58.5	19.6	211.5
20	2.43	87.8	17.1	210.5
21	2.03	132	14.6	213
22	1.62	198	12.0	222
23	1.22	296	9.3	234
24	0.81	444	6.4	248
25	0.41	667	3.4	266
26	0	1000	0.1	287

formulation by Lorenz (1960).

Vorticities (also stream functions) are defined at the midpoints of the twenty-five layers of the model, where as vertical velocities (also tracer mixing ratios and temperatures) are defined at each of the 26 levels, i.e., at the layers' interfaces.

The horizontal velocity field $\vec{V}$ is divided into a non-divergent (or rotational) part $\hat{k} \times \nabla\psi$, where ψ is the stream function, and a divergent (or non-notational) part, $-\nabla\chi$, where χ is the velocity potential, i.e.,

$$\vec{V} = \hat{k}x\nabla\psi - \nabla\chi$$

Velocity $\vec{V}$ is thus composed of u and v components (eastward and northward, respectively) and these are related to latitude and longitude by,

$$u = a \cos\phi \frac{d\lambda}{dt} = -\frac{1}{a \cos\phi} \frac{\partial\chi}{\partial\lambda} - \frac{1}{a} \frac{\partial\psi}{\partial\phi}$$

$$v = a \frac{d\phi}{dt} = \frac{1}{a \cos\phi} \frac{\partial\psi}{\partial\lambda} - \frac{1}{a} \frac{\partial\chi}{\partial\phi}$$

where a is the radius of the earth.

The vertical component of relative vorticity ζ and the horizontal divergence of the horizontal velocity field, δ , are given by

$$\zeta = k.\nabla x\vec{V} = \nabla^2\psi = \frac{\partial v}{\partial x} - \frac{\partial u}{\partial y}$$

$$\delta = \nabla.\vec{V} = -\nabla^2\chi = \frac{\partial u}{\partial x} + \frac{\partial v}{\partial y}$$

The quasi-geostrophic balance condition takes the form,

$$\nabla.f\nabla\psi = g\nabla^2 z$$

where $f = 2\Omega \sin\phi$, is the Coriolis parameter and $\Omega = 7.292.6^{-5}$ (radians sec^{-1}) is the earth's rotation rate. Using the hydrostatic relation and the euqation of state, we then get the thermal wind relation

$$\nabla.f\nabla\frac{\partial\psi}{\partial Z} = R\nabla^2 T$$

For Z as the vertical coordinate, vertical advection velocity is defined by

$$W = \frac{dZ}{dt} = -\frac{1}{P}\frac{dP}{dt} \quad .$$

Our model uses precalculated vorticity fields ζ , from which ψ, $\nabla\psi$ and the temperature fields are derived using the following relations,

$$\psi = L\zeta$$

where L is defined as the operator $L \equiv \nabla^{-2}$

$$\nabla\psi = \frac{\partial\psi}{\partial x} + \frac{\partial\psi}{\partial y} = v - u$$

$$T = L\left(\frac{1}{R}\nabla . f\nabla\frac{\partial\psi}{\partial Z} \right) \quad .$$

Our model solves the prediction equation for the tracer's mixing ratio m, $m = \frac{n}{n_m}$,

where n is the tracer's number density and n_m is the total number density, equivalent to the normal constituents of dry air (N_2, O_2, CO_2),

$$n_m = \frac{p}{kT}$$

where k, is the Boltzman constant.

The tracer's prediction equation has the form,

$$\frac{\partial m}{\partial t} = -(\hat{k}x\nabla\psi - \nabla\chi).\nabla m - W\frac{\partial m}{\partial Z}$$

$$+ \frac{1}{n_m}(\frac{dn}{dt})_c + \frac{1}{H_o^2 P} \frac{\partial}{\partial Z}(K_d \; P \; \frac{\partial m}{\partial Z})$$

where $(\frac{dn}{dt})_c$ is the net rate of local tracer generation (number per unit volume per unit time) -- due to combining all local chemical sources minus all local chemical sinks, and K_d is the vertical eddy-diffusion coefficient (a prescribed function of Z). Neglecting the small term $\nabla\chi \ll kx\nabla\psi$, we get,

$$\frac{\partial m}{\partial t} = - J(\psi,m) - W\frac{\partial m}{\partial Z} + \frac{1}{n_m}(\frac{dn}{dt})_c + \frac{1}{H_o^2 P} \frac{\partial}{\partial Z}(K_d P\frac{\partial m}{\partial Z})$$

where J is the Jacobian.

For any tracer the model predicts separately the changes in the horizontal average mixing ratio $\bar{m}$ as well as deviations from the horizontal average m', i.e., there are in practice two material prediction equations:

$$\frac{\partial m'}{\partial t} = - J(\psi,m') - W\frac{\partial \bar{m}}{\partial Z} + \frac{1}{H_o^2 P} \frac{\partial}{\partial Z}(K_d P\frac{\partial m'}{\partial Z}) + (\frac{1}{n_m} \frac{dn}{dt})'_c$$

$$\frac{\partial \bar{m}}{\partial t} = -\frac{1}{P}\frac{\partial}{\partial Z}\{P(\overline{Wm'})\} + \frac{1}{H_o^2 P}\frac{\partial}{\partial Z}\left(K_d P \frac{\partial \bar{m}}{\partial Z}\right) + \left(\overline{\frac{1}{n_m}\frac{dn}{dt}}\right)_c$$

we use the fact that $-J(\psi,\bar{m}) = 0$

In the horizontal the truncated series of spherical harmonics,

$$\Pi_n^{\ell}(\sin\phi)\exp(i\ell\lambda)$$

are used to represent the various fields, e.g., for the vorticity field,

$$\nabla^2\psi(\lambda,\phi,Z_j,t) = \sum_{n=\ell}^{N_\ell}\sum_{\ell=-L}^{L} C_{\ell n}(t,j)\Pi_n^{\ell}(\sin\phi)\exp(i\ell\lambda)$$

where Π_n^{ℓ} are Legendre polynomials and $C_{\ell n}$ are the expansion coefficients. Fields of W, T, and m and various intermediate derivatives and combinations of variables needed in the computation are all represented in the same way. The truncation used has $L = 6$, $N_\ell = 6,6,7,8,9,10,11$ for $|\ell| = 0,1,2,3,4,5,6$ respectively, giving 79 degrees of freedom in each variable at each vertical level. Nonlinear terms are computed using the spectral interaction method, except for the highly nonlinear chemical generation term $(\frac{1}{n_m}\frac{dn}{dt})_c$. This term is computed at each time step in the physical space grid, (Table 2), and by using a fast-Fourier transform, is moved backward and forward between the spectral and grid representations of its values. All variables used in the model are non-dimensional.

The computational procedure uses the "4-cycle" version of the time differencing scheme of Lorenz (1971), for the material prediction equation. The atmospheric chemical local generation term for the four tracers: $CFC\ell_3$, $CF_2C\ell_2$, $CC\ell_4$, N_2O includes photochemical destruction by far uv radiation and reaction of the tracer with $O(^1D)$ radicals in stratospheric levels and for $CH_3CC\ell_3$ it includes, in addition, the reaction with OH free radicals. e.g., for $CH_3CC\ell_3$ we have,

$$\frac{1}{n_m}\left(\frac{dn}{dt}\right)_c = -\left\{J_{CH_3CC\ell_3} + k_{OH}n_{OH} + k_{O(^1D)}n_{O(^1D)}\right\} m$$

where,

$$CH_3CC\ell_3 + h\nu \xrightarrow{J_{CH_3CC\ell_3}} \text{Products}$$

$$CH_3CC\ell_3 + OH \xrightarrow{k_{OH}} CH_2CC\ell_3 + H_2O$$

$$CH_3CC\ell_3 + O(^1D) \xrightarrow{k_{O(^1D)}} CH_2CC\ell_3 + OH$$

$$J_{CH_3CC\ell_3} = \int \alpha_{CH_3CC\ell_3}(\Lambda) I(\Lambda) \exp(-\Sigma\xi_{tracers} - \xi_{O_2} - \xi_{O_3}) d\Lambda$$

where

$$\xi_i = \frac{\alpha_i(\Lambda) N_i}{\cos\varphi}$$

$\alpha_i(\Lambda)$ is the absorption cross section (cm^2 $molecule^{-1}$) of the i'th tracer (as a function of wavelength Λ), $I(\Lambda)$ is the incident solar radiation (as a function of wavelength Λ), in units of

(photons cm^{-2} sec^{-1}), N_i is the number of molecules of species i in the (1 cm^2) vertical column above the point of interest, φ is the solar zenite angle. The term $J_{CH_3CC\ell_3}$ so evaluated, will be given in (sec^{-1}) units. Since absorption bands of all the tracers overlap the absorption bands of ozone and oxygen, the latter two species must be included in the exponent term of the integral $J_{CH_3CC\ell_3}$, to account for the depletion of solar energy by them (the main depletion is due to ozone and $\Sigma\xi_{tracers}$ is very small, and is in practice neglected in the calculations, ξ_{O_2}, ξ_{O_3} are maintained).

The reaction rate of $CH_3CC\ell_3$ with OH radicals is given in units of (cm^3 $molecule^{-1}$ sec^{-1}), n_{OH} the number density of OH radicals is given in (molecules cm^{-3}), so that $k_{OH}n_{OH}$ will have units of (sec^{-1}) same as for J. The rate constant k_{OH} is a function of temperature, and is given in the form:

$$k_{OH} = A\exp\left(-\frac{B}{T}\right) \qquad (cm^3 molecule^{-1} sec^{-1})$$

where A and B are experimentally determined constants.
$O(^1D)$ radicals typical vertical number density distribution is determined by writing the balance between the following chemical reactions:

$$O_3 + h\nu \xrightarrow{J_{O_3}} O(^1D) + O_2 \qquad \Lambda \leq 310 \text{ nm}$$

$$O(^1D) + M \xrightarrow{k_1} O + M$$

$$O(^1D) + H_2O \xrightarrow{k_2} 2OH$$

the reaction with water is neglected (in the stratosphere, this sink for $O(^1D)$ is negligible in comparison to the k_1 sink). Thus we can write the balance for $O(^1D)$ in stratospheric levels,

$$k_1 \, n_{O(^1D)} \, n_m = J_{O_3} \, n_{O_3}$$

and,

$$n_{O(^1D)} = \frac{J_{O_3} n_{O_3}}{k_1 n_m} = \frac{J_{O_3}}{k_1} m_{O_3}$$

and

$$\frac{1}{n_m}\left(\frac{dn}{dt}\right)_c = -\left(J_{CH_3CC\ell_3} + k_{OH} n_{OH} + k_{O(^1D)} \frac{J_{O_3}}{k_1} m_{O_3} \right) m$$

this additional sink was treated in the model calculations

as a small "correction" to the $J_{CH_3CC\ell_3}$ calculation, i.e.,

$$\frac{1}{n_m}\left(\frac{dn}{dt}\right)_c = -\left(J_{eff} + k_{OH} n_{OH} \right)_m$$

$$\text{where } J_{eff} = J_{CH_3CC\ell_3} + k_{O(^1D)} \frac{J_{O_3}}{k_1} m_{O_3}$$

and was calculated in the model once every ten days, and not in each time step of the calculation.

For the tracers $CFC\ell_3$, $CF_2C\ell_2$, $CC\ell_4$, N_2O no OH sink was included in the calculation, only photodissociation and the reaction of the tracer with stratospheric $O(^1D)$ radicals, were considered.

The spectral fields of $\nabla^2\psi$, W, and mozone needed for our model integration of the tracer prediction equations, are taken from a recent run (run 34) of the Cunnold *et al.* (1975) dynamical model which is discussed in the following section. These fields are used as input data for our tracer model runs, in each time step of the "4-cycle" Lorenz numerical scheme.

Details of the model input data, initialization, boundary conditions and chemistry are given in section 2.2. To give a sense of the overall operation of the model an outline of a typical model run follows. The model runs for each of the five tracers, start with reading an initial two-dimensional field of tracer for the month of July 1978,

assuming it to be the value for July 16, 1978. This initial two-dimensional tracer distribution is based on global surface measurements and on measured or calculated vertical profiles. Following the initial two-dimensional distribution, the model code reads the tracer's surface source parameters (yearly global emissions and the surface distribution of these emissions). Next are read the tracer's absorption cross sections with their appropriate temperature dependence (if available), and the details of the tracer's oceanic sink where applicable. The values read in next are the dry air number density vertical profile, various mathematical constants including the interaction coefficients, initial fields of ozone and OH free radicals, absorption cross-sections for ozone and oxygen, ultraviolet photon fluxes and vertical profiles of Z, P and average temperatures.

In the next step all the initial two-dimensional fields are converted to initial three-dimensional fields by putting the same zonal values around the latitude circles. This is done for ozone mixing ratios, ozone column values, and tracer mixing ratios. The model then reads in the appropriate (according to the date) spectral fields of vorticities, vertical velocities and ozone mixing ratios. An initial field of the tracer is then created in spectral form, from the initial grid form of the three-dimensional field. For consistency at this point, the grid field is then recreated from the deduced spectral field, and any negative values of the

tracer mixing ratios thus created, are set to zero in the latter grid form. Then the spectral tracer field is regenerated. Vorticities $\nabla^2\Psi$ are then transformed into stream functions ψ, and using the thermal wind relation, temperatures are calculated from the stream functions (all in spectral representation). Next, the temperature field in grid format is created from the spectral temperature field, to be used later in the photochemical and chemical calculations. Now the time step is specified. Mid-level values of the stream functions are then calculated. Next ozone mixing ratios are created in grid form, from the spectral field, and again negative values thus generated in the grid field, are set to zero -- these grid values of ozone, are necessary for the photochemical calculations. The photodissociation integral J is calculated next, in a three-dimensional grid field, taking the date into account. In the following steps the various contributions to the tracer's prediction equation, are calculated: horizontal and vertical advection, vertical eddy diffusion, photochemistry and chemistry, anthropogenic source, and oceanic sink. The chemical-photochemical net generation term, $\frac{1}{n_m}(\frac{dn}{dt})_c$ is determined for each vertical level at the 240 grid points and then converted to spectral form, by the fast-Fourier transformation, and added to the other terms in the $\frac{\partial m}{\partial t}$ equation, which are also all calculated in the spectral form. The source term for the tracer which is its daily release from human activity at the

surface of the continents, is accounted for at the grid points of the lowest layer of the model. Each grid point has its own contribution, depending on the amount of tracer released there - this source contribution, is also transformed into the spectral form before being added to the other terms in the $\frac{\partial m}{\partial t}$ equation. Prediction using the N = 4 N-cycle scheme is done next, and the whole cycle is then started all over again, depending on the total integration time needed for each particular run. The initial tracer field and the field calculated after each five days of integration are printed out, as well as the zonally-averaged tracer mixing ratios at the 26 model levels and 19 latitudes (90°N, 80°N, ..., 10°N, Eq, 10°S, ..., 80°S, 90°S), and finally the tracer mixing ratios for the surface level 26 at 240 model grid points (15 latitudes x 16 longitudes). After each day of integration the following diagnostic terms are printed: total atmospheric tracer content, the tracer instantaneous lifetime, the daily input and the daily loss of tracer, the tracer mixing ratios at 5 ALE station locations where surface measurements are available, the tracer zonally-averaged mixing ratio at the latitudes of these 5 latter locations, and finally the tracer's globally averaged surface mixing ratio. After each month of integration, the model also prints out the monthly-mean tracer mixing ratios at the latter 5 ALE station locations, with their appropriate standard deviations. The tracer mixing ratio spectral field is stored on an output tape after

the completion of each run for further integration or analysis. Integration of the tracer mixing ratio prediction equation in time steps of two hours, requires about eight seconds per model day (twelve time steps), where the major part of this time is consumed in handling the input data tapes (namely reading the fields of the precalculated vorticity, vertical velocity and ozone mixing ratio, every other time step). This integration time is about 20 % of the time needed for the integration of the MIT/GIT model -- where ozone was the tracer, and where 3 prediction equations were integrated. Some important conversion factors and constants which are used in our model calculation are summarized in Table 4.

2.1.2 The MIT/GIT ozone mathematical model

The MIT/GIT model Cunnold *et al.* (1975, 1980) solves three prediction equations:

(i) the vorticity prediction equation,

$$\frac{\partial}{\partial t} \nabla^2\psi = -J(\psi, f+\nabla^2\psi) - \nabla . f \frac{\partial X}{\partial P} - \nabla . \frac{\partial}{\partial P}(PF)$$

where X is defined as,

$$X = - \int_{P_{top}}^{P} \chi dP \qquad \text{or} \qquad \chi = - \frac{\partial X}{\partial P}$$

and F denotes friction,

Table 4 : Conversion Factors and Constants.

Dimensional to non-dimensional conversion factors, (dimensional quantity = conversion factor * non-dimensional quantity).

Quantity	Conversion Factor
Time	$\frac{1}{2\Omega}$
W	2Ω
T	$\frac{4}{R}\Omega^2 a^2$
1 day	$\frac{1}{4\pi}$

Constant	Description	Value
Ω	earth rotation	7.292E-5 [rad /sec]
a	earth radius	6.371E6 [m]
R	dry air universal gas constant	.287 [joul/(gm*deg)]
C_p	dry air heat capacity (cons. press.)	$\frac{7}{2}$ R
k	Boltzman constant	1.38E-29 [joul/deg]
H_o	scale height	7000 [m]
N_m	column dry air	2.12E25*P [mol./cm^2]
Z	non-dim. vertical increment	0.40574
Z_{top}	non-dim. top	10.13675
Z_{bottom}	non-dim. bottom	0
k_d	surface drag coefficient	1.6E-6 [1/sec]
N_{O_2}	column oxygen	0.4444E25*P [mol./cm^2]

at $Z=0$, $F = k_d \nabla\psi_o$, $W = \frac{1}{H_o} J(\psi_o, z_o)$

where k_d the surface drag coefficient
and z_o the orography

at $Z_{top} > Z > 0$ $\qquad F = \frac{K_d}{H_o^2} P \frac{\partial \nabla\psi}{\partial Z}$

where $K_d(Z)$ is the vertical diffusion coefficient of the tracer, a prescribed function of Z.

and at $Z=Z_{top}$, $F=0$, $W=0$.

(ii) the temperature prediction equation,

$$\frac{\partial T'}{\partial t} = -J(\psi, T') - W\left(\frac{dT_s}{dt} + \frac{R}{C_p} T_s \right) + \frac{q'}{C_p}$$

the model does not predict any changes in the horizontally-averaged temperature $\overline{T}(z)$ from the reference distribution $T_s(z)$ (e.g., for the standard atmosphere),

$$T = \overline{T}(Z) + T'(\lambda,\phi,Z,t)$$

q' is the rate of heating per unit mass, minus its horizontal average.

$\left(\frac{dT_s}{dZ} + \frac{R}{C_p}T_s \right)$ is the static stability and its values are presceibed in the model as a function of Z.

(iii) the ozone mixing ratio prediction equation,

$$\frac{\partial m}{\partial t} = -J(\psi,m) - W\frac{\partial m}{\partial Z} + \frac{1}{n_m}\left(\frac{dn}{dt}\right)_c + \frac{1}{H_o^2 P}\frac{\partial}{\partial Z}\left(K_d P \frac{\partial m}{\partial Z}\right)$$

with the appropriate boundary conditions for ozone.

The model uses three diagnostic relations,

(i) Hydrostatic

$$RT' = g\frac{\partial z'}{\partial Z}$$

(ii) Balance

$$g\nabla^2 z' = \nabla . f\nabla\psi$$

(iii) Continuity $PW = \nabla^2 X$

The MIT/GIT model has been run in several forms for ozone (e.g., see Cunnold *et al.*, 1975, 1980; Prinn *et al.* 1978). These runs all used time steps of one hour in each

cycle. Some results for run 17 are redrawn in Figures 1, 2, 3, 4a, 4b, 4c. Figure 1 shows the measured zonal wind cross-section as reported by Newell (1969) and as calculated by the model for the solstice. Figure 2 shows the zonally-averaged temperature distribution as observed and as calculated by the model for the solstice. Figure 3 shows the mean meridional circulation patterns for the solstice as produced by the model. Figure 4a shows the columnar ozone variation in the Northern hemisphere compared to observations, Figure 4b shows calculated and observed ozone mixing ratios during typical solsticial seasons, Figure 4c shows the calculated and observed two-dimensional (latitude-altitude) ozone distribution for summer and winter. These figures show very good agreement between measurement and calculations for ozone. Although the model was not tested for the circulation and chemistry of tropospheric tracers, this good agreement for ozone was the basis for choosing the transport parameters from this model for the 3-D tracer model developed for this thesis. In the future we can choose vorticities, vertical velocities, and ozone concentrations from observations or from other three-dimension general circulation models. The question of the time steps and spatial resolution required in our model would then need to be reassessed.

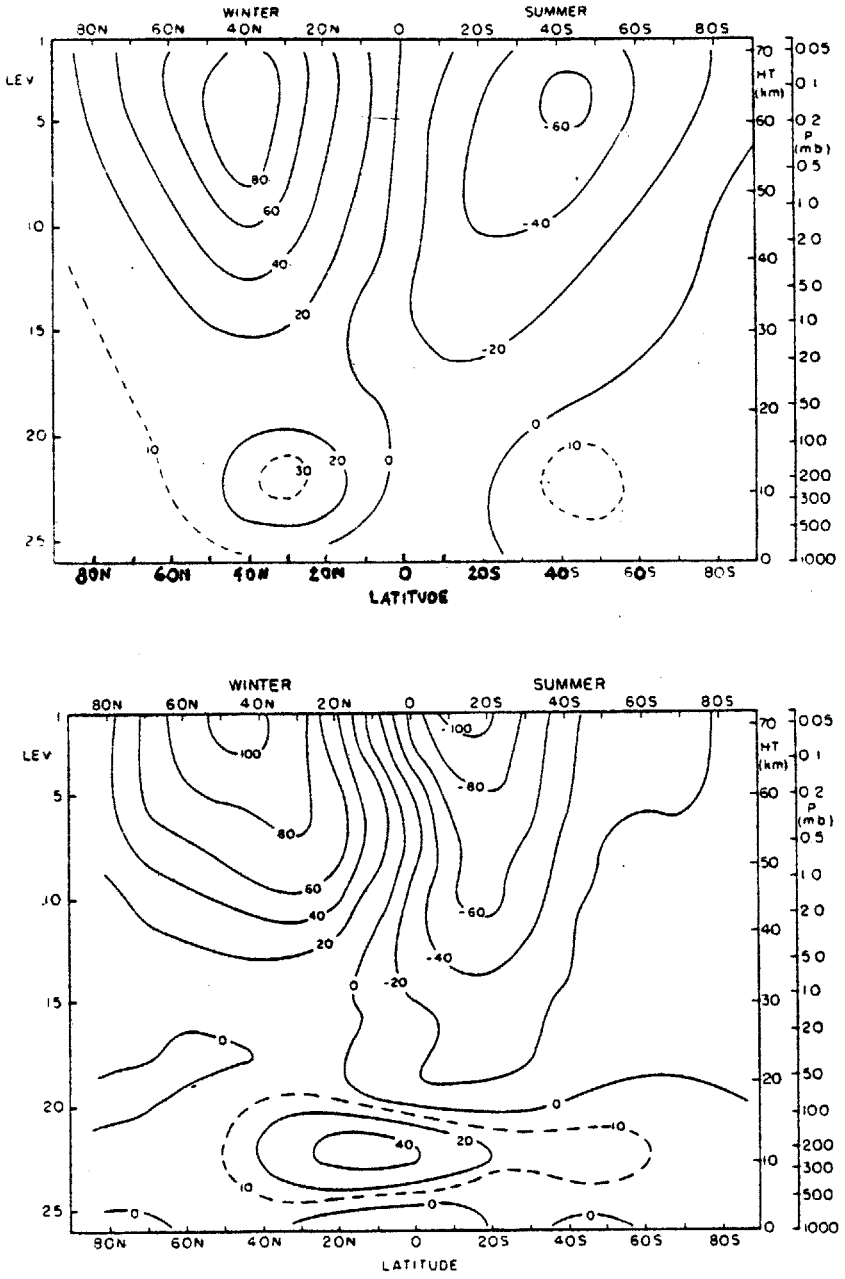


Figure 1: Northern hemisphere winter and summer mean zonal wind (m/sec), measurements (top) and model calculations, Run 17 (bottom), after Prinn et al. (1978).

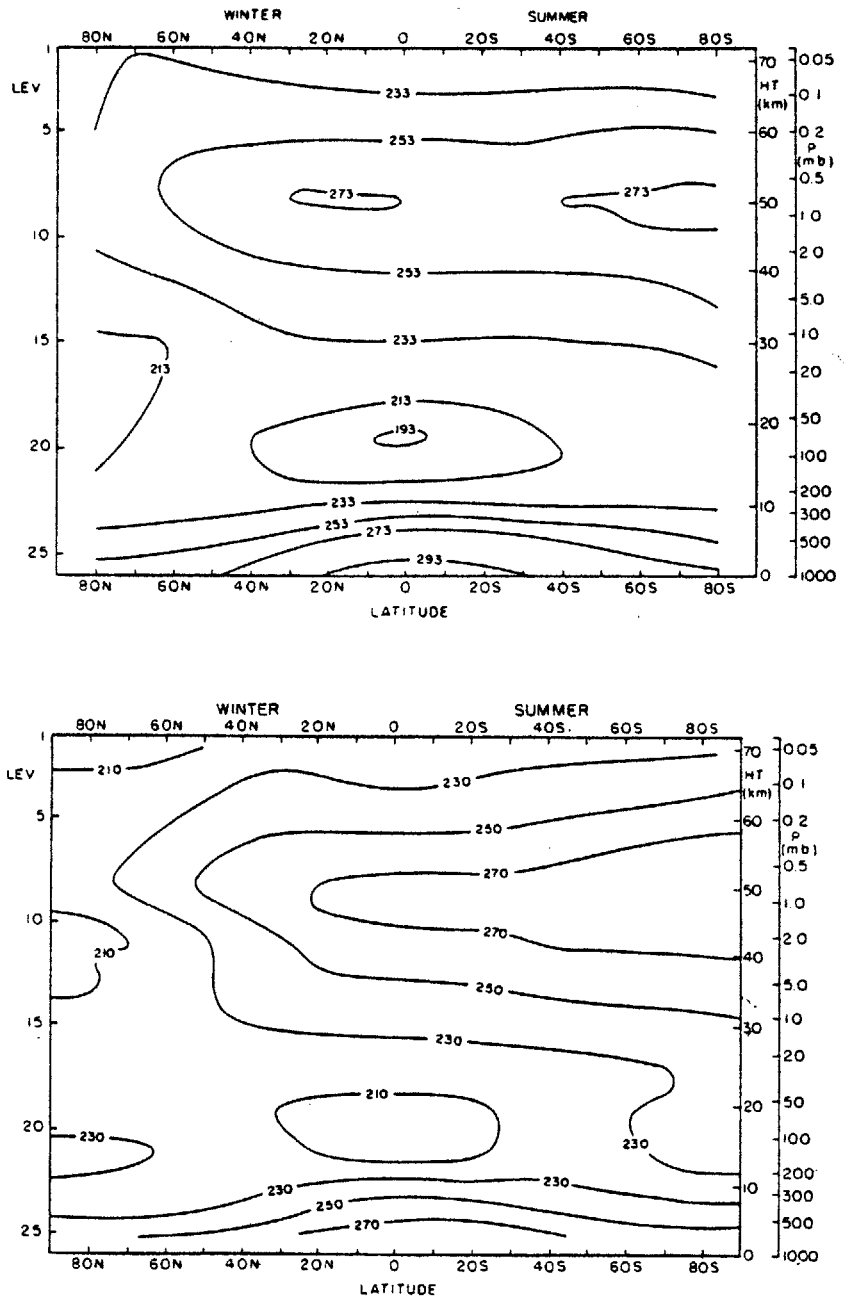


Figure 2: Northern hemisphere winter and summer mean zonal temperatures (°K), measurements (top) and model Run 17 calculations (bottom), after Prinn et al. (1978).

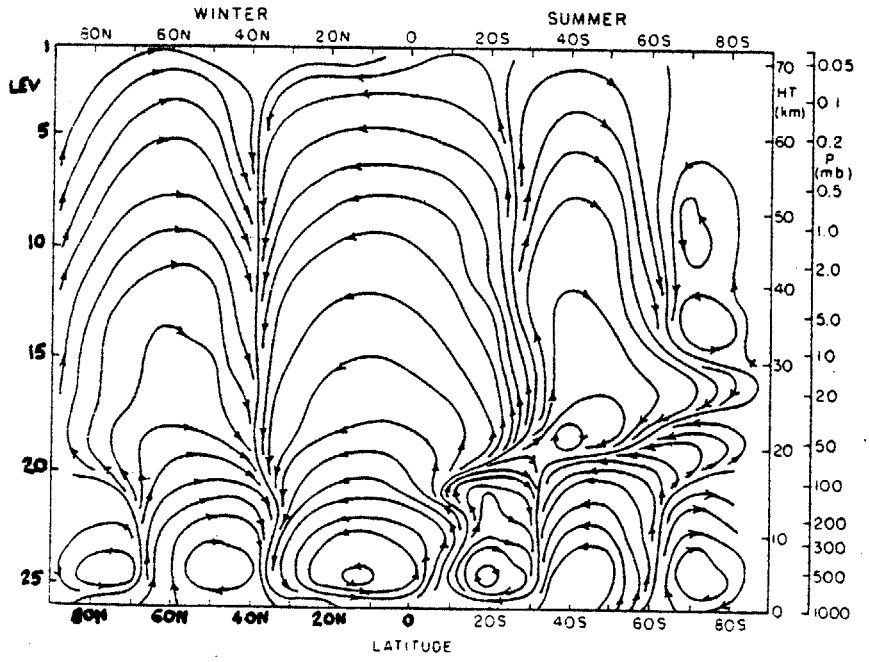


Figure 3: Northern hemisphere winter and summer mean meridional circulation as predicted in Run 17 of the model, after Prinn et al. (1978).

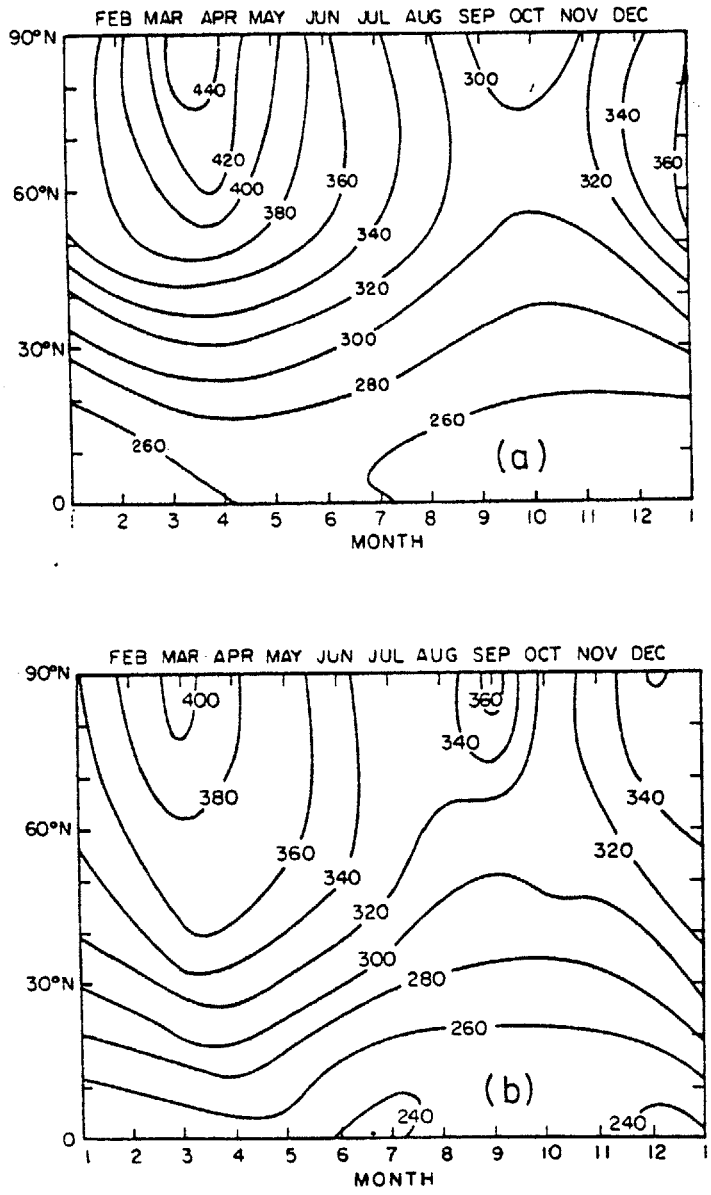


Figure 4a: The columnar ozone variation (Dobson units) in the Northern hemisphere. Model results from Run 17,(b) are compared to measurements,(a), after Cunnold et al. (1980).

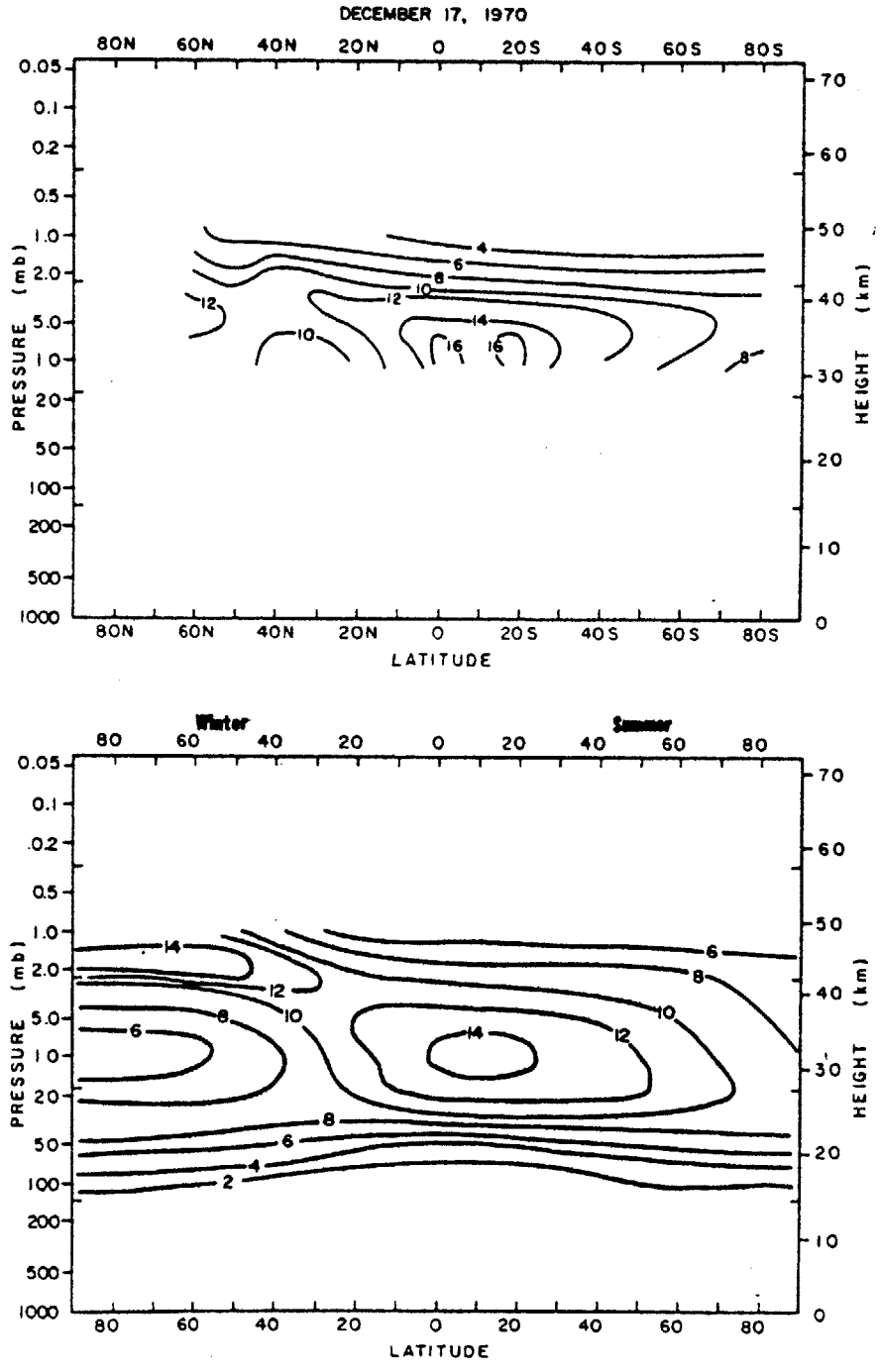


Figure 4b: Calculated ozone mixing ratios (ppm), lower figure, compared against observations, upper figure, for a typical solsticial season, after Cunnold et al. (1980).

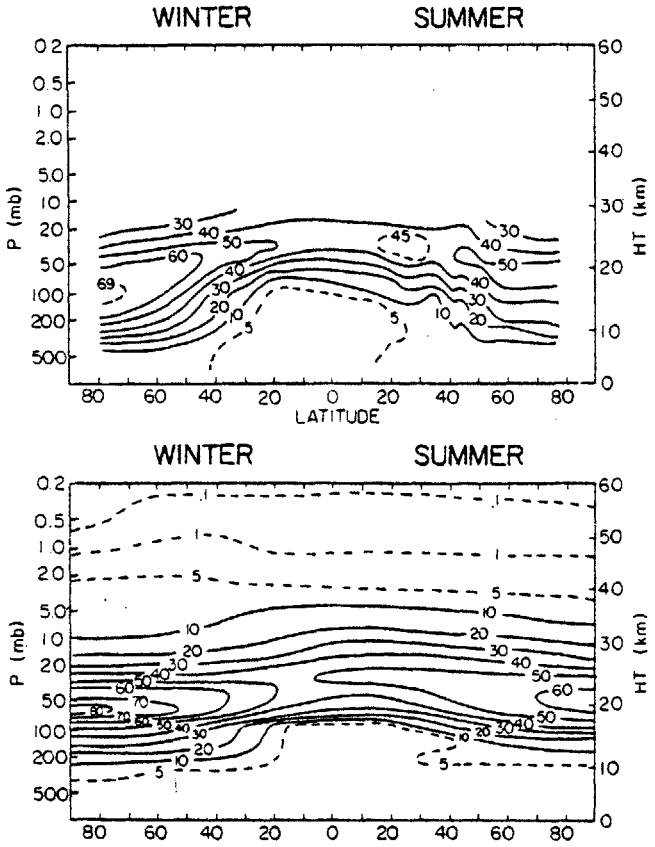


Figure 4c: The distribution of ozone (units 10^{11} mol dm^{-3}) as a function of latitude and height from model Run 17 (lower figure) compared against observations (upper figure), after Cunnold et al. (1980).

2.2 Initialization, Input Data, and Boundary Conditions

2.2.1 Two-dimensional initial profile

Integration was started using an initial two-dimensional tracer field constructed from observations. For surface concentrations the monthly-mean values of $CFC\ell_3$, $CF_2C\ell_2$, $CC\ell_4$, N_2O and $CH_3CC\ell_3$, as measured at 4 of the 5 ALE stations (Table 5) during the month of July 1978 are used (Cunnold *et al.*, 1982a, 1982b; Simmonds *et al.*, 1982; Prinn *et al.*, 1982b). The ALE stations measure $CFC\ell_3$, $CF_2C\ell_2$, $CC\ell_4$, N_2O and $CH_3CC\ell_3$, three to four times a day, using electron-capture gas chromatography, and compute the concentrations by comparison with an on-site standard. Initial concentrations are given in Table 6. Using these latter surface values as a basis a smoothed latitudinal distribution for each species was constructed (see Figures 5a, b, c). In the vertical for $CFC\ell_3$ and for $CF_2C\ell_2$, two separate vertical profile estimates were used. The first is a profile calculated in a one-dimensional model by Crutzen *et al.* (1978) which effectively served as an upper limit (their values turned out to be somewhat too high in our model stratosphere). The second is a profile measured by Fabian (1981) and Fabian *et al.* (1981), at one specific location in Germany ($\sim$44°N) which served effectively as a lower limit (these values turned out to be somewhat too low for a global vertical profile in our model stratosphere). For $CH_3CC\ell_3$, $CC\ell_4$, and N_2O only one vertical profile was used, namely that of Crutzen *et al.*

Table 5 : ALE Stations Locations.

	Station Number and Name	Location		Date at which Measurement began
1.	Adrigole, Ireland	52°N	10°W	July 1978
2.	Cape Meares, Oregon	45°N	124°W	January 1980
3.	Ragged Point, Barbados	13°N	59°W	July 1978
4.	NOAA Site, American Samoa	14°S	171°W	July 1978
5.	Cape Grim, Tasmania	41°S	145°E	July 1978

Table 6: July 1978 Surface Monthly Averaged Mixing ratios as Measured by Gas-Chromatographs at the ALE Stations. Standard deviations are given in parentheses. These are absolute mixing ratios obtained after multiplication of reported mixing ratios by the appropriate calibration factor ξ (see Prinn et al., 1982a).

ALE Site	CH_3CCl_3 (pptv)	$CFCl_3$ (pptv)	CF_2Cl_2 (pptv)	CCl_4* (pptv)	N_2O (ppbv)
1	140.1(5.7)	166.9(3.3)	273.7(7.1)	123.4(4.4)	308.2(1.7)
3	124.5(7.2)	159.8(2.6)	269.0(3.0)	118.9(2.8)	303.2(1.7)
4	88.9(3.6)	145.0(1.7)	241.7(2.3)	114.0(1.8)	300.3(2.6)
5	86.0(4.3)	142.1(1.7)	241.9(1.2)	118.0(2.4)	304.2(3.1)

* uses $\xi = 0.84$; current best estimate for ξ for CCl_4 in the ALE program is 0.81 .

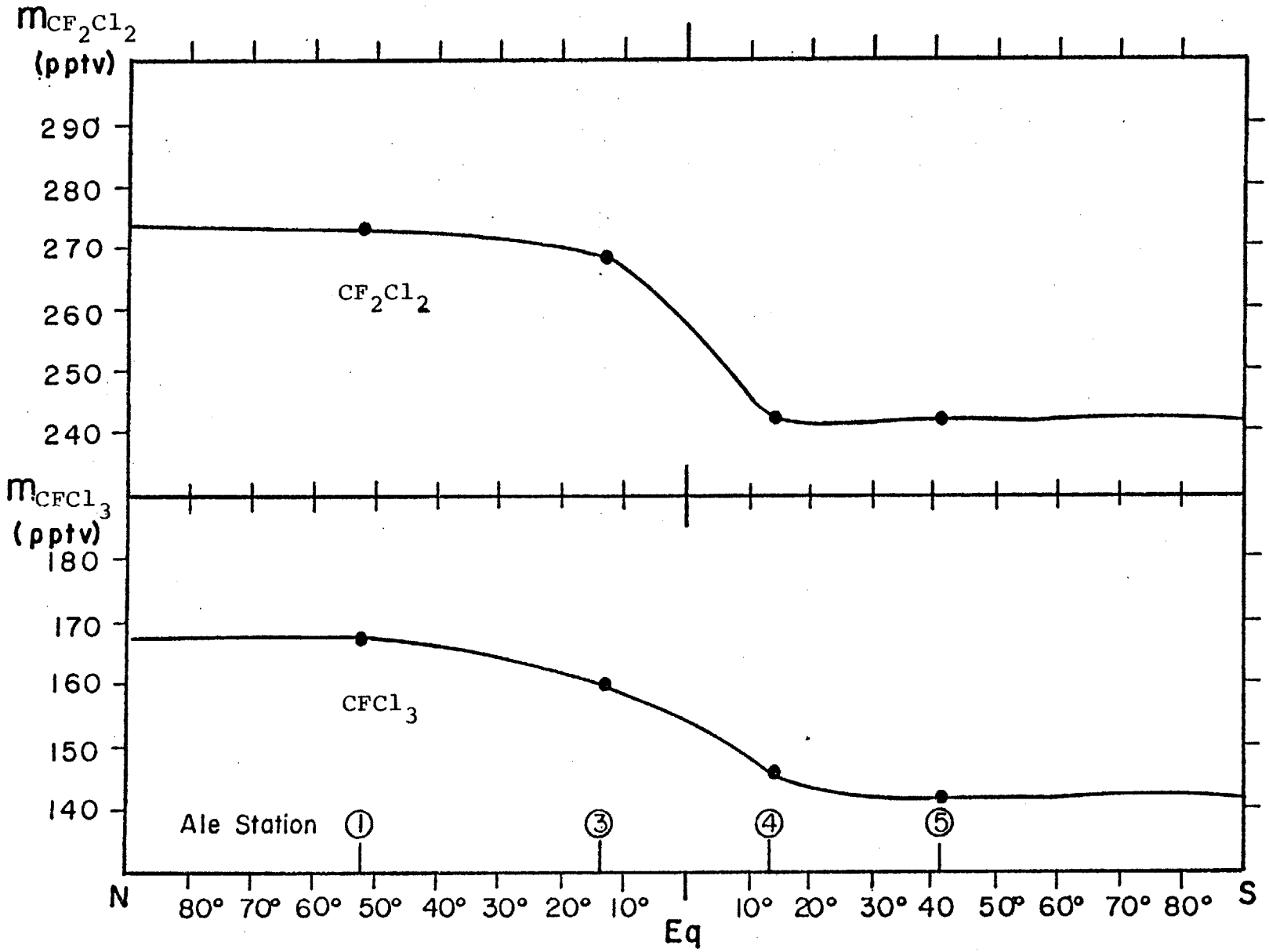


Figure 5a : Initial $CFCl_3$, CF_2Cl_2 latitudinal distribution, July 1978.

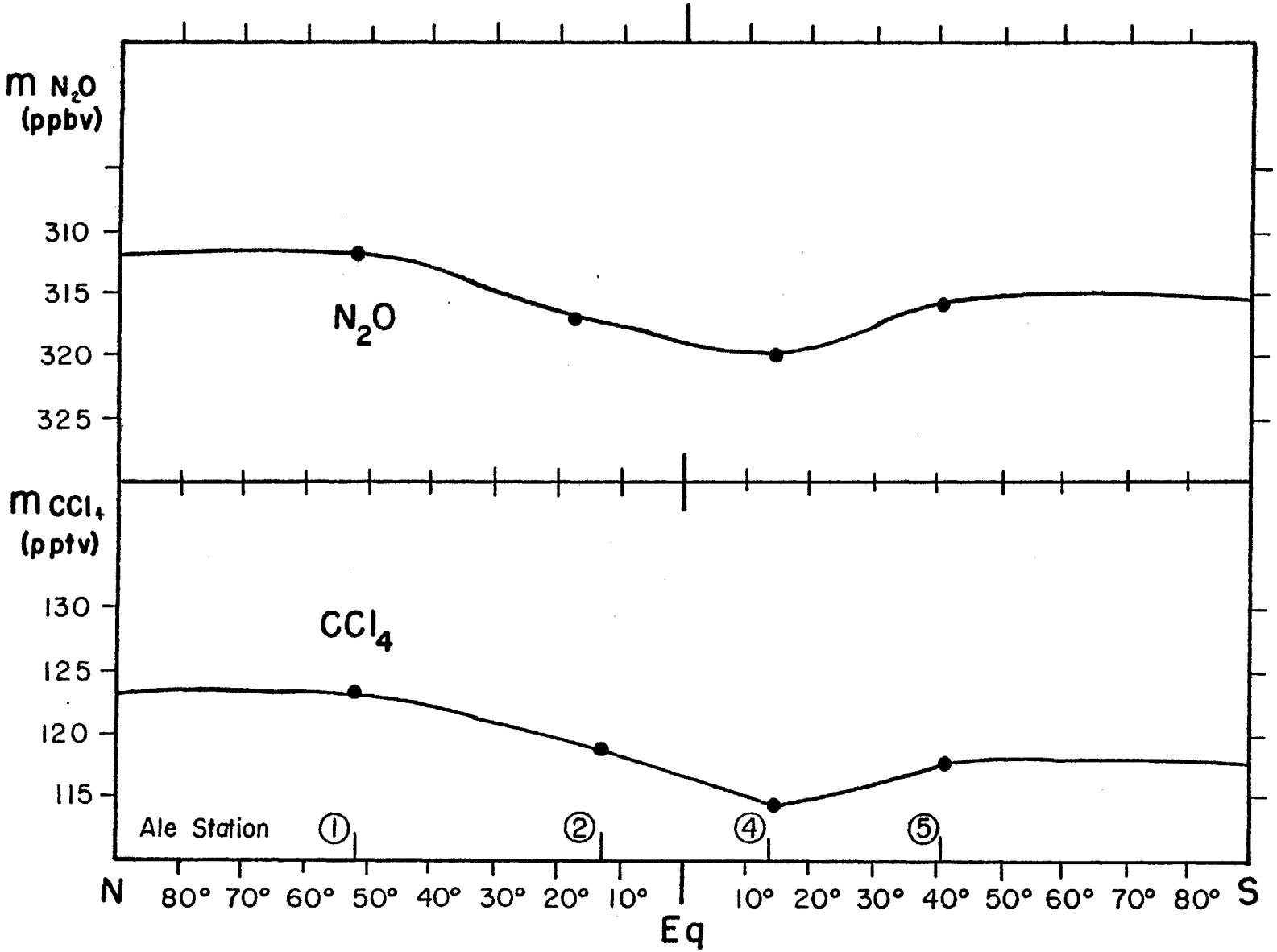


Figure 5b : Initial CCl_4 and N_2O latitudinal distribution, July 1978.

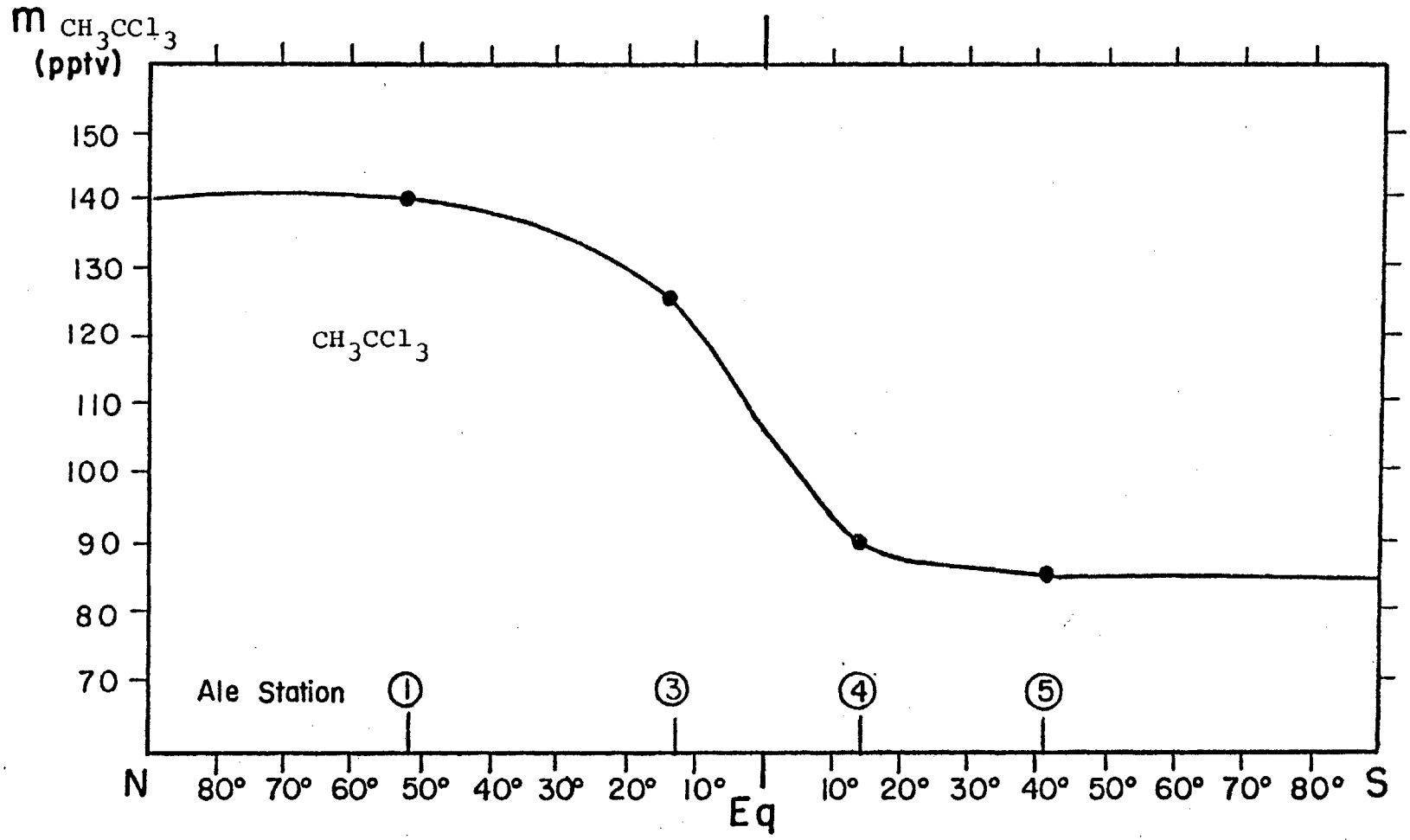


Figure 5c : Initial CH_3CCl_3 latitudinal distribution, July 1978.

(1978). These vertical profiles were taken as a basis for the definition of a dimensionless vertical distribution function which was then multiplied by the surface concentration at each latitude as given in Figures 5a, b, c. The initial vertical profiles are summarized in Table 7 and Figures 6a, b, c. This two-dimensional (latitude, altitude) initial distribution was assumed to be applicable at all longitudes. That is, we started with a distribution which was independent of longitude.

2.2.2 Anthropogenic Source

The amounts of the tracers released since 1951 until 1981 are based on CMA reports which were summarized and analyzed by Cunnold *et al.* (1982a) for $CFC\ell_3$, by Cunnold *et al.* (1982b) for $CF_2C\ell_2$, by Simmonds *et al.* (1982) for $CC\ell_4$, and by Prinn *et al.* (1982b) for $CH_3CC\ell_3$. In each of these latter ALE references the fraction of the emissions of the various tracers in each semi-hemisphere (90°N-30°N, 30°N-0°, 0°-30°S, 30°S-90°S) is also deduced and reported. The source for N_2O was taken from Levy *et al.* (1979). In this case the source was homogeneous and its value was 15×10^{12} gm per year for each year in our model runs. The global amounts of each tracer released are summarized in Table 8.

The geographic distribution of the sources on the surface of the globe is based on the aforementioned ALE references but more details were added concerning the latitudinal

Table 7 : Initial Vertical Profiles.

Level	Height (Km)	CH_3CCl_3 (pptv)	$CFCl_3$ FAB (pptv)	$CFCl_3$ CRU (pptv)	CF_2Cl_2 FAB (pptv)	CF_2Cl_2 CRU (pptv)	CCl_4 (pptv)	N_2O (ppbv)
9	48.2					0.1		18.0
10	45.0				0.1	1.3		28.3
11	41.9				1.0	4.4		47.5
12	38.8				3.1	12.0	0.1	58.5
13	35.9	0.3		0.2	8.5	27.8	0.4	98.9
14	33.0	1.2	0.3	1.0	18.7	52.2	1.2	120.2
15	30.2	4.0	1.4	4.3	36.1	84.0	4.5	141.3
16	27.5	9.2	5.7	16.9	54.9	106.6	17.0	182.2
17	24.8	18.7	18.0	42.1	70.6	135.0	37.0	194.2
18	22.2	39.1	40.8	75.4	103.5	166.9	67.7	219.2
19	19.6	55.4	76.7	109.3	151.0	196.6	87.2	250.4
20	17.1	69.1	95.3	127.7	187.1	215.7	110.1	275.8
21	14.6	79.7	120.5	137.1	214.0	229.4	111.6	283.8
22	12.0	92.7	136.8	145.5	237.6	242.2	117.7	293.8
23	9.3	102.7	151.5	152.3	253.8	254.7	117.8	302.4
24	6.4	106.4	151.4	152.2	254.6	255.0	118.6	302.9
25	3.4	108.8	153.1	153.2	256.4	256.5	118.8	303.9
26	0.1	108.8	153.1	153.2	256.4	256.5	118.8	303.9

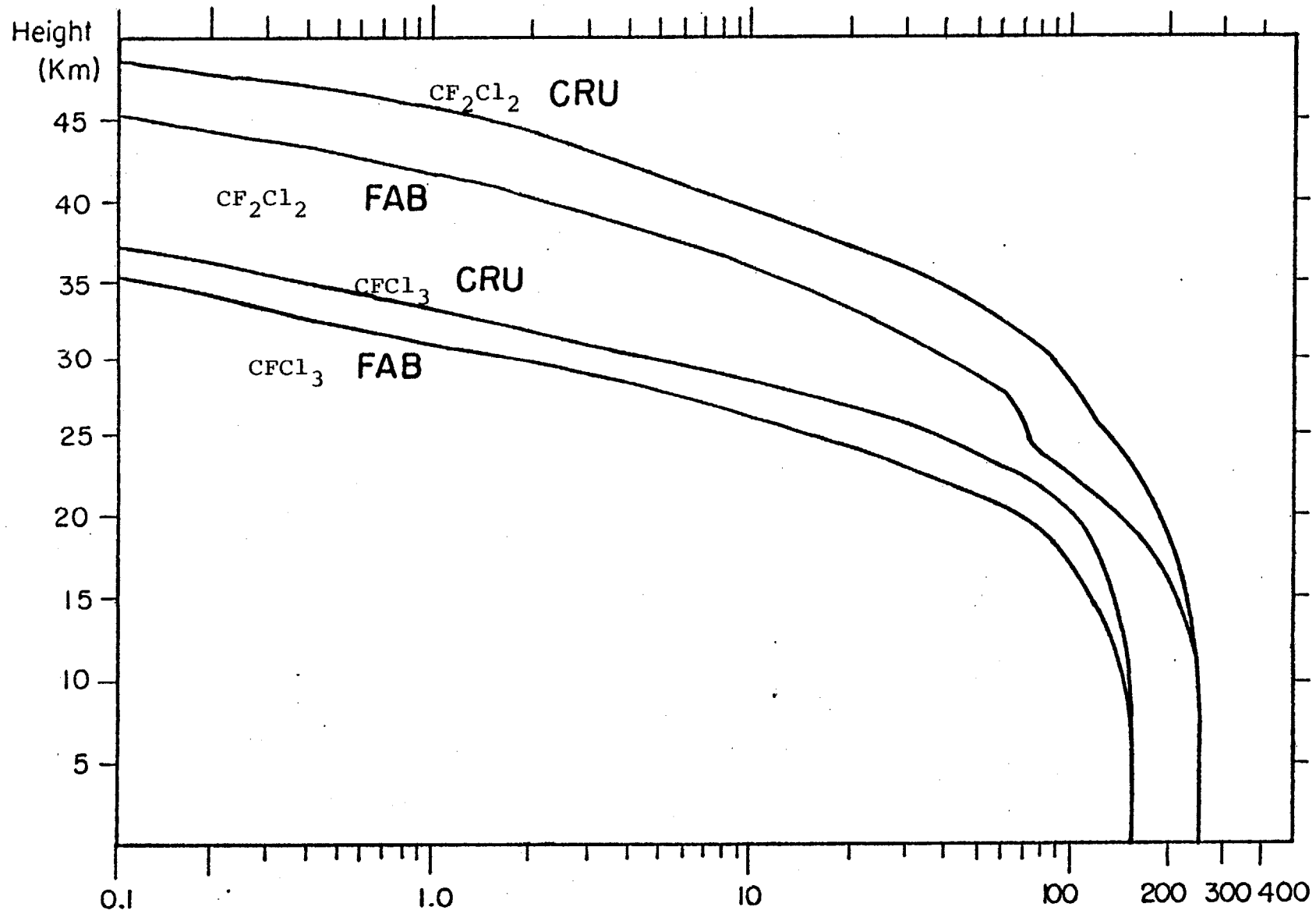


Figure 6a: $CFCl_3$, CF_2Cl_2 initial vertical profiles.

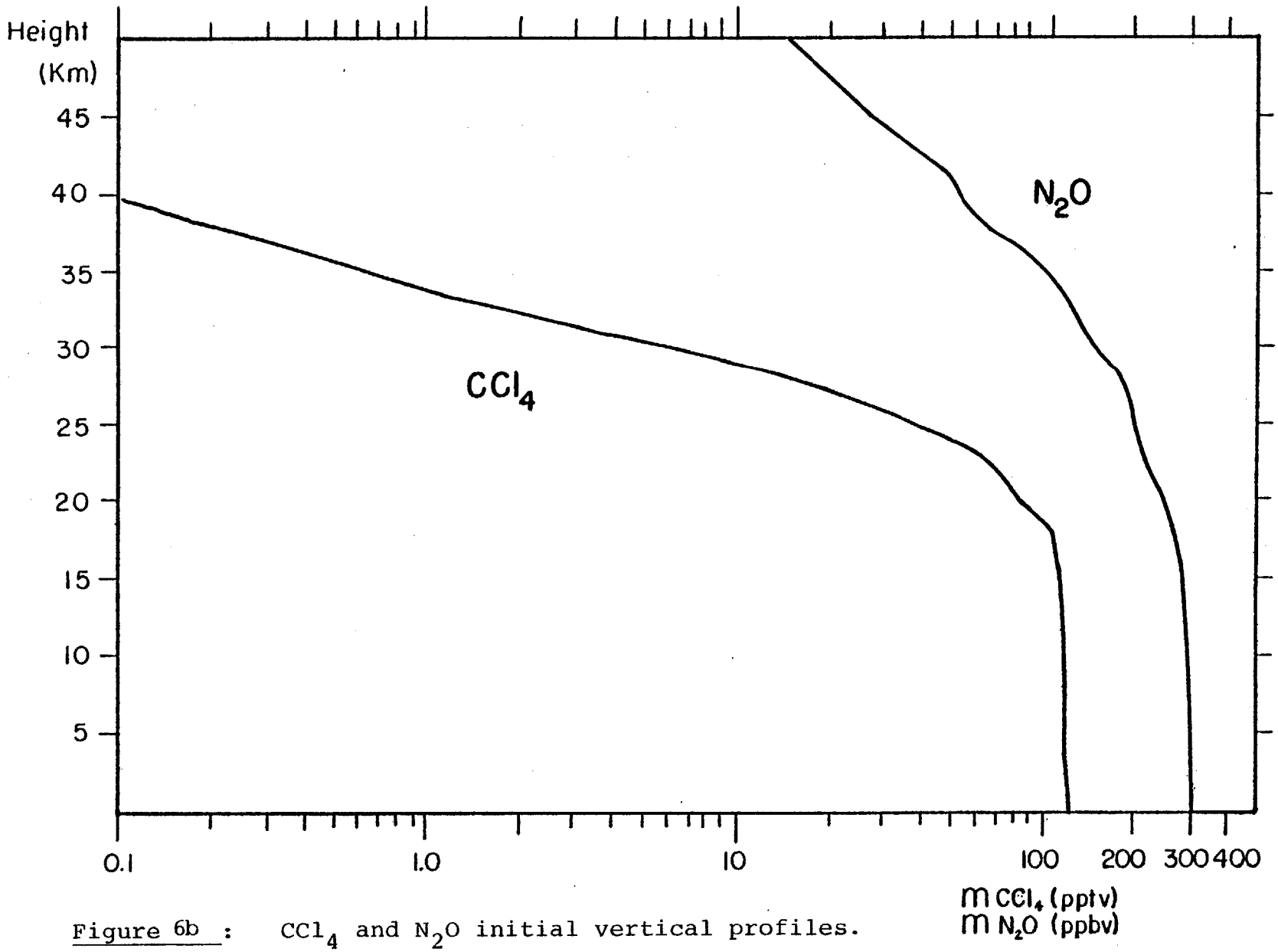


Figure 6b : CCl_4 and N_2O initial vertical profiles.

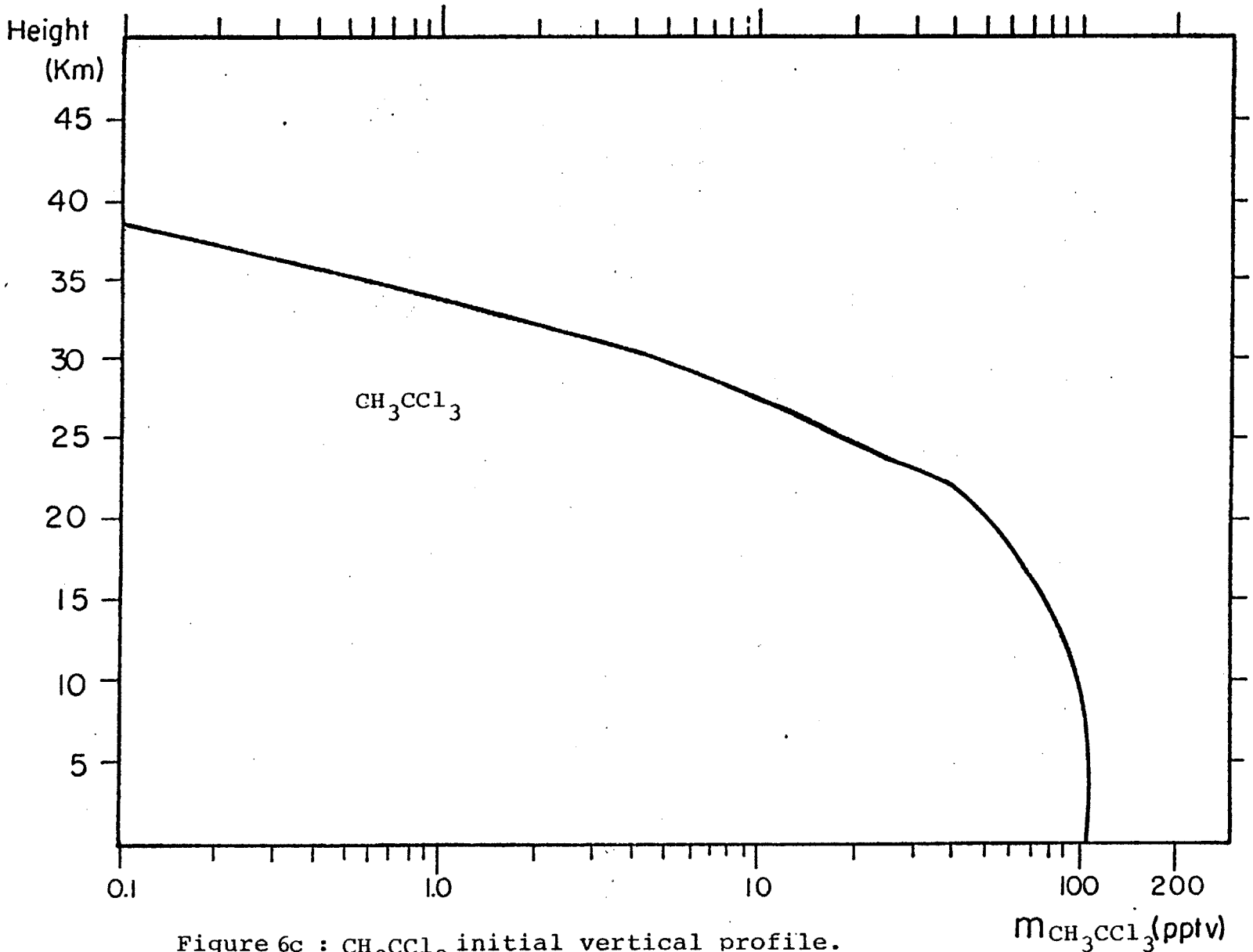


Figure 6c : CH_3CCl_3 initial vertical profile.

Table 8: CH_3CCl_3, $CFCl_3$, CF_2CCl_2, CCl_4 Releases to Atmosphere (10^9 gm per year).

Year	CH_3CCl_3 (a)	$CFCl_3$ (b)	CF_2Cl_2 (c)	CCl_4 (d)
1951	0.1	7.6	32.4	65.0
1952	0.2	11.0	33.7	46.5
1953	1.0	14.9	37.8	50.7
1954	2.7	18.5	42.8	31.2
1955	8.0	23.0	48.1	40.7
1956	12.4	28.7	56.0	30.8
1957	19.6	32.1	63.7	35.7
1958	20.7	30.2	66.9	31.4
1959	30.3	30.8	74.6	35.9
1960	36.1	40.4	88.9	39.7
1961	38.0	52.1	99.6	42.2
1962	56.2	65.2	114.2	51.7
1963	50.7	79.9	133.7	59.5
1964	56.6	94.9	155.2	68.6
1965	72.9	108.2	175.1	72.4
1966	108.7	121.1	194.6	87.1
1967	130.5	137.5	219.6	101.3
1968	145.0	157.3	250.6	107.1
1969	148.1	183.4	284.0	128.5
1970	154.5	208.8	311.9	156.3
1971	166.7	229.5	336.3	162.6
1972	230.1	258.4	367.2	96.0
1973	339.8	295.9	407.3	106.5
1974	362.4	326.9	443.3	119.8
1975	364.2	318.7	435.5	100.1
1976	415.4	310.4	423.1	107.3
1977	449.3	314.2	411.3	103.4
1978	483.0	**300.3 (299.1)	**390.6 (386.5)	99.2
1979	512.2	**283.0 (281.2)	**391.0 (390.6)	93.0
1980	507.5	**270.8 (269.9)	**398.2 (394.0)	97.2
1981	*502.1 (509.4)	*270.8	*398.2	* 97.2

References: (a)-Prinn et al. (1982b) (b)-Cunnold et al. (1982a)
(c)-Cunnold et al. (1982b) (d)-Simmonds et al.(1982)

* - Estimated values. For CH_3CCl_3 our estimate differs from the more recent estimate by Prinn et al. (1982b), noted in paretheses.

** - $CFCl_3$ and CF_2Cl_2 releases are based on CMA report of December 1981 and are slightly different from the updated values given in CMA report of February 1982, shown in parentheses (less than 1.1% difference).

variation.

The percentages emitted in each of the surface grid points were determined considering the following factors:

(i) The existence of at least 60% land cover in the area represented by each grid point.

(ii) The existence of a populated industrialized country in the area represented by each grid point, which according to CMA reports produced, imported or used the various chemical compounds studied in this thesis.

The latitudinal semihemispheric distribution of sources as computed and reported in the ALE references, was always maintained.

The amount released daily in a certain year was calculated using a smoothed function of the yearly amount released during the previous year and the following year. Let us define the daily amount released during day j of year i as I_{ij}, where I_{ij} is the linear function

$$I_{ij} = A_i + jB_j \qquad j=1,360$$

we would like to find A_i and B_i, imposing the following conditions:

(i) The amount released durind the first day (j=1) of the year i will be defined as C_1

$$C_1 = \frac{1}{2}(M_{i-1} + M_i)\frac{1}{360}$$

where M_i is the amount released during year i.

(ii) The amount released during the last day (j=360) of year i will be defined as C_{360},

$$C_{360} = \frac{1}{2}(M_i + M_{i+1})\frac{1}{360}$$

from the linear function we have also the relations $C_1 = A_i' + B_i'$; $C_{360} = A_i' + 360B_i'$ where A_i' and B_i' will presently be defined. Solving for A_i' and B_i' we get,

$$A_i' = \frac{1}{359} (360C_1 - C_{360})$$

$$B_i' = \frac{1}{359} (C_{360} - C_1)$$

A_i' and B_i' should be normalized for each year i, so that the total amount released durind year i,

$$M_i' = \sum_j A_i' + jB_i'$$

will be equal to the amount M_i as reported by the CMA. Let us define the weighting factor W as

$$WM_i' = M_i \qquad \text{or} \qquad W = \frac{M_i}{M_i'}$$

so that finally we get,

$$A_i = WA_i' \quad ; \quad B_i = WB_i' \quad .$$

The values used for the surface distribution of the sources of the five tracers, are summarized in Tables 9a and 9b, where percentages of the global total emitted in each of the 240 surface grid points are shown. The model calculates for each tracer, the amount of the daily anthropogenic input at each of the surface grid points based upon the the data shown in Tables 8-9: Nitrous oxide source was assumed to be homogeneous over continents and oceans, and was evenly divided among all surface grid points between 57.5°N and 57.5°S. The mass of tracer added daily in each of the surface grid points, was translated into a mixing ratio increase by assuming that this tracer mass was added to the total atmospheric mass in a "box" whose base is the area represented by each grid point on the surface, which is bounded below

Table 9a: Anthropogenic Surface Source Distribution for $CFCl_3$, CCl_4, and CF_2Cl_2. Percentages*100 at each surface grid point for the years 1978-1981. ($CFCl_3$ and CCl_4 upper values, CF_2Cl_2 lower values)

NLONG	1	2	3	4	5	6	7	8	9	10	11	12	13	14	15	16
NLAT																
1																
2																
3	755 762	755 762														
4	755 762	755 762										872 878	872 878	872 878		
5							370 370					872 878	872 878			
6		178 152	178 152		178 152	178 152										
7	178 152	178 152	178 152			178 152								178 152		
8															120 150	
9															120 150	
10															120 150	
11		40 40		43 55		43 55	43 55		43 55							
12								43 55						43 55		
13																
14																
15																

Table 9b: Anthropogenic Surface Source Distribution for CH_3CCl_3. Percentages*100 at each surface grid point. (upper values are for 1978-1979, lower values are for 1980-1981).

NLONG	1	2	3	4	5	6	7	8	9	10	11	12	13	14	15	16
NLAT																
1																
2																
3	909 906	909 906										1100 1094	1100 1094	1100 1094		
4	909 906	909 906										1100 1094	1100 1094			
5							500 500									
6		16 18	16 18		16 18	16 18										
7	16 18	16 18	16 18			16 18								16 18		
8															19 20	
9															19 20	
10															19 20	
11		37 42		22 23		22 23	22 23		22 23							
12								22 23								
13														22 23		
14																
15																

by the surface and above by the pressue level halfway between levels 25 and 24 (approximately 4.9km). The area represented by each grid point (in a fixed latitude) is given in Table 10, the area s was calculated using

$$ds = 2\pi r dy \quad , \quad r = a\cos\phi \quad , \quad dy = rd\phi$$

$$ds = 2\pi a^2 \cos\phi d\phi \quad .$$

The area of a belt Δs, on the Earth's surface between latitudes ϕ_1 and ϕ_2 is

$$\Delta s = 2\pi a^2 \int_{\phi_1}^{\phi_2} \cos\phi d\phi = 2\pi a^2 (\sin\phi_1 - \sin\phi_2)$$

and the area s of each grid point is that belt, is $\frac{1}{16}\Delta s$. The mass of air included in each grid point box is calculated by using

$$dw' = \rho dz \quad , \quad p = \rho RT \quad , \quad \frac{\partial p}{\partial z} = -\rho g$$

where dw' is the mass per unit area and ρ is the density of dry air. Hence,

$$dw = -\frac{1}{g} dp$$

Table 10: Area (s) and Mass (w) of each Grid Point.

NLAT	Latitude	ϕ_1	ϕ_2	$\sin\phi_1$	$\sin\phi_2$	s (10^{16} cm^2)	w (10^{18} gm)
1	80.5°N	90°N	74.75°N	1.0	0.9625	0.5977	2.7076
2	69 °N	74.75°N	63.25°N	0.9625	0.893	1.1078	5.0183
3	57.5°N	63.25°N	51.75°N	0.893	0.7853	1.717	7.778
4	46 °N	51.75°N	40.25°N	0.7853	0.6461	2.219	10.052
5	34.5°N	40.25°N	28.75°N	0.6461	0.481	2.632	11.923
6	23 °N	28.75°N	17.25°N	0.481	0.2965	2.941	13.323
7	11.5°N	17.25°N	5.75°N	0.2965	0.1002	3.129	14.174
8	0°	5.75°N	5.75°S	0.1002	-0.1002	3.194	14.469
9	11.5°S	5.75°S	17.25°S	-0.1002	-0.2965	3.129	14.174
10	23 °S	17.25°S	28.75°S	-0.2965	-0.481	2.941	13.323
11	34.5°S	28.75°S	40.25°S	-0.481	-0.6461	2.632	11.923
12	46 °S	40.25°S	51.75°S	-0.6461	-0.7853	2.219	10.052
13	57.5°S	51.75°S	63.25°S	-0.7853	-0.893	1.717	7.778
14	69 °S	63.25°S	74.75°S	-0.893	-0.9625	1.1078	5.0183
15	80.5°S	74.75°S	90°S	-0.9625	-1.0	0.5977	2.7076

and $$w = -\frac{1}{g}\int_{p_2}^{p_1} dp = \frac{1}{g}(p_1 - p_2)$$

Here w denotes the mass of the atmospheric slice per unit area between pressure levels p_1 and p_2 . For our specific slice p_1 = Psurface = 1000mb, and $p_2 = 0.5(p_{24} + p_{25}) = 555.5$mb and the numerical value for w is therefore w = 453 gm per 1 cm^2. The masses w = sw' represented by each grid point box are also shown in Table 10.

As mentioned earlier, the added mass at each grid point is converted to the increase in tracer mass mixing ratio by dividing the tracer mass added by the mass of air associated with each grid point. This increase in mass mixing ratio is then multiplied by the ratio of the molecular weights of air and tracer, thus converting mass-mixing ratio to volume mixing ratio. In each time step the appropriate volume mixing ratio increase for each surface grid point (which depends on the length of each time step), is added to the tracer volume-mixing ratio incremental net increase caused by all other processes (advection, diffusion, chemical and photochemical reactions), after converting the values from grid to spectral representation.

2.2.3 Photochemical Dissociation

Each tracer considered absorbs uv radiation in stratospheric levels and is dissociated according to the following reactions,

$$CFC\ell_3 + h\nu \xrightarrow{J_{CFC\ell_3}} CFC\ell_2 + C\ell$$

$$CF_2C\ell_2 + h\nu \xrightarrow{J_{CF_2C\ell_2}} CF_2C\ell + C\ell$$

$$CC\ell_4 + h\nu \xrightarrow{J_{CC\ell_4}} CC\ell_3 + C\ell$$

$$N_2O + h\nu \xrightarrow{J_{N_2O}} N_2 + O(^1D)$$

$$CH_3CC\ell_3 + h\nu \xrightarrow{J_{CH_3CC\ell_3}} CH_3CC\ell_2 + C\ell$$

where $J_{tracer} = \int \alpha(\Lambda) I(\Lambda) \exp\{-(\sum_{tracers} \xi_{tracer}) - \xi_{O_2} - \xi_{O_3}\} d\Lambda$

$$\xi_i^n = \frac{\alpha_i(\Lambda) N_i}{\cos\varphi}$$

where n is wavelength or frequency, I is solar intensity, α_i and N_i are respectively the absorption cross-section and column abundance of species i, and φ is the angle between the sun's rays and the local vertical. Since the contribution of $\sum_{tracers} \xi_{tracer}$ in the exponent is very low, it is neglected. The integral J_{tracer} is calculated numerically using

$$J_{tracer} = \sum_j \alpha(\Lambda_j) I(\Lambda_j) \exp(-\xi_{O_2} - \xi_{O_3}) \qquad (sec^{-1})$$

where here $I(\Lambda_j)$ is the solar flux at a specific wavelength (Λ_j) as tabulated by Ackerman (1971). Values for the absorption cross-sections $\alpha(\Lambda_j)$ for $CFC\ell_3$, $CF_2C\ell_2$, $CC\ell_4$,

N_2O and $CH_3CC\ell_3$ were taken from WMO(1981), NASA(1979), Vanlaethem *et al.* (1979). Wherever available, the temperature dependence of $\alpha(\Lambda_j)$ was included in the model calculations. For $CH_3CC\ell_3$, values for the absorption cross-sections as published by Vanlaethem *et al.* (1979), which are somewhat lower than those in NASA (1979), were used in calculating the photodissociation integral $J_{CH_3CC\ell_3}$. All the $\alpha(\Lambda_j)$ cross-section values used in our model calculations, are given in Tables 11a, b, c. In the model calculation a daily average value for the photodissociation integral J_{tracer} is utilized. The day by day variation of the solar zenith angle throughout the year is included in the model calculations. Sample calculations as done by the model are given in Tables 12a, b. These calculations are for J values of $CH_3CC\ell_3$, $CFC\ell_3$, $CF_2C\ell_2$, $CC\ell_4$ and N_2O (horizontally averaged for January 1st) as a function of height. Beside these values, the photochemical lifetimes of the various tracers are also shown, in each vertical level of the model.

The laboratory O_2 absorption cross-sections which we (and all other recent workers) are using have been placed in doubt for the wavelength region 200-210 nm (the Herzberg continuum) by recent measurements in the real atmosphere (Frederick and Mentall, 1982). Therefore, we will also present calculations using suitably modified O_2 cross-sections to demonstrate the effect of the uncertainty in O_2 cross-sections on our reported results.

Table 11a: $CFCl_3$ and CF_2Cl_2 Absorption Cross Sections (NASA, 1979).

Λ (nm)	α $CFCl_3$ ($10^{-20}cm^2$)				α CF_2Cl_2 ($10^{-20}cm^2$)
	213°K	232°K	252°K	298°K	296°K
186.0	-	-	-	243.0	106.0
187.8	-	-	-	217.0	85.4
189.6	-	-	-	186.0	64.6
191.4	161.0	161.0	164.0	159.0	48.7
193.2	137.0	137.0	141.0	133.0	35.3
195.1	110.0	110.0	114.0	111.0	24.5
197.0	88.5	88.5	91.3	90.3	16.6
199.0	69.1	69.1	72.1	73.0	10.8
201.0	53.1	54.3	56.6	57.3	6.87
203.0	40.2	41.1	43.0	45.2	4.36
205.1	28.6	30.0	31.7	33.3	2.59
207.3	19.8	21.1	22.6	23.9	1.50
209.4	13.3	14.2	15.2	16.8	0.89
211.6	8.5	9.1	9.9	11.5	0.51
213.9		5.7	6.4	7.6	0.29
216.2		3.4	3.9	5.0	0.17
218.6		2.0	2.3	3.1	0.095
221.0				2.0	0.05
223.5				1.2	0.05
226.0				0.8	0.05

CF_2Cl_2 - Temperature dependence formula (NASA, 1979)

$$\alpha_T = \alpha_{296} \exp[3.6E\text{-}4(\Lambda - 184.9)(T - 296)]$$

α_{296} is the F12 cross section at 296°K

Λ in nm, T in °K.

Table 11b: CCl_4 and N_2O Absorption Cross Sections, (WMO 1981).

Λ (nm)	α_{CCl_4} ($10^{-20}cm^2$)	Λ (nm)	α_{CCl_4} ($10^{-20}cm^2$)
174	995	208	52.8
176	1007	210	47.3
178	976	212	39.6
180	772	214	33.4
182	589	216	27.6
184	450	218	22.1
186	318	220	17.0
188	218	222	12.8
190	142	224	9.5
192	98.9	226	7.1
194	73.3	228	5.6
196	67.6	230	4.11
198	65.1	232	3.05
200	64.1	234	2.24
202	61.4	236	1.52
204	60.1	238	1.25
206	56.5		

N_2O Absorption Cross Section Function:

$$\ln\alpha_{N_2O}(\Lambda,T) = A_1 + A_2\Lambda + A_3\Lambda^2 + A_4\Lambda^3 + A_5\Lambda^4 + (T - 300)\exp(B_1 + B_2\Lambda + B_3\Lambda^2 + B_4\Lambda^3)$$

$T(^oK)$ Λ(nm) range: Λ(173-240)nm, T(194-302)^oK

$A_1 = 68.21023$ $A_2 = -4.071805$ $A_3 = 4.301146E\text{-}2$

$A_4 = -1.77784E\text{-}4$ $A_5 = 2.520672E\text{-}7$ $B_1 = 123.4014$

$B_2 = -2.116255$ $B_3 = 1.111572E\text{-}2$ $B_4 = -1.881085E\text{-}5$

Table 11c: CH_3CCl_3 Absorption Cross Sections.

Λ (nm)	α (10^{-20} cm^2)					
	NASA(1979)	Vanlaethem et al. (1979)				
		295°K	270°K	250°K	230°K	210°K
182.6	-	305.0	-	-	-	-
184.3	-	278.0	-	-	-	-
186.0	325.0	250.0	-	-	-	-
187.8	284.0	225.0	-	-	-	-
189.6	246.0	200.0	-	-	-	-
191.4	215.0	175.0	-	-	-	-
193.2	189.0	152.0	-	-	-	-
195.1	168.0	129.0	-	-	-	-
197.0	148.0	108.0	-	-	-	-
199.0	128.0	88.0	-	-	-	-
201.0	111.0	72.5	-	-	-	-
203.0	95.4	59.0	-	-	-	-
205.1	80.5	46.0	-	-	-	-
207.3	63.9	35.5	35.5	35.5	35.5	35.5
209.4	51.1	25.8	25.8	25.8	25.7	25.1
211.6	39.4	19.0	18.7	18.4	17.9	17.4
213.9	28.1	12.8	12.3	11.9	11.4	10.9
216.2	19.6	8.40	7.81	7.48	7.06	6.68
218.6	12.5	5.40	4.86	4.56	4.27	3.97
221.0	8.3	3.58	3.11	2.86	2.63	2.42
223.5	5.1	2.33	1.96	1.77	1.58	1.42
226.0	2.9	1.48	1.20	1.05	0.918	0.814
228.6		0.900	0.702	0.594	0.504	0.432
231.2		0.560	0.420	0.344	0.286	0.230
233.9		0.330	0.238	0.186	0.148	0.114
236.7		0.196	0.133	0.102	0.075	0.053
239.5		0.115	0.075	0.048	0.037	0.023

Table 12a: Photodissociation Rates (J) and Photochemical Lifetimes (τ). Horizontally-averaged, January 1 values, as a function of height, as calculated by the model are given for CH_3CCl_3, $CFCl_3$, and CF_2Cl_2.

Level	Height (Km)	$J_{CH_3CCl_3}$ (s^{-1})	$\tau_{CH_3CCl_3}$	J_{CFCl_3} (s^{-1})	τ_{CFCl_3}	$J_{CF_2Cl_2}$ (s^{-1})	$\tau_{CF_2Cl_2}$
2	69.0	2.00E-5	13.9 h	1.33E-5	20.9 h	2.08E-6	5.6 d
3	66.3	1.96E-5	14.2 h	1.31E-5	21.2 h	1.98E-6	5.9 d
4	63.5	1.91E-5	14.5 h	1.27E-5	21.9 h	1.86E-6	6.2 d
5	60.6	1.85E-5	15.0 h	1.23E-5	22.6 h	1.73E-6	6.7 d
6	57.6	1.77E-5	15.7 h	1.18E-5	23.5 h	1.58E-6	7.3 d
7	54.5	1.67E-5	16.6 h	1.12E-5	24.8 h	1.43E-6	8.1 d
8	51.4	1.55E-5	17.9 h	1.04E-5	26.7 h	1.28E-6	9.0 d
9	48.2	1.39E-5	20.0 h	9.24E-6	30.1 h	1.10E-6	10.5 d
10	45.0	1.16E-5	24.0 h	7.67E-6	36.2 h	8.62E-7	13.4 d
11	41.9	8.95E-6	31.0 h	5.89E-6	47.2 h	6.21E-7	18.6 d
12	38.8	6.19E-6	44.9 h	4.05E-6	2.9 d	3.98E-7	29.1 d
13	35.9	3.79E-6	3.1 d	2.48E-6	4.7 d	2.30E-7	1.7 m
14	33.0	2.03E-6	5.7 d	1.33E-6	8.7 d	1.17E-7	3.3 m
15	30.2	9.41E-7	12.3 d	6.09E-7	19.0 d	5.13E-8	7.5 m
16	27.5	3.66E-7	31.6 d	2.32E-7	1.7 m	1.88E-8	1.7 y
17	24.8	1.19E-7	3.2 m	7.47E-8	5.2 m	6.21E-9	5.2 y
18	22.2	3.31E-8	11.7 m	2.04E-8	1.6 y	1.77E-9	18.2 y
19	19.6	7.98E-9	4.0 y	4.82E-9	6.7 y	4.64E-10	69.3 y
20	17.1	1.45E-9	22.2 y	8.51E-10	37.8 y	1.05E-10	306 y
21	14.6	1.94E-10	166 y	1.09E-10	295 y	3.81E-11	844 y
22	12.0	2.31E-11	1392 y	1.33E-11	2417 y	9.53E-12	3374 y

h - hours d - days m - months y - years

Table 12b: As for Table 12a but for CCl_4 and N_2O.

Level	Height (Km)	J_{CCl_4} (s^{-1})	τ_{CCl_4}	J_{N_2O} (s^{-1})	τ_{N_2O}
2	69.0	3.64E-5	7.6 h	6.80E-7	17.0 d
3	66.3	3.54E-5	7.8 h	6.64E-7	17.4 d
4	63.5	3.45E-5	8.1 h	6.46E-7	17.9 d
5	60.6	3.34E-5	8.3 h	6.30E-7	18.4 d
6	57.6	3.22E-5	8.6 h	6.08E-7	19.0 d
7	54.5	3.06E-5	9.1 h	5.87E-7	19.7 d
8	51.4	2.85E-5	9.7 h	5.57E-7	20.8 d
9	48.2	2.54E-5	10.9 h	5.02E-7	23.1 d
10	45.0	2.10E-5	13.2 h	4.14E-7	27.9 d
11	41.9	1.57E-5	17.7 h	3.13E-7	1.2 m
12	38.8	1.04E-5	26.7 h	2.11E-7	1.8 m
13	35.9	6.01E-6	46.2 h	1.27E-7	3.0 m
14	33.0	3.06E-6	3.8 d	6.67E-8	5.8 m
15	30.2	1.35E-6	8.6 d	3.04E-8	1.1 y
16	27.5	5.09E-7	22.7 d	1.15E-8	2.8 y
17	24.8	1.61E-7	2.4 m	3.80E-9	8.5 y
18	22.2	4.49E-8	8.6 m	1.07E-9	30.0 y
19	19.6	1.11E-8	2.9 y	2.72E-10	118 y
20	17.1	2.07E-9	15.5 y	5.60E-11	574 y
21	14.6	2.55E-10	126 y	1.53E-11	2101 y
22	12.0	2.36E-11	1362 y	3.50E-12	9186 y

h - hours d - days m - months y - years

2.2.4 Reaction of $CH_3CC\ell_3$ with OH radicals

The second order reaction rate constant k_{OH} for the reaction

$$CH_3CC\ell_3 + OH \xrightarrow{k_{OH}} CH_2CC\ell_3 + H_2O$$

is expressed in form

$$k_{OH} = A\exp(-\frac{B}{T}) \qquad (cm^3\ molecule^{-1}\ sec^{-1})$$

Some experimental data for A, B and k_{OH} at $\sim$25°C, are listed in Table 13. The value used in the model calculation for $CH_3CC\ell_3$ is the one recommended by NASA (1979). The other less recent values are apparently too high, probably due to impurities in the methylchloroform used in the experiments. The stratospheric OH free radical distribution for the model calculation with $CH_3CC\ell_3$, was taken from run 34 of the MIT/GIT dynamical-chemical model which is in turn based on a two-dimensional model (Prinn *et al.*, 1975). This two-dimensional OH distribution applies only for the stratosphere (model vertical levels 1 through 22) and is summarized in Table 14. For initialization purposes of the $CH_3CC\ell_3$ run, altitude, latitude, and time dependent values for the OH free radical number density in the troposphere were assumed as discussed in more detail in Chapter 3.

Table 13 : Experimental Values for k_{OH}.

$$k_{OH} = A \exp\left(-\frac{B}{T}\right)$$

A	B	k_{OH} (cm^3 $molecule^{-1}$ s^{-1})		
		296°K	298°K	Reference
(5.49±1.40)E-12	1832±98	1.12E-14	1.17E-14	a
(5.41±1.84)E-12	1831±95	1.18E-14	1.23E-14	b
-	-	1.50E-14	-	c
3.7E-12	1627	1.52E-14	1.59E-14	d
1.95E-12	1331	2.17E-14	2.24E-14	e
2.40E-12	1394	2.16E-14	2.23E-14	f
5.40E-12	1820	1.15E-14	1.20E-14	g

References:
a - Jeong and Kaufman (1979)
b - Kurylu et al. (1979)
c - Howard and Evenson (1977)
d - Watson et al. (1977)
e - Chang and Kaufman (1977)
f - Clyne and Holt (1979)
g - NASA(1979) recommended value based on a and b.

Table 14: MIT/GIT Model Stratospheric OH Free Radical Concentrations, December 30 daily-averaged values (10^4 mol cm^{-3}). (June 30 values are a mirror image of December 30 values, across the equator).

NLAT	1	2	3	4	5	6	7	8	9	10	11	12	13	14	15
LEVEL															
1	0	0	47	78	100	120	140	160	170	180	180	170	170	210	190
2	0	0	59	95	120	140	160	180	200	200	200	200	210	250	230
3	0	0	74	120	140	160	190	210	230	230	240	240	250	310	280
4	0	0	94	140	170	190	220	250	270	270	270	290	310	380	340
5	0	0	120	190	220	240	280	310	330	330	340	360	400	490	440
6	0	0	170	260	300	330	380	420	440	440	450	490	550	690	620
7	0	0	250	380	440	470	530	600	630	630	650	710	800	1000	900
8	0	0	340	510	570	600	660	740	780	790	810	880	980	1200	1100
9	0	0	360	570	670	730	820	900	960	970	1000	1100	1200	1500	1300
10	0	0	370	620	780	1300	1000	1100	1200	1200	1300	1300	1500	1800	1500
11	0	0	350	640	840	1000	1100	1200	1300	1300	1400	1400	1400	1700	1500
12	0	0	260	490	680	840	980	1100	1200	1200	1200	1200	1200	1500	1300
13	0	0	230	420	570	710	820	920	980	1000	990	1000	1100	1300	1300
14	0	0	210	390	520	610	670	720	750	780	810	840	910	1200	1100
15	0	0	170	330	440	500	520	530	550	590	630	670	730	950	920
16	0	0	120	220	290	340	370	390	410	430	460	500	560	750	740
17	0	0	76	140	190	240	270	300	300	300	320	360	420	550	530
18	0	0	46	92	150	210	250	260	250	250	260	290	330	410	370
19	0	0	18	71	170	260	280	240	210	210	250	280	290	330	280
20	0	0	6	88	230	290	240	160	140	210	280	280	250	290	310
21	0	0	6	89	210	260	200	110	120	210	280	270	220	240	280
22	0	0	2	61	160	210	180	120	110	170	220	220	190	200	210

2.2.5 Reactions with $O(^1D)$

The rate constants for the reaction of each tracer with $O(^1D)$ are summarized in Table 15. As discussed in section 2.1.1, the $O(^1D)$ concentrations are specifically computed in the model using the computed rates of $O(^1D)$ generation by photo-dissociation of O_3 and $O(^1D)$ destruction by collisional quenching. Rate constants for collisional quenching are also summarized in Table 15. In Figure 7 we show typical $O(^1D)$ densities computed in the model and also for comparison purposes the $O(^1D)$ densities computed by Crutzen *et al.* (1978). When compared to tracer destruction by photodissociation the reaction with $O(^1\mathbf{D})$ was found to be small ($\leq$ 2% for $CFC\ell_3$ and $\leq$ 12% for $CF_2C\ell_2$).

2.2.6 Oceanic Sink

The role of the ocean as a possible sink or source for N_2O, $CC\ell_4$ and $CFC\ell_3$ was discussed by Liss and Slater (1974). For $CFC\ell_3$, $CF_2C\ell_2$ and $CC\ell_4$ it was discussed by Singh (1979) and for $CH_3CC\ell_3$ it was considered by Neely and Plonka (1978). Following Liss and Slater (1974), we calculate the flux of any tracer from the atmosphere to the ocean using,

$$\text{Flux} = k_{ex}\Delta c$$

where k_{ex} is the exchange constant (cm hour^{-1}) which is a measure of the flux per unit concentration gradient and

Table 15 : Reaction Rate Constants of $O(^1D)$.

Reaction	Rate Constant ($cm^3\ mol.^{-1}\ s^{-1}$)	Reference
$O(^1D) + M \xrightarrow{k_1} O + M$	$k_1 = 3.2E\text{-}11$	1
$O(^1D) + H_2O \xrightarrow{k_2} 2OH$	$k_2 = 2.3E\text{-}10$	1
$O(^1D) + CH_3CCl_3 \xrightarrow{k_3} CH_2CCl_3 + OH$	$k_3 = 4.0E\text{-}10$	2
$O(^1D) + CFCl_3 \xrightarrow{k_4} CFCl_2 + ClO$	$k_4 = 2.2E\text{-}10$	2
$O(^1D) + CF_2Cl_2 \xrightarrow{k_5} CF_2Cl + ClO$	$k_5 = 1.4E\text{-}10$	2
$O(^1D) + CCl_4 \xrightarrow{k_6}$ Products	$k_6 = 3.5E\text{-}10$	2
$O(^1D) + N_2O \xrightarrow{k_7} N_2 + O_2$	$k_7 = 4.4E\text{-}11$	2
$O(^1D) + N_2O \xrightarrow{k_8} 2NO$	$k_8 = 7.2E\text{-}11$	2

References: (1) Chameides and Tan (1981).
(2) WMO (1981).

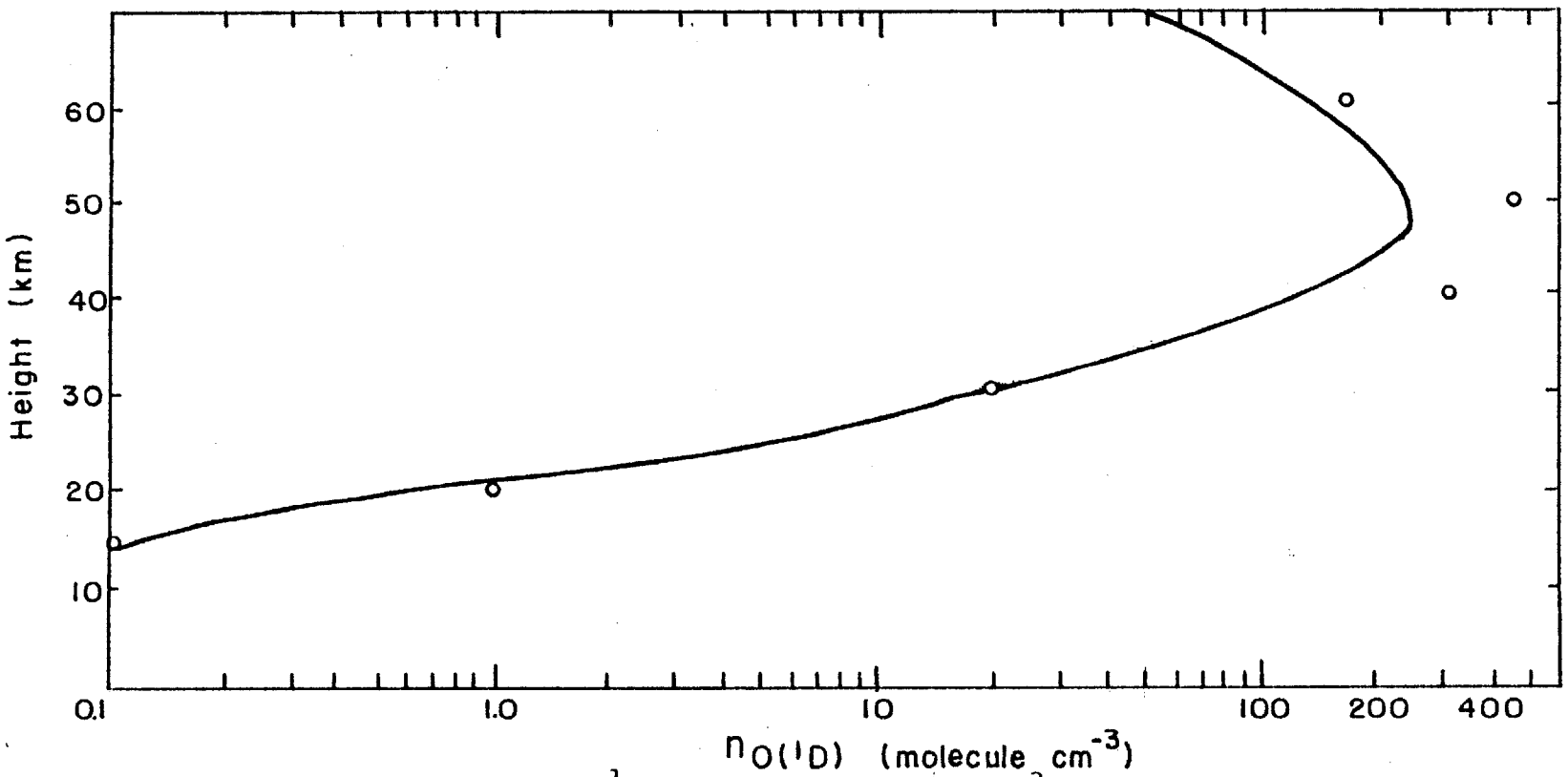


Figure 7: Horizontally averaged $O(^1D)$ number density (mol cm^{-3}) as calculated by the model for January 16, solid line, and as given by Crutzen el al. (1978), open circles.

Δc is the concentration difference between the atmosphere and the ocean. The quantity k_{ex}^{-1} is the "resistance" to the transfer and is composed of the resistance to the transfer through the gas phase boundary layer and the resistance to the transfer through the liquid phase boundary layer, where both boundary layers are in contact with one another at the interface between ocean and atmosphere. We thus have the relation,

$$\frac{1}{k_{ex}} = \frac{1}{k_\ell} + \frac{1}{Hk_g}$$

where k_ℓ is the exchange constant in the liquid phase part of the exchange boundary layer (and k_ℓ^{-1} is the transfer "resistance" in the liquid part of the boundary layer); k_g is the exchange constant in the gas phase part of the exchange boundary layer (and $\frac{1}{Hk_g}$ is the transfer "resistance" in the gas phase part of the boundary layer); and finally H is the Henry constant (which expresses the ratio in equilibrium conditions of the mass of tracer mixed in a known volume of air over the mass of the tracer dissolved in the same volume of water). The values of k_g and k_ℓ are known experimentally for water and CO respectively. For use with other compounds, the following conversion equations are used,

$$k_g(\text{tracer}) = k_g(H_2O)\left\{\frac{M_{H_2O}}{M_{\text{tracer}}}\right\}^{1/2} \quad ; \quad k_g(H_2O)=3000\text{cm/hr}$$

$$k_\ell(\text{tracer}) = k_\ell(CO_2)\left\{\frac{M_{CO_2}}{M_{\text{tracer}}}\right\}^{1/2} \quad ; \quad k_\ell(CO_2)=20\text{cm/hr}$$

where M_i is the molecular weight of species i. The various values of k_g,k_ℓ,H and k_{ex} for the five tracers are summarized in Table 16. In order to assess the magnitude of the oceanic sink or source for each of the species, one must know their concentration in the ocean surface water as compared to their mixing ratios in the atmospheric layer just above the ocean surface. Measurements of the five tracers relevant to this thesis in the ocean are very sparse, and therefore the assessment of even the direction of the flux is subject to a large uncertainty. Liss and Slater (1974) estimate that N_2O has a large source in the ocean of about $1.2\text{x}10^{14}$ gm per year. For $CC\ell_4$ they estimate an oceanic sink of $1.4\text{x}10^{10}$ gm per year which is approximately 14% of the current anthropogenic source. For $CFC\ell_3$ they estimate an oceanic sink of about $5.4\text{x}10^{9}$gm per year, which is approximately 2% of the current anthropogenic source. Singh *et al.* (1979) estimate that ocean water is supersaturated with respect to $CFC\ell_3$ and $CF_2C\ell_2$, so that the ocean is considered to be a rather poor sink for these two tracers. For $CC\ell_4$ Singh *et al.* (1979) estimate an oceanic sink of about $3.2\text{x}10^{10}$gm per year, or about 32% of the current anthropogenic source. For $CH_3CC\ell_3$, Singh (1981) estimates that the air concentration of $CH_3CC\ell_3$

Table 16 : Oceanic Sink Constants.

Tracer	M	k_g (cm/hr)	k_ℓ (cm/hr)	H 20°C (air/water)	k_{ex} (cm/hr)	Water Solubilty (20°C, ppm)
$CFCl_3$	137.4	1086	11.3	33.3 (1)	11.3	1100 (1)
CF_2Cl_2	120.9	1158	12.1	16.7 (1)	12.1	280 (1)
CCl_4	153.8	1026	10.7	0.91 (1)	10.6	785 (1)
N_2O	44.0	1918	20.0	0.79 (2)	19.7	-
CH_3CCl_3	133.4	1102	11.5	1.41 (1)	11.4	480 (1)

References: (1) Pearson and McConnell (1975).
(2) Slinn et al. (1978).

note that $k_\ell \simeq k_{ex}$ i.e. most of the resistance is in the liquid phase.

is always in equilibrium with its oceanic concentration, while the residence time of $CH_3CC\ell_3$ in the ocean is very long (longer than 50 years), so that the oceanic sink for $CH_3CC\ell_3$ is also very small and certainly ineffective compared to its tropospheric OH sink.

In order to assess the effect of the oceanic sink in our model calculation, we consider a "perfect-sink" and a "partial-sink". A perfect sink is a sink where at the beginning of each time step the tracer concentration in the ocean water is taken as zero (due to an imaginary very fast destruction mechanism of the tracer dissolved in the ocean water and then the downward flux is evaluated using $k_{ex}\Delta c$. A partial sink is a sink where from one time step to the next, the tracer concentration in the ocean water does not change from its equilibrium value determined at the previous time step. Now a flux from atmosphere to ocean will occur only if the tracer concentration in the air above the ocean, increases with time. (Here we do not allow the tracer to escape from the sea to the atmosphere, thus calculating an upper limit for the partial sink). The perfect sink case corresponds to the maximum flux possible from atmosphere to ocean and is considered here only in order to show the maximum value that can be achieved by an oceanic sink. The oceanic sink term is calculated in grid form, taking into account what fraction of the surface area represented by each grid point was composed of land, water or ice (the seasonal

dependence is considered for sea-ice). This contribution was then transformed into spectral form.

The picture as described here for the oceanic sink term is over-simplified and is really affected by such factors as wind speed, ocean surface temperatures, salinity and oceanic currents. The overall effect of each of these factors, is not known yet in a predictable form, (see Broecker and Peng, 1974; Slinn *et al.*, 1978; Peng *et al.*, 1979).

2.2.7 Other Sinks

Alyea *et al.* (1978) suggested a possible effective dessert sink for halocarbons and nitrous oxide, by absorption on dust and sand particles, followed by photodissociation by the long wave solar radiation (Λ>300nm). Also, Pieroti *et al.* (1978) measured an average $CH_3CC\ell_3$ mixing ratio of (102$\pm$4)pptv in dustry Saharan air vs. (112$\pm$6)pptv in non-dustry Saharan air.

A washout effect by rain was suggested by Ohta *et al.* (1977). They measured lower average daily concentrations of $CH_3CC\ell_3$ in a clear Tokyo day, than on a cloudy day, and much lower values on a rainy day, in the ratio of:

$$\text{cloudy} : \text{clear} : \text{rainy} = 1 : 0.92 : 0.60$$

These suggested two additional sinks were not explicitly

included in the model calculations due to a lack of a suitable way of quantitatively assessing their importance.

2.2.8 Boundary Conditions

The lower boundary condition was chosen so as to be consistent with the assumption that the layer from the surface up to halfway between level 24 and 25 is well-mixed, i.e., $m_{26} = m_{25}$. Calculations were done only down to level 25 and the m values for level 26 were set equal to the m values of level 25 at the end of each time step.

The upper boundary condition was chosen so as to ensure that there was no accumulation of tracer there. In particular each amount of tracer transported from below, was immediately destroyed by "psuedo-photodissociation" during each individual time step. The amount of destruction resulting from this top boundary assumption was continuously recorded and was always unimportant compared to the true chemical destruction for each species (well below 0.1%).

3. RESULTS

3.1 General results

3.1.1 Numerical Stability and Convergence

The integration time step Δt, for each of the four steps in the Lorenz 4-cycle, was reduced from 24 hours to 12, 8, 4, 2 and 1 hour. Instability occurred with Δt = 24, 12, and 8 hours after only four time steps, while with

Δt=4 hours instability only occurred after almost 6 months of integration (990 time steps). Stability was achieved with Δt=2 hours at least for three full years of integration. Convergence was confirmed by comparing results of runs with Δt = 1, 2 and 4 hours which yielded almost identical results (the run with Δt=4 hours was almost identical to the other runs with Δt = 1, 2 hours up to the point where instability occurred). The time step chosen for the production runs was thereforeΔt=2 hours. Since data from the original ozone model was available only for Δt=4 hours (although the original ozone model was run with time steps of Δt=1 hour), the model was run with linearly interpolated fields of data (vorticities, vertical velocities and ozone mixing ratios).

3.1.2 Model Diagnostic Parameters

The model results were diagnosed by calculating and checking each day (every 12 time steps) the following parameters:

(i) Atmospheric total tracer content -- gradual increase is expected

(ii) Daily-averaged loss due to sinks (photodissociation and the reactions with $O(^1D)$ and OH radicals where applicable).

(iii) Daily-averaged global tracer lifetime.

(iv) Zonally-averaged vertical profile at 19 latitudes.

(v) Tracer mixing ratios at the five ALE station

locations.

(vi) Horizontally-averaged surface tracer mixing ratio-gradual increase, is expected

The required balance between the calculated daily increase of the total tracer atmospheric content, the total daily loss and the total daily input by the sources at the surface is checked continuously.

The tracer's lifetime was calculated each day by using the definition,

$$\tau = \frac{\text{Integrated Atmospheric content of the tracer}}{\text{Integrated photochemical destruction rate of the tracer}}$$

where integration was done over all the grid points of the model in all latitudes, longitudes and levels.

The lifetime τ, is the instantaneous lifetime of the tracer appropriate for the day of integration, and is different from the steady-state lifetime, for all species with a measureable trend.

3.2 Results for the Fluorocarbons $CFC\ell_3$ and $CF_2C\ell_2$

The changes in the calculated lifetimes τ for $CFC\ell_3$ and $CF_2C\ell_2$ are given in Figures 8a and 8b respectively. In each case starting with the Crutzen initial vertical profile (lower curve), the lifetime increases over the first 4 months, as excess tracer is destroyed in stratospheric levels, while starting with the Fabian initial vertical profile

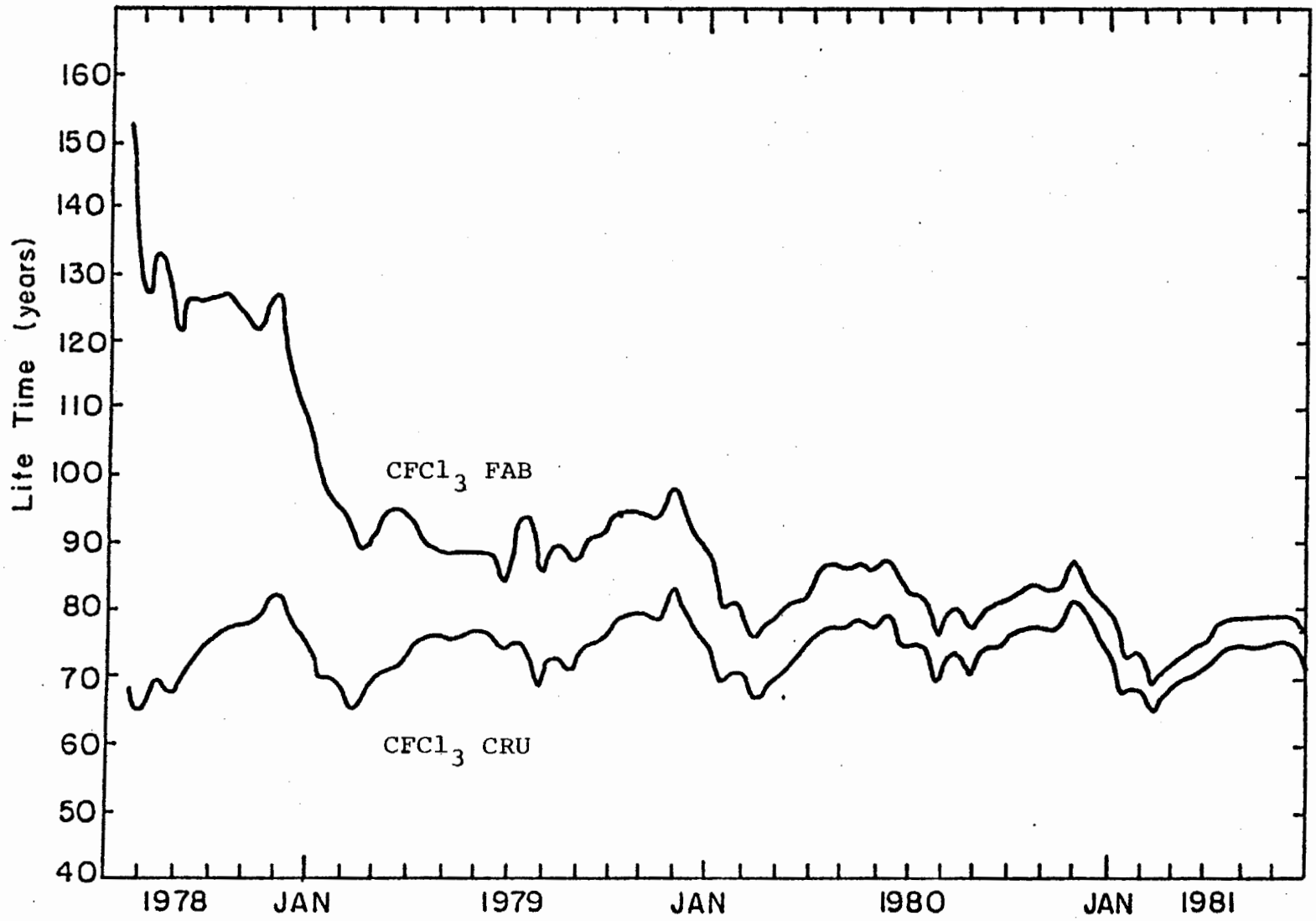


Figure 8a : $CFCl_3$ lifetime trend.

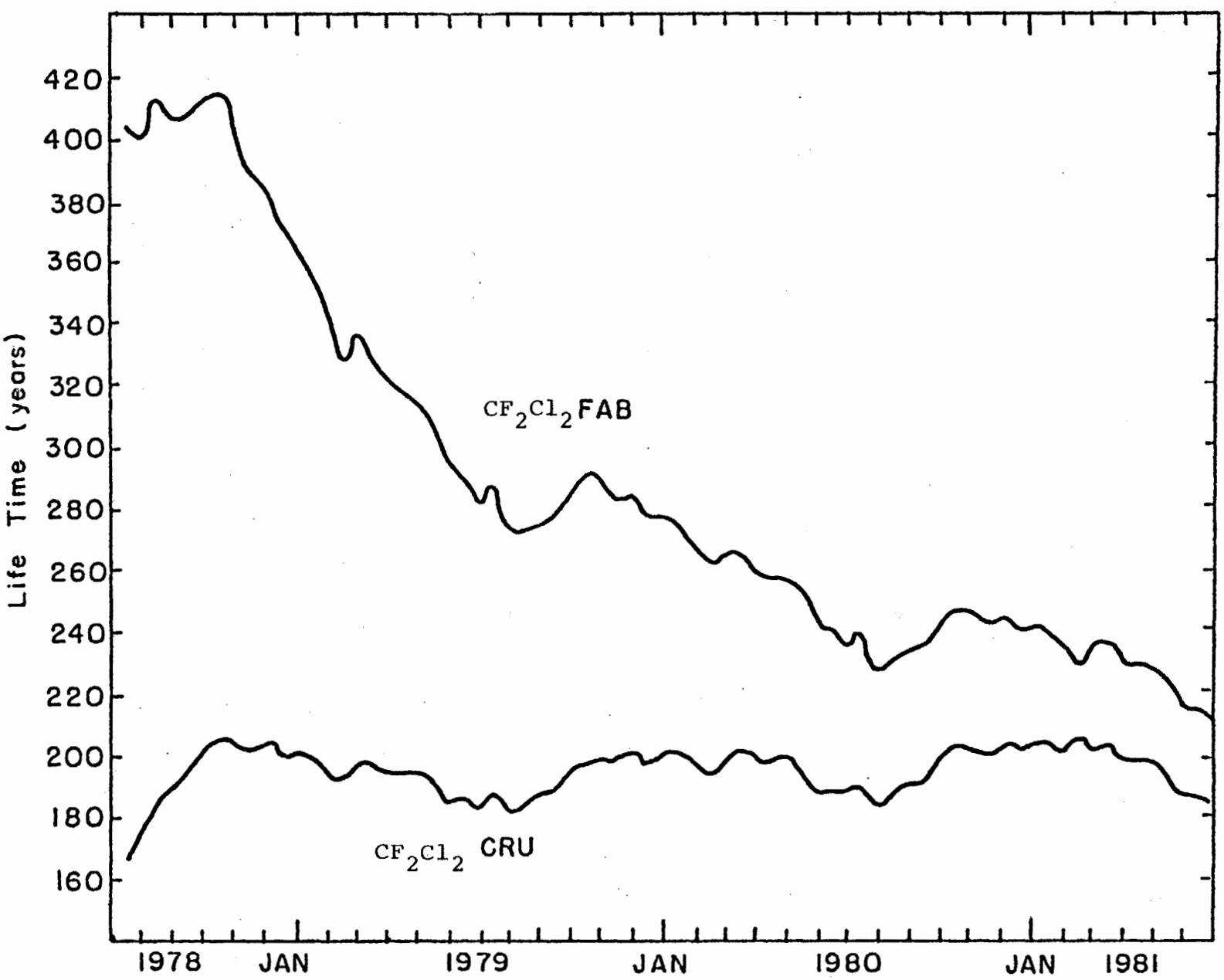


Figure 8b : CF_2Cl_2 lifetime trend.

(upper curve), the lifetime gradually decreases, as tracer is transported upward to the stratosphere, to make up for deficiencies in stratospheric levels. Both trends gradually level off and merge to yield a lifetime of 78 years (annually-averaged) for $CFC\ell_3$, and a lifetime of $\sim$220 years for $CF_2C\ell_2$ (annually-averaged). As stated earlier, the value of the lifetime thus calculated, is the instantaneous value of the lifetime, i.e., the value for the appropriate date when it was calculated. Until the tracer reaches a steady-state, this instantaneous value of the lifetime will gradually decrease with time. This decrease is very difficult to observe in the calculated trends, since it is very small for only three years of integration. The estimated decrease in the lifetime of $CFC\ell_3$ using the two-dimensional model, steady-state τ = 65 years calculation of Sze an Ko (1981), is 78-65 = 13 years from 1980 until year 2100, i.e., an average of $\sim$0.1 years per one calendar year.

An annual cycle in the lifetime of both $CFC\ell_3$ and $CF_2C\ell_2$ was found, where for $CFC\ell_3$ we can also observe a clear semiannual cycle (Figures 8a and 8b). The annual cycle for $CF_2C\ell_2$ has a minimum in August and a maximum in February. The semiannual cycle for $CFC\ell_3$ has a minimum in February and August and a maximum in June and December (i.e., solsticial). The stratospheric tracer mixing ratios for $CFC\ell_3$ are strongly peaked near the equator ($\pm$ 10° latitude). A large portion of the tracer destruction therefore takes place in the equatorial stratosphere and maximum global destruction is

expected near equinoxes and minimum near the solstices producing the observed semiannual lifetime cycle. The details of the semiannual cycle for $CF_2C\ell_2$ are apparently blurred because its lifetime is much longer than that of $CFC\ell_3$, and its peak concentration in the equatorial stratosphere is much less obvious than that of $CFC\ell_3$ (Figures 13 and 14). In one-dimensional models we cannot predict this semiannual cycle, because these models do not have latitudinal variations of tracer concentrations.

The annual (rather than semi-annual) cycle for $CF_2C\ell_2$ is obtained because maximum stratospheric concentrations of this compound are found in the Northern hemisphere and maximum destruction is therefore expected in the Northern hemisphere summer. In Figure 9 we plotted the latitudinal dependence of the zonally-averaged column destruction of $CFC\ell_3$ and $CF_2C\ell_2$ as calculated in June 30 and December 30 of 1980. The plots for $CFC\ell_3$ are symetric (mirror images across the equator), while the plots for $CF_2C\ell_2$ are not, showing the higher Northern hemisphere summer destruction of $CF_2C\ell_2$. This effect for $CF_2C\ell_2$ explains the predominance of its annual cycle in the lifetime trend.

The two lifetime values based upon the two initial vertical profiles (Crutzen and Fabian profiles) are still different after three years of integration, because the total atmospheric content based on these profiles is different. Using the Fabian profile, we have a smaller overall atmospheric

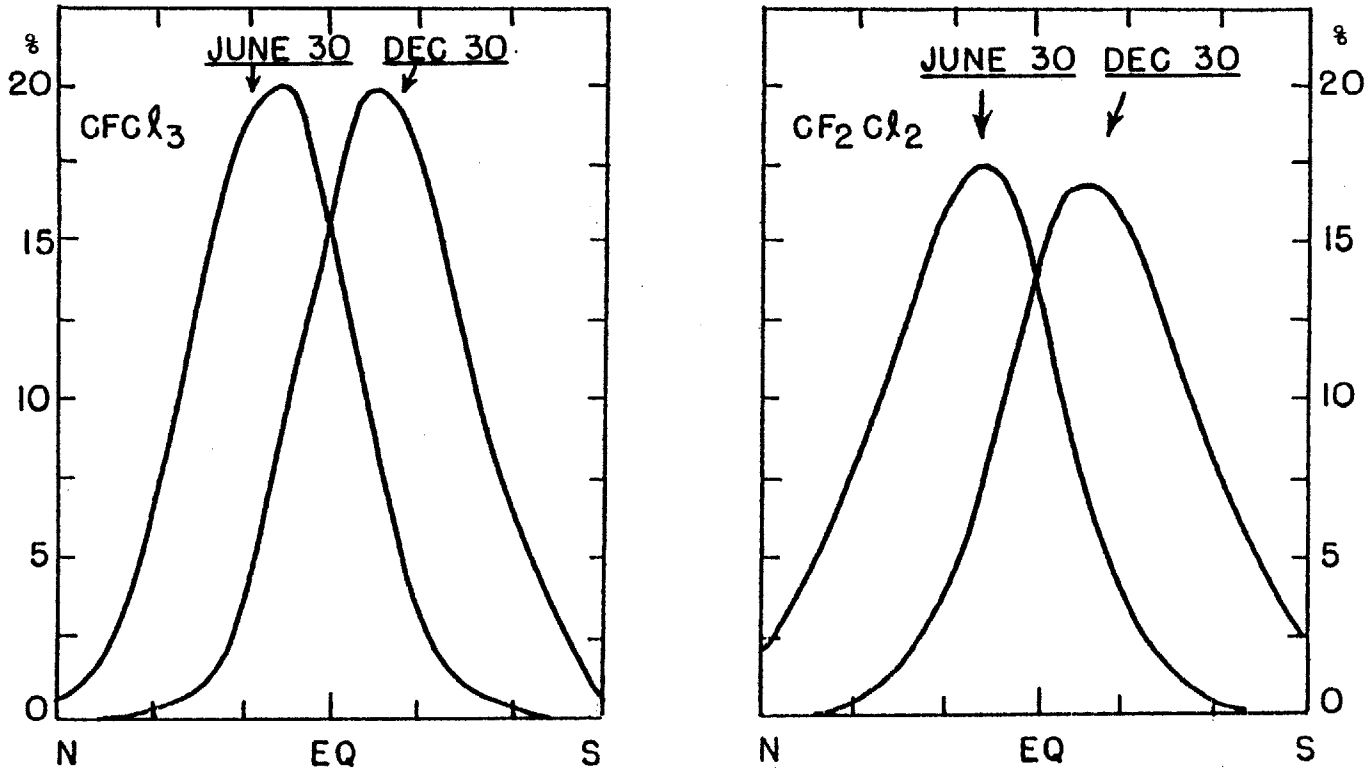


Figure 9: Zonally-averaged column destruction of $CFCl_3$ and CF_2Cl_2 (percentage as a function of latitude), as calculated by the model for June 30 and December 30, 1980.

tracer content than in using the Crutzen profile. Because the calculated lifetimes are so long, it will take decades of model running in order to get the two contents to converge. This difference in total tracer atmospheric content is also creating different tracer trends at the surface: even though we begin with the same surface values initially, the surface concentrations in the Crutzen and Fabian runs begin to slightly diverge as integration is pursued. This is because vertical mixing affects the surface concentrations as time progresses and the two vertical profiles are different.

A crucial test of the circulation and chemistry in our model involves a comparison of the trends as calculated by the model and as actually measured in the atmosphere, in particular at the five ALE stations. Looking at the trends of the fluorocarbons $CFC\ell_3$ and $CF_2C\ell_2$ at the five ALE station locations as calculated by the model and as actually measured at the ALE sites (Cunnold *et al.*, 1982a, 1982b) we find rather good agreement (see Figure 10). We note that the major source of fluorocarbons for the Southern hemisphere involves their transportation in the atmosphere from the Northern hemisphere and not their use and release in the Southern hemisphere itself. Thus the general agreement between calculated and observed trends for the fluorocarbons in Tasmania is a good confirmation of the validity of the model at least for global-scale mixing. A quantitative comparison is given in Table 17. Here the trends at the

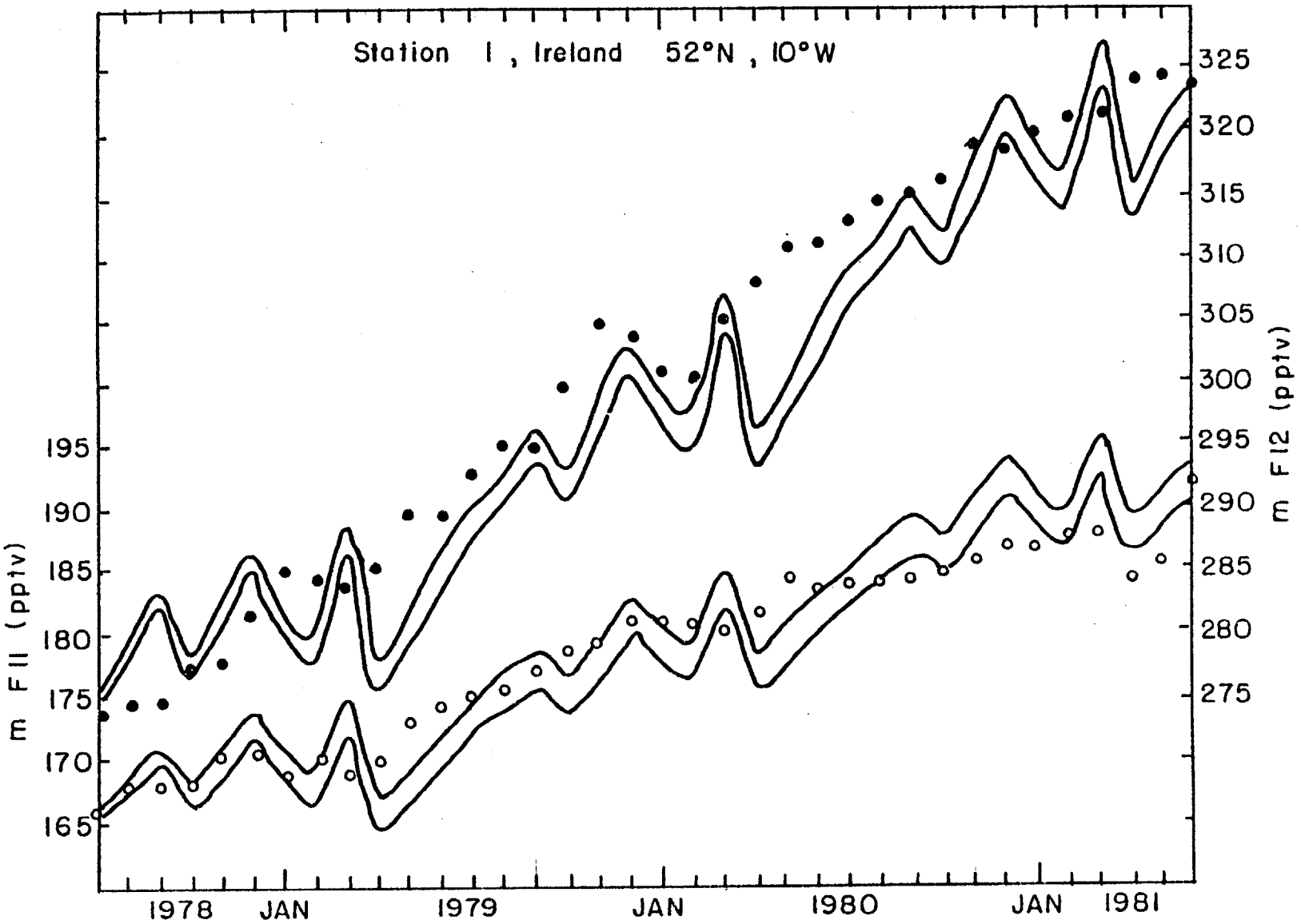


Figure 10a: The $CFCl_3$ and CF_2Cl_2 monthly-mean trends. Solid lines are calculated trends, the upper line used the Crutzen initial profile, the lower line used the Fabian initial profile, and the circles denote ALE station measurements. Station 1, Ireland.

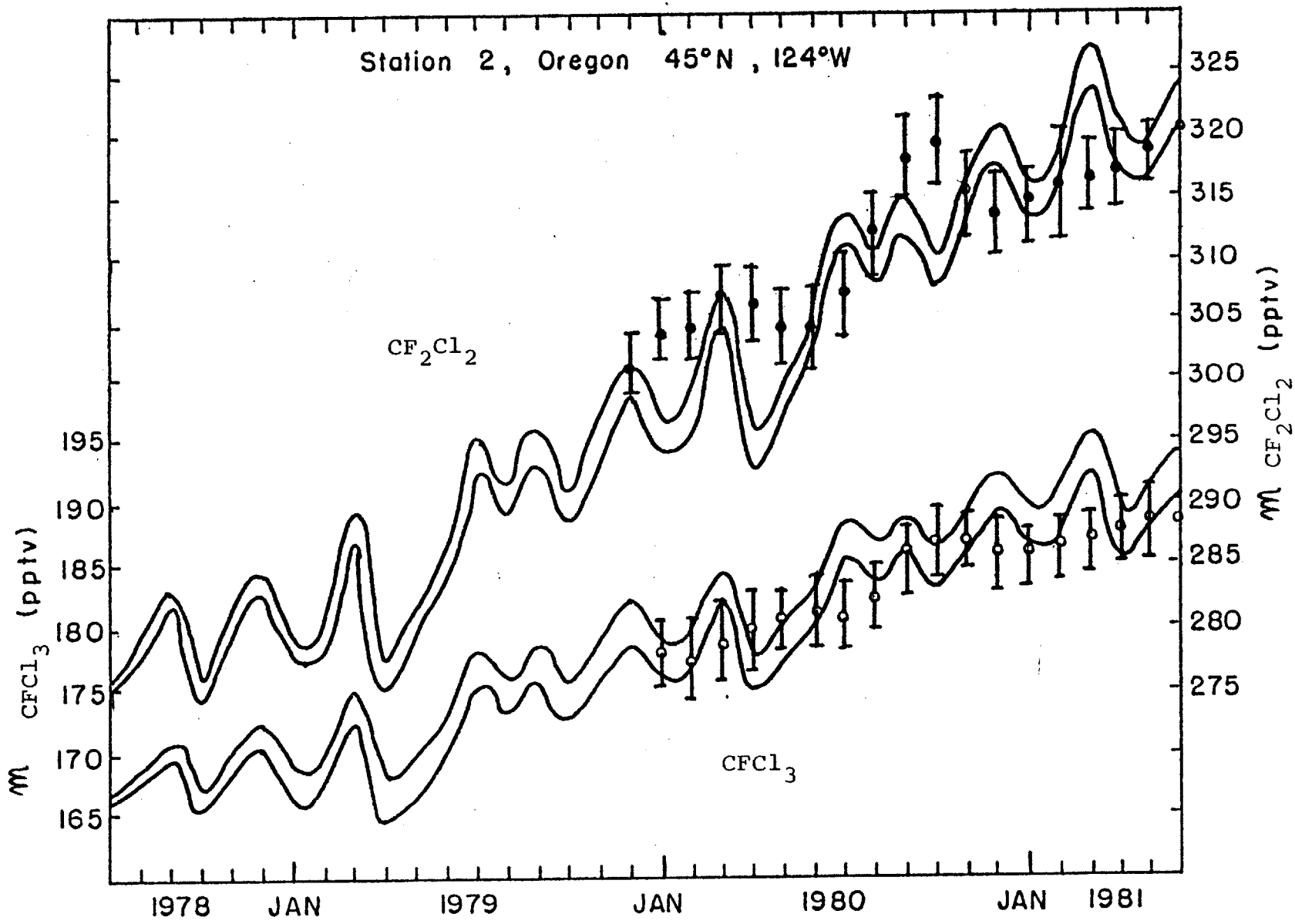


Figure 10b : Same as figure 10a, but for Station 2, Oregon.

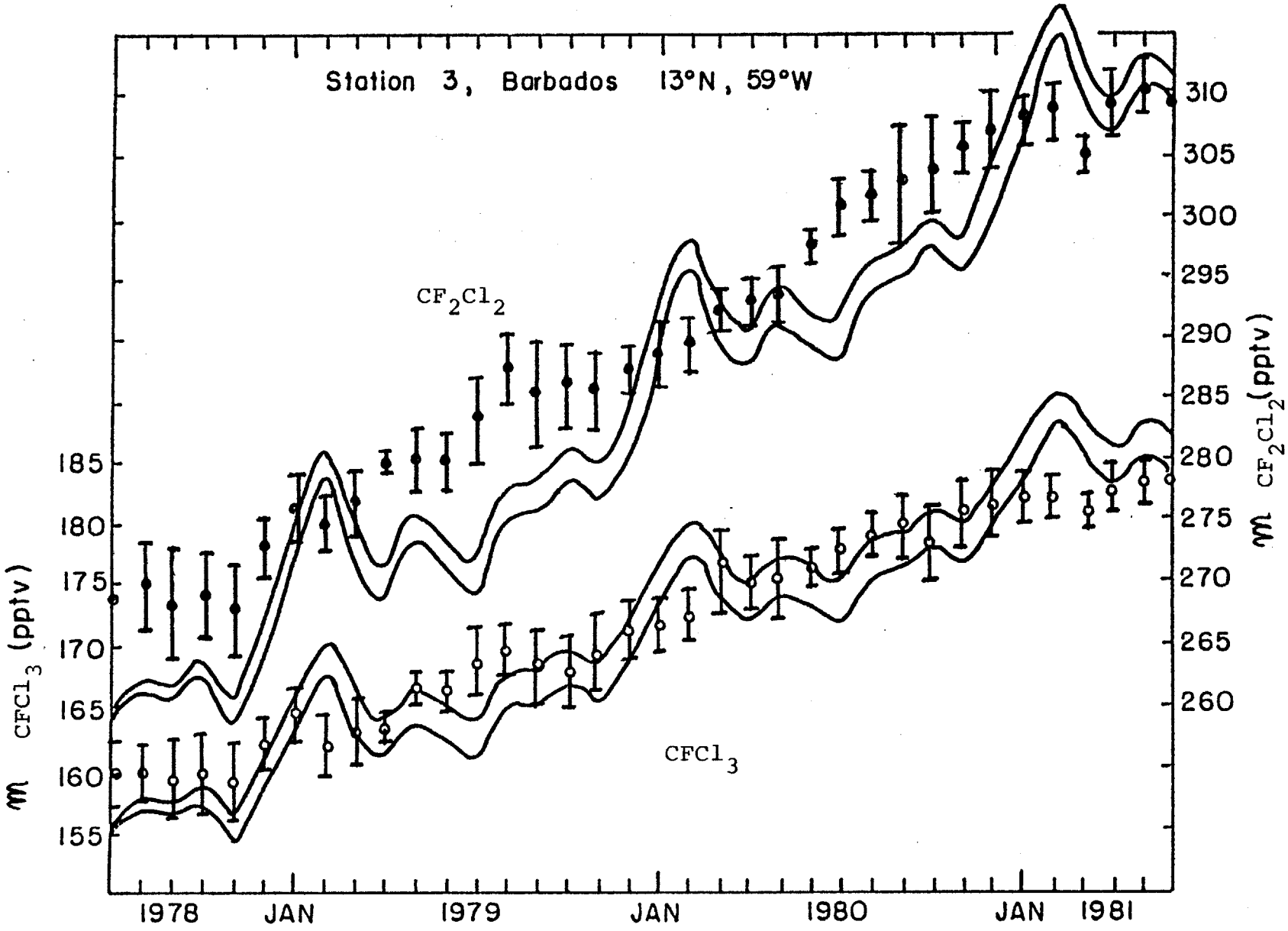


Figure 10c : Same as figure 10a , but for Station 3, Barbados.

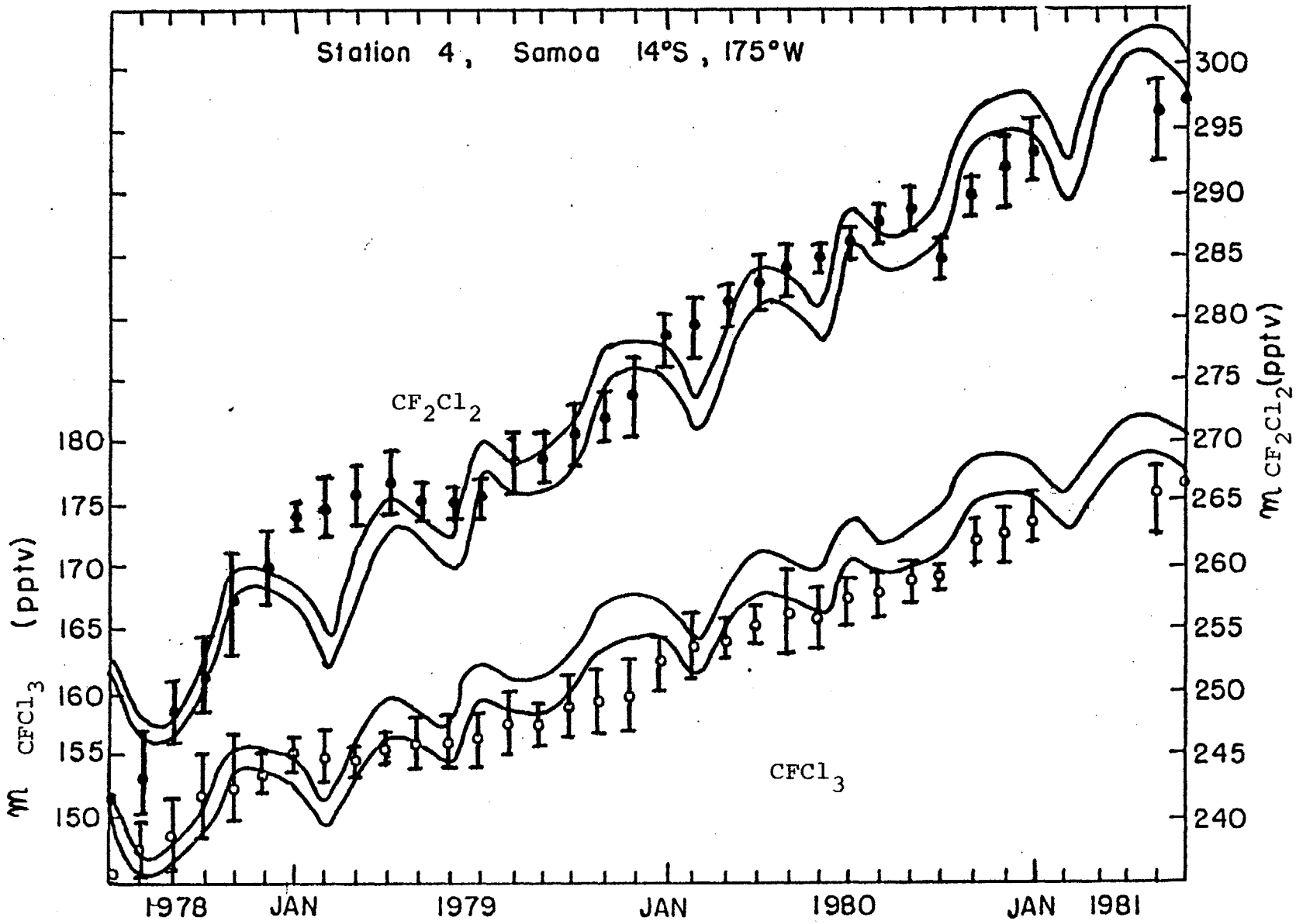


Figure 10d : Same as figure 10a , but for Station 4, Samoa.

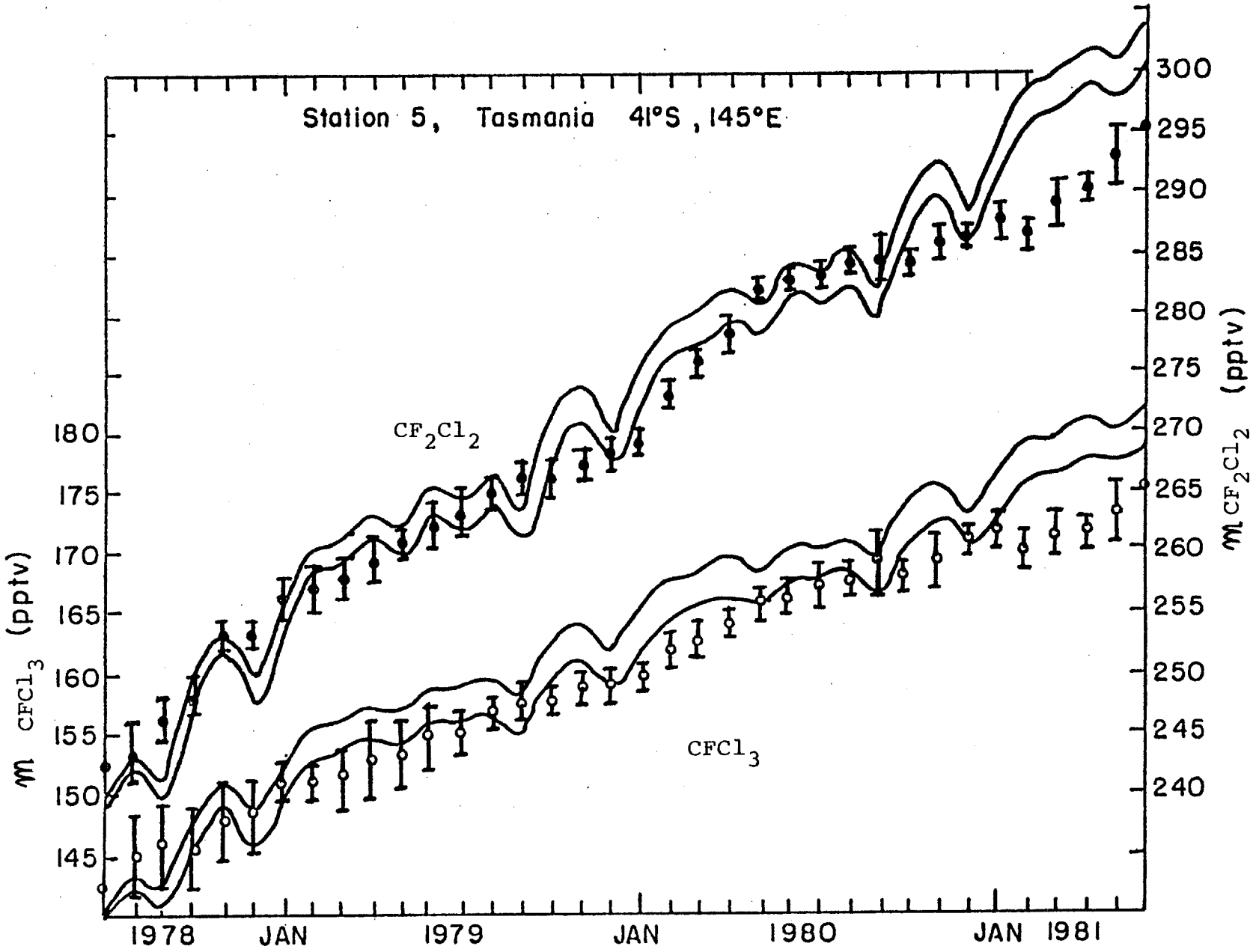


Figure 10e : Same as figure 10a , but for Station 5, Tasmania.

Table 17: Experimental and Calculated Tends, based on Three Years of Data. Trends are given in percent per year and mixing ratios m_0 and m_H are given in pptv.

Station	Experimental			Calculated					
				Fabian			Crutzen		
	trend	m_0	m_H	trend	m_0	m_H	trend	m_0	m_H
				$CFCl_3$					
1	4.95±0.13	166	179	4.76±0.26	165	177	5.11±0.23	166	179
2	5.47±0.33*	167*	179*	4.67±0.26	165	177	5.10±0.23	166	179
3	6.33±0.15	156	172	6.26±0.19	154	169	6.43±0.19	156	172
4	6.10±0.15	147	161	6.63±0.23	146	161	6.76±0.22	148	164
5	6.43±0.17	145	160	7.68±0.24	143	160	8.14±0.29	144	162
				CF_2Cl_2					
1	5.95±0.17	274	300	5.24±0.21	273	295	5.52±0.20	274	297
2	3.83±0.43*	301*	310*	5.10±0.21	274	295	5.40±0.20	274	297
3	5.30±0.14	267	289	6.44±0.19	257	283	6.57±0.19	258	285
4	6.19±0.26	250	275	6.58±0.21	245	271	6.67±0.20	247	273
5	6.38±0.20	245	270	7.41±0.20	242	270	7.63±0.22	243	272

* - numbers based only on 19 months of data.

five ALE stations locations (in precent per year) were calculated based on a weighted linear fit.

$$\ln(w_i m_i) = Aw_i + Bw_i t_i \quad .$$

Here m_i is the monthly mean mixing ratio calculated (or measured) at each ALE site in month t_i and w_i is the weighting factor for each monthly-mean calculation (or ALE measurement). This latter factor is given by

$$w_i = \frac{1}{\sigma_i^2}$$

where σ_i is the standard deviation of the monthly-mean calculation (or ALE measurement). Month one is July 1978, and for each calculation (or measurement), 36 data points were used (i.e., 36 months). In ALE station 2 (Oregon), only 19 months of data were available. In Table 17, m_0 and m_H are also compared, where m_0 denotes the monthly-average mixing ratio calculated by the weighted linear fit for the beginning of the time period (t=0), and m_H denotes the monthly-average mixing ratio calculated by the weighted linear fit for the middle of the time span of the data used (t = 18).

Looking at the details of the tracer mixing ratios and and their trends in the various ALE sites, (Figure 10) we can observe in the calculated mixing ratios some persistent

features which tend to repeat each year. In site 1 (Ireland) for example, we can see the same cycle repeated in the calculated values each year: namely a monthly-average mixing ratio decrease from December to February, a sharp increase in March, a sharp decrease in April, a gradual increase from May through September, a slight decrease in October and gradual increase in November and December. This pattern repeats itself in each year of the model run for $CFC\ell_3$ as well as for $CF_2C\ell_2$. Since we are using the same vorticity fields each year, this repetitive feature is a characteristic of the model transport. In the measured values at site 1 (Ireland) we can also observe some similarities to the calculated values. For example, the flattening and the slight decrease in the experimental values during the months of November through February, is somewhat similar to the decrease observed in the calculated values during December through February. Generally the fluctuations in the calculated mixing ratios in site 1 for $CFC\ell_3$ and $CF_2C\ell_2$ are larger than the fluctuations in the experimental trends. When comparing $CFC\ell_3$ and $CF_2C\ell_2$ in site 1, both calculated and experimental fluctuations for $CFC\ell_3$ seem to be smaller than the fluctuations of $CF_2C\ell_2$, and this simply reflects the higher mixing ratios and larger source strength of $CF_2C\ell_2$. In ALE site 3 (Barbados) we can observe a clear annual cycle in the calculated values with a maximum during February, it is difficult however to identify such an annual cycle in the measurements. As we go

farther away from the antropogenic sources in the Northern hemisphere, we find smaller fluctuations both in the experimental and the calculated trends of $CFC\ell_3$ and $CF_2C\ell_2$ in the Southern hemisphere. It is difficult to see similarities in the small time-scale fluctuation patterns between the calculated and experimental trends of $CFC\ell_3$ and $CF_2C\ell_2$ in ALE sites 4 and 5 (Samoa and Tasmania), through it seems that a smoothing of the calculated oscillations may improve the similarity. When we compare the weighted-linear fits of the calculated and experimental mixing ratio values (Table 17), we can see that generally the model tends to under-estimate the Northern hemisphere trends and over-estimate the Southern hemisphere trends both for $CFC\ell_3$ and for $CF_2C\ell_2$. This general feature of the model is, we believe, a result of the low truncation (wave number 6) of the spectral representation. Both $CFC\ell_3$ and $CF_2C\ell_2$ are anthropogenic pollutants, having a concentration gradient across the equator and it is probable that the low truncation tends to smooth that gradient.

For both the species $CFC\ell_3$ and $CF_2C\ell_2$, the use in the model calculation of the initial experimental Fabian vertical profile results in a better fit to the measured trends than the use of the initial Crutzen vertical profile.

Vertical profiles as calculated by the model are compared to three sets of measurements. The first set was made on November 9, 1979 in Germany at 44°N (Fabian *et al.*,1981).

The second set was made on February 1, 1979 in Wyoming at 41°N (Goldan *et al.*, 1980), and finally the third set of measurements was made on March 29, 1979 in Brazil at 5°S (Goldan *et al.*, 1980). The results of the model calculations are compared with these observations in Figures 11a, b, c. Some of the vertical profiles fit observations very closely, especially the equatorial $CFC\ell_3$ profile (Figure 11b). Disagreement between calculated and measured vertical profiles, are not systematic and the reasons for any disagreements may be different for each individual case. In general, incorrect calculated vertical profile values may be caused by erroneous photodissociation integral calculations (J values), by incorrect values of experimental cross-sections, or by incorrect ozone concentrations. Another potential source of error may be incorrect vertical mixing rates. The fact that the calculated vertical profiles presented are zonally averaged, while the measurements are done at a specific longitude and time, may cause disagreements due to longitudinal and time variations in the individual measurements from their zonally-averaged values. Typical of this kind of disagreement, is the vertical experimental $CFC\ell_3$ profile of November 9, 1979 at 45°N (Figure 11c) where around 30km we find large variations in the measured $CFC\ell_3$ concentrations which we believe is due to local transport effects.

In Figures 12a and 12b we show the latitudinal surface variations the fluorocarbons $CFC\ell_3$ and $CF_2C\ell_2$. These are the zonally-averaged values calculated by the model in 19

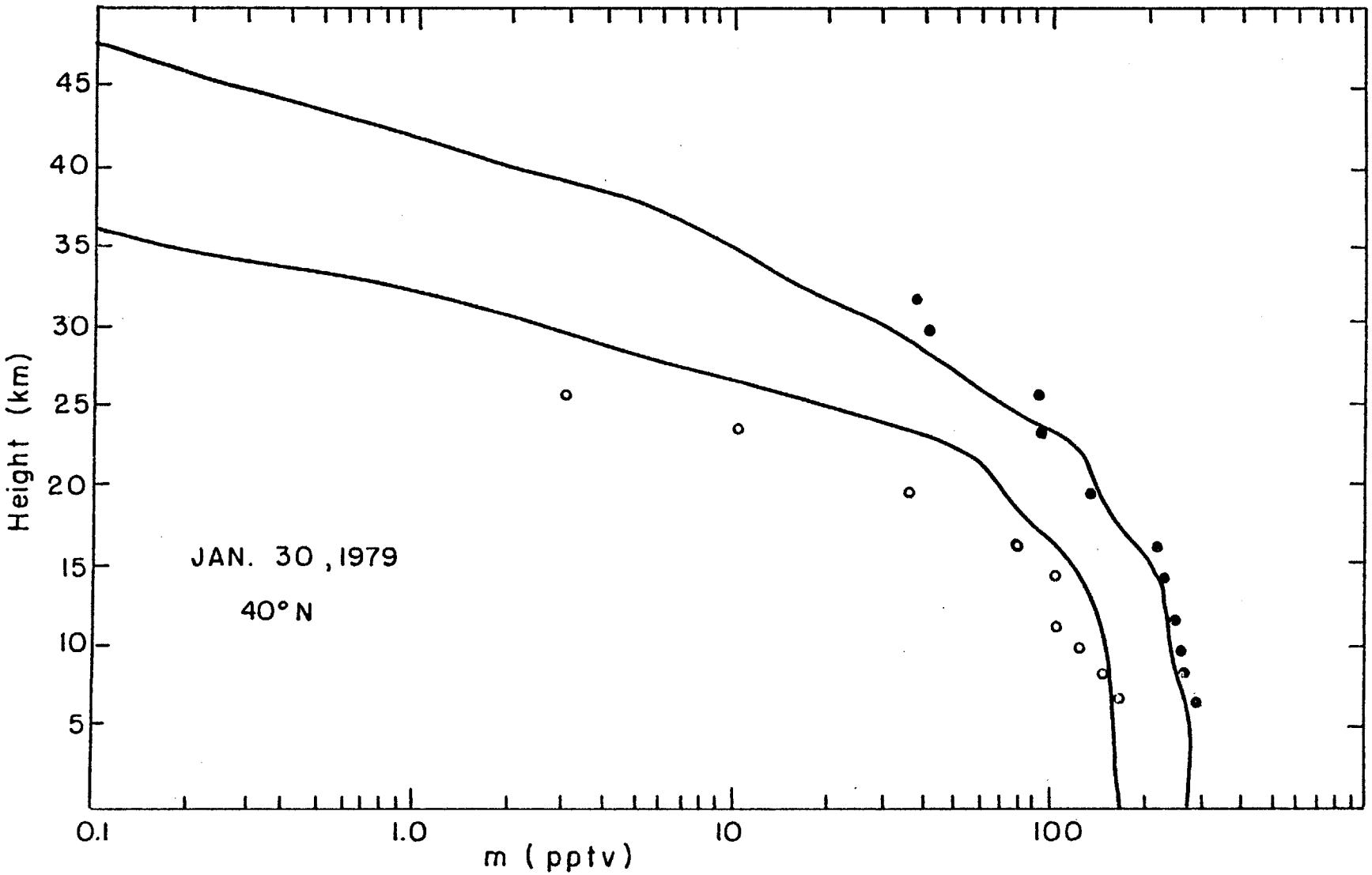


Figure 11a: $CFCl_3$, CF_2Cl_2 vertical profiles, calculated solid lines are zonally-averaged values for January 30, 1979 at 40°N, circles are measurements at 41°N, February 1, 1979 as reported by Goldan et al. (1980).

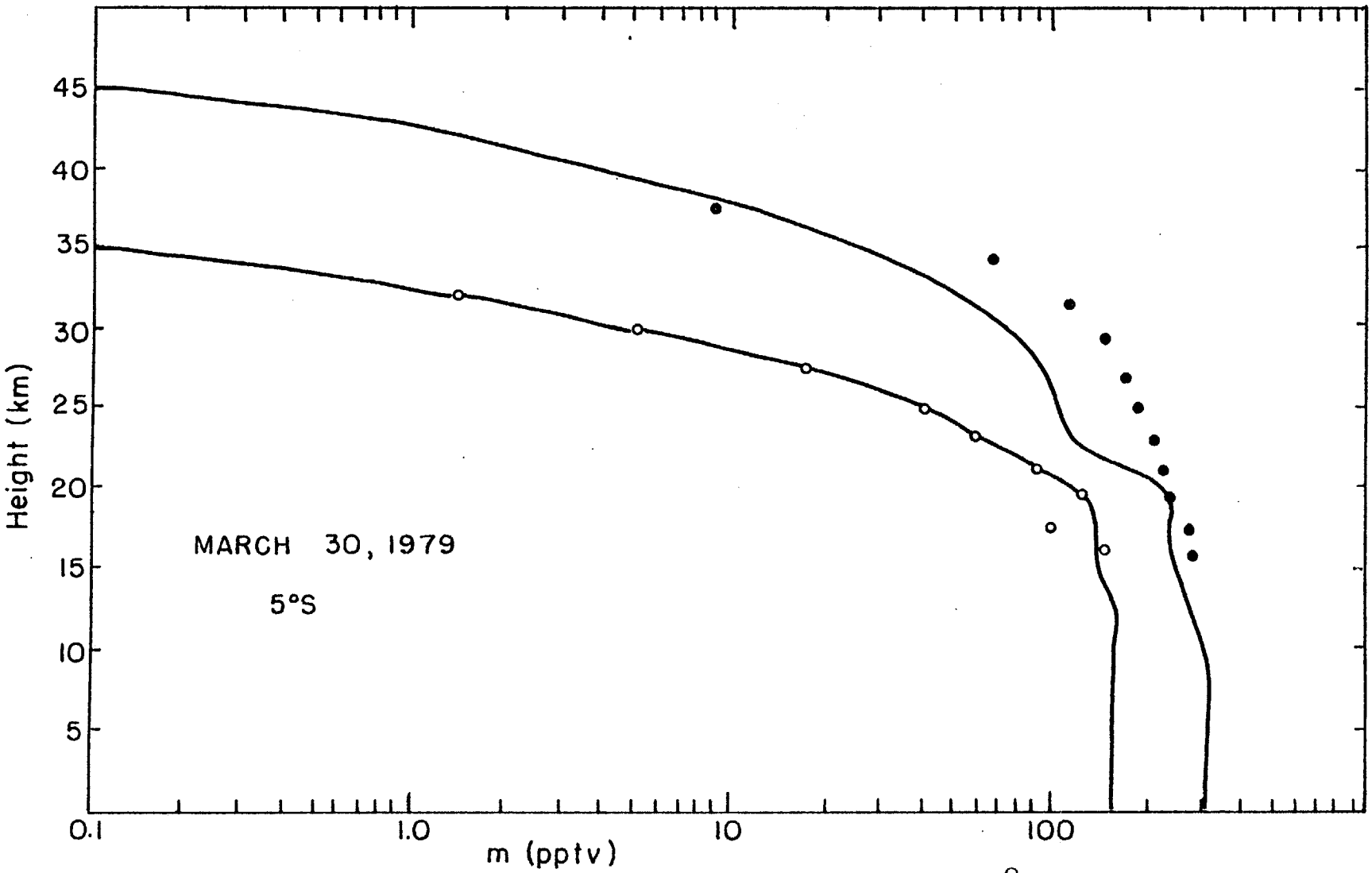


Figure 11b: Same as figure 11a, calculated lines are for March 30, 1979 5°S, measurements are for March 29, 1979 5°S, Goldan et al. (1980).

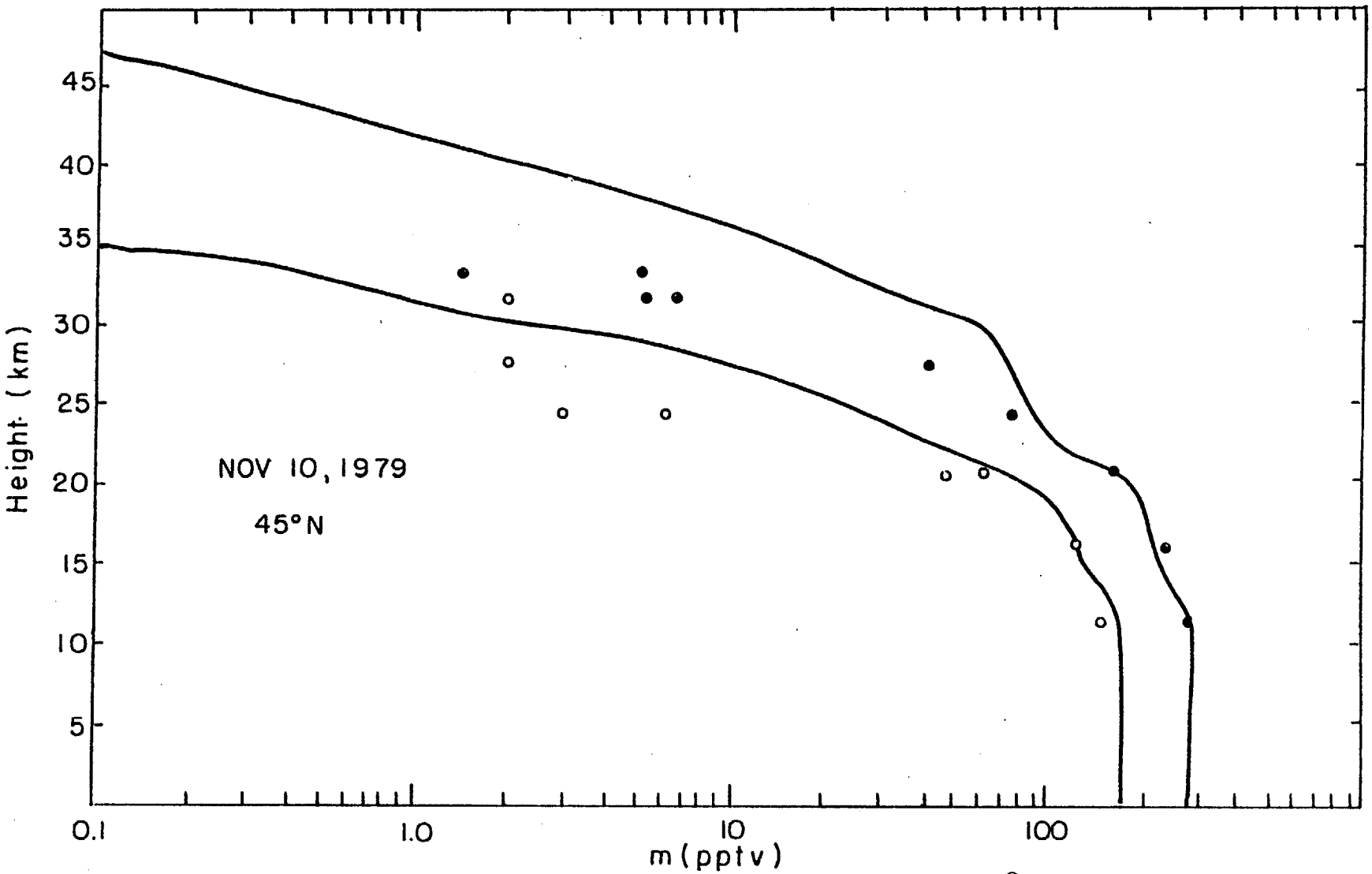


Figure 11c: Same as figure 11a, calculated lines are for November 10, 1979 45°N, measurements are for November 9, 1979 44°N, Fabian et al. (1981).

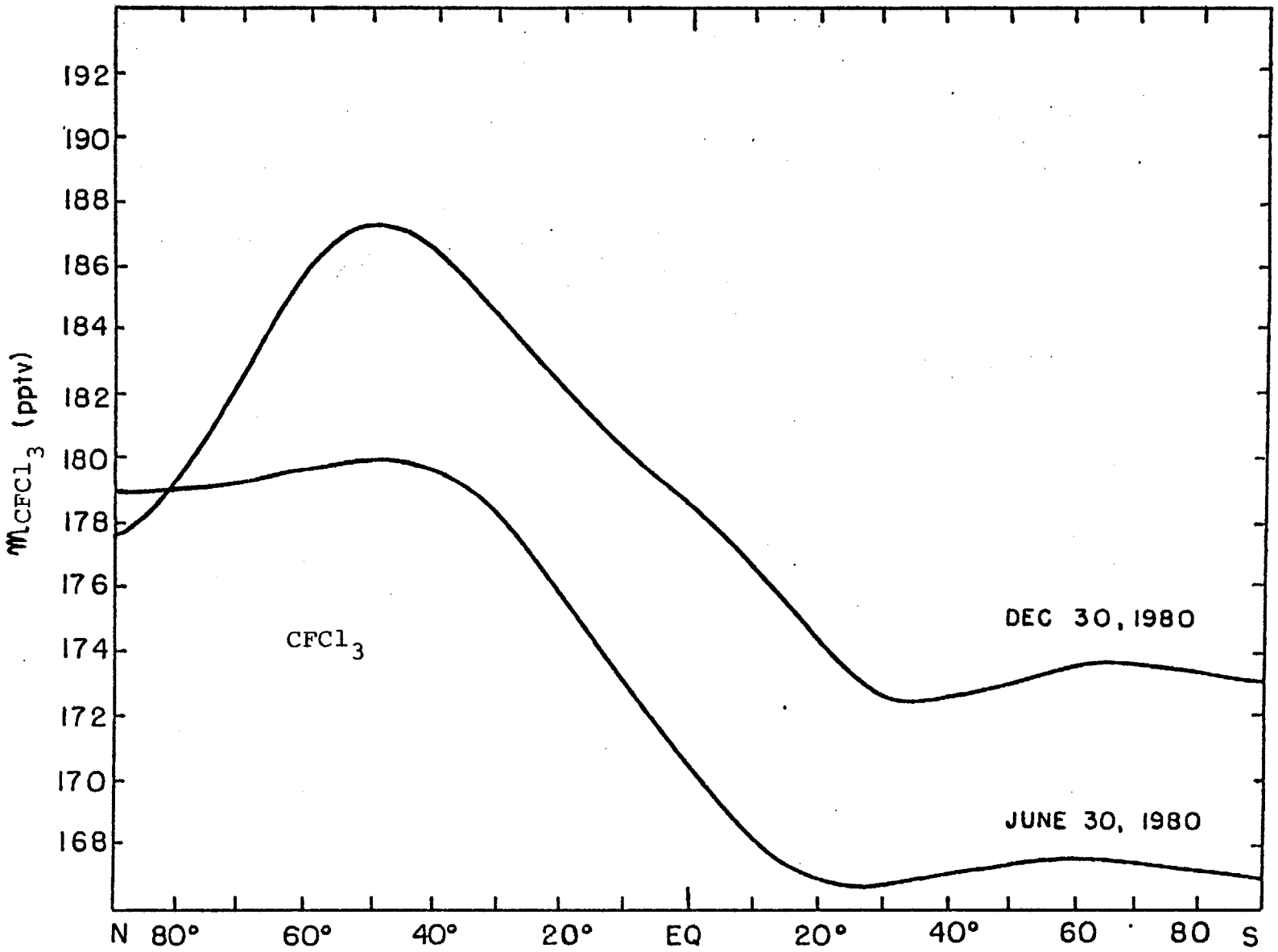


Figure 12a : $CFCl_3$ surface distribution as calculated by the model for June 30 and December 30, 1980, (zonally averaged values).

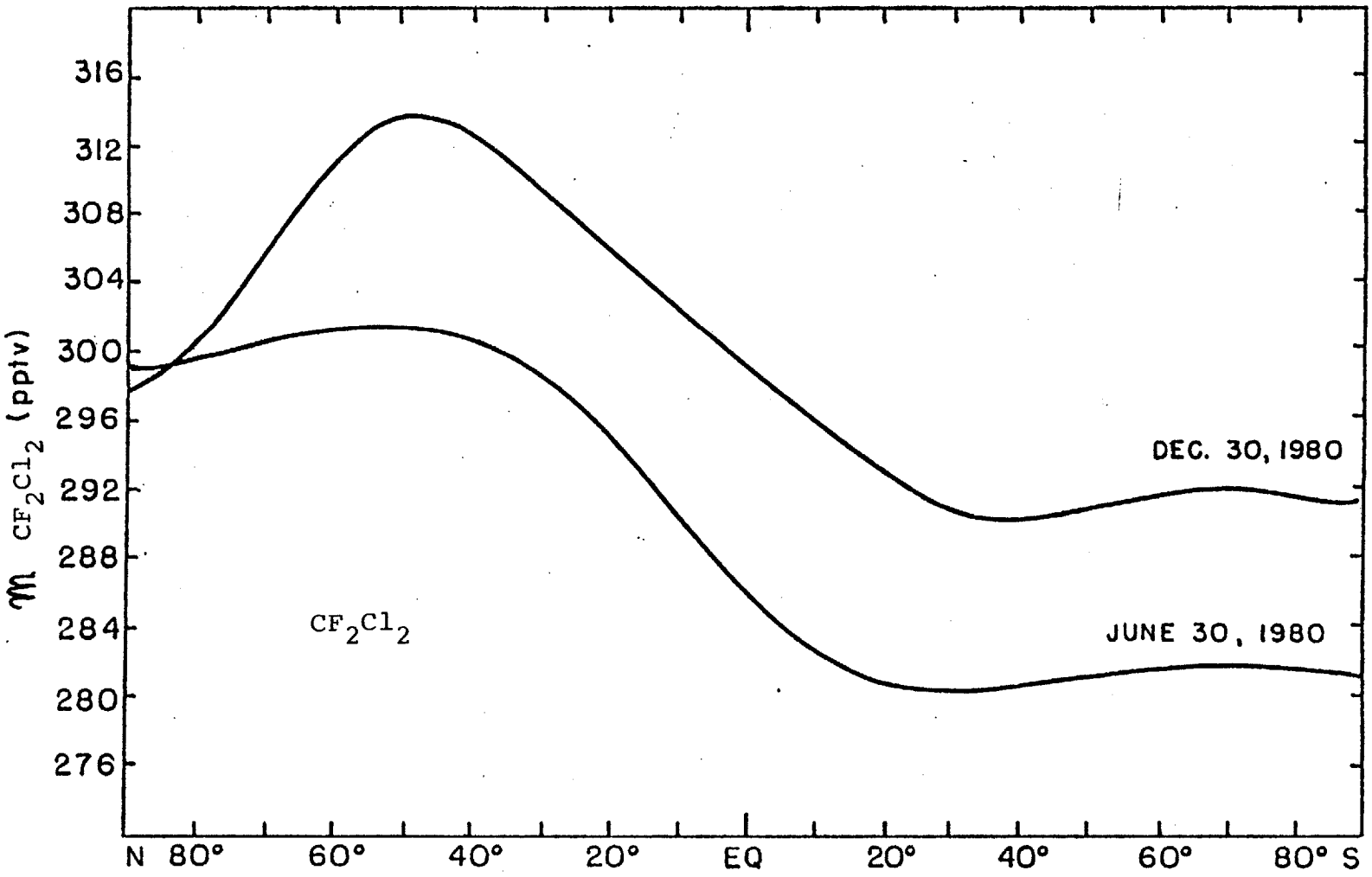


Figure 12b : Same as figure 12a , but for CF_2Cl_2.

latitudes (after 24 and 30 months of integration) for the dates June 30 and December 30, 1980. Figures 13 and 14 show the zonally-averaged two-dimensional (latitude, altitude) distributions of $CFC\ell_3$ and $CF_2C\ell_2$ respectively for December 30, 1980 as given by the model.

Finally in Figures 15 and 16 we plot the surface two-dimensional (latitude, longitude) distributions of $CFC\ell_3$ and $CF_2C\ell_2$ respectively. The mixing ratios in these figures are monthly-averaged calculated values for the month of January 1981. These figures give us the details of the horizontal tracer distribution, which is a unique feature of the three-dimensional model. The peaks of the distributions coincide with the anthropogenic source emission locations, as shown for example in figure 17 for $CFC\ell_3$. The highest tracer concentrations occur in Europe due to local emissions amplified by transport across the Atlantic ocean from continental USA. The northern hemisphere mid-latitudes show a strong standing wave pattern, in pollutants distribution, while the southern hemisphere is much more homogeneous.

3.3 Results for Carbon Tetrachloride and Nitrous Oxide

Model lifetime trends for $CF\ell_4$ and N_2O are given in Figure 18. Similar to the $CFC\ell_3$ and $CF_2C\ell_2$ runs for the Crutzen initial profile, we find an increase in lifetime as excess tracer is photochemically destroyed in stratospheric levels in the first year and a half of integration. The

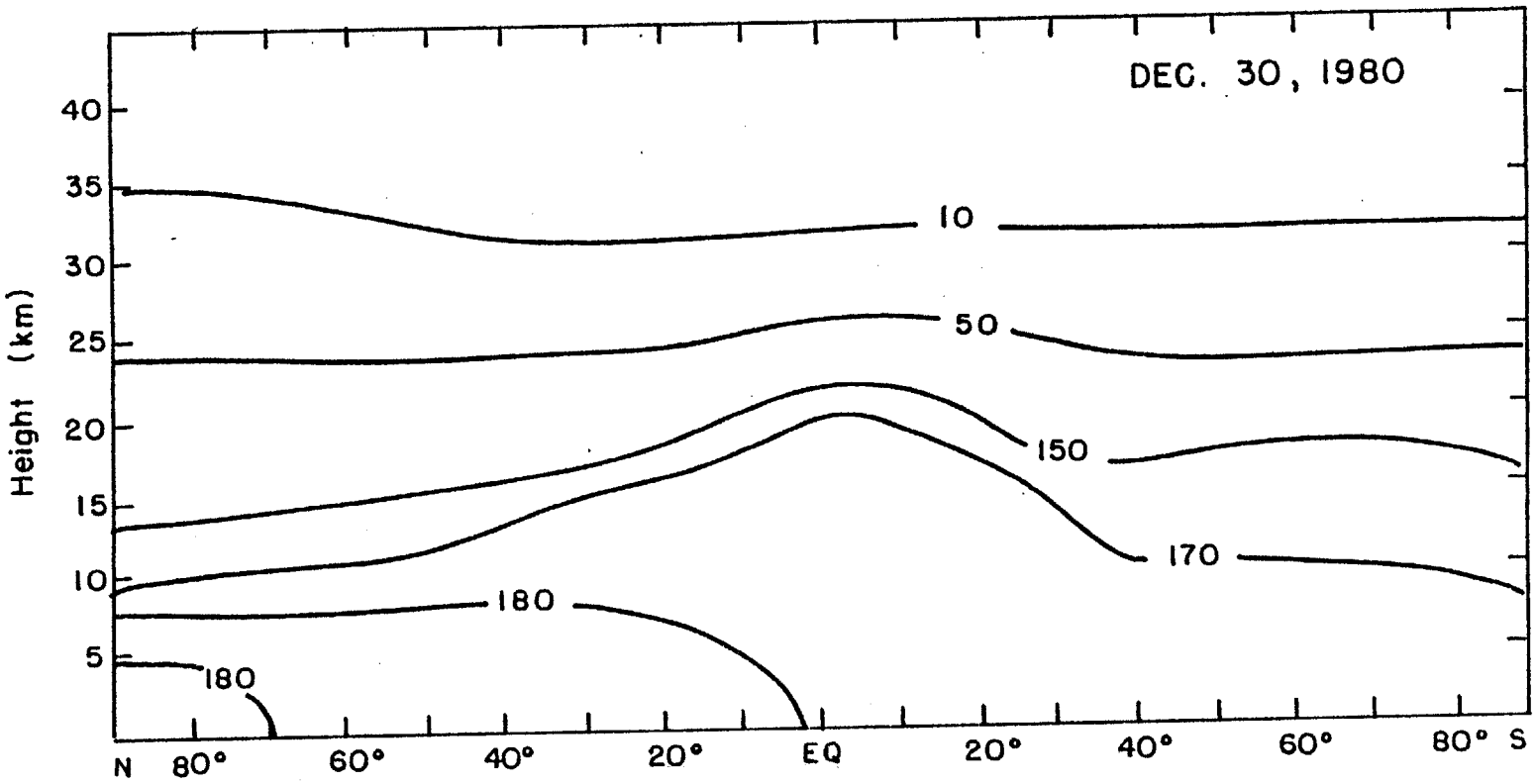


Figure 13: Zonally-averaged $CFCl_3$ 2-D distribution (pptv), calculated for December 30, 1980.

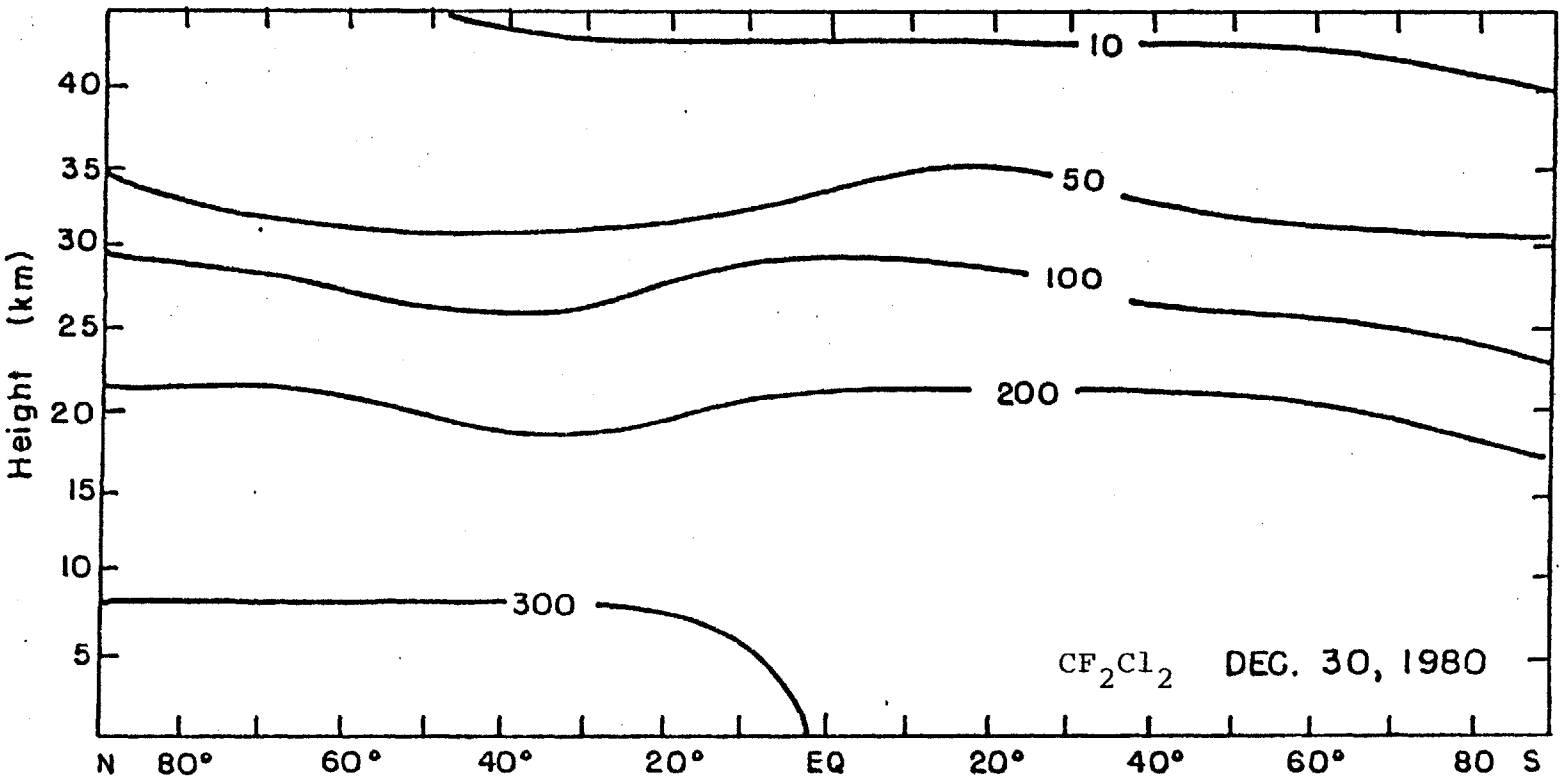


Figure 14 : Same as figure 13 , but for CF_2Cl_2 .

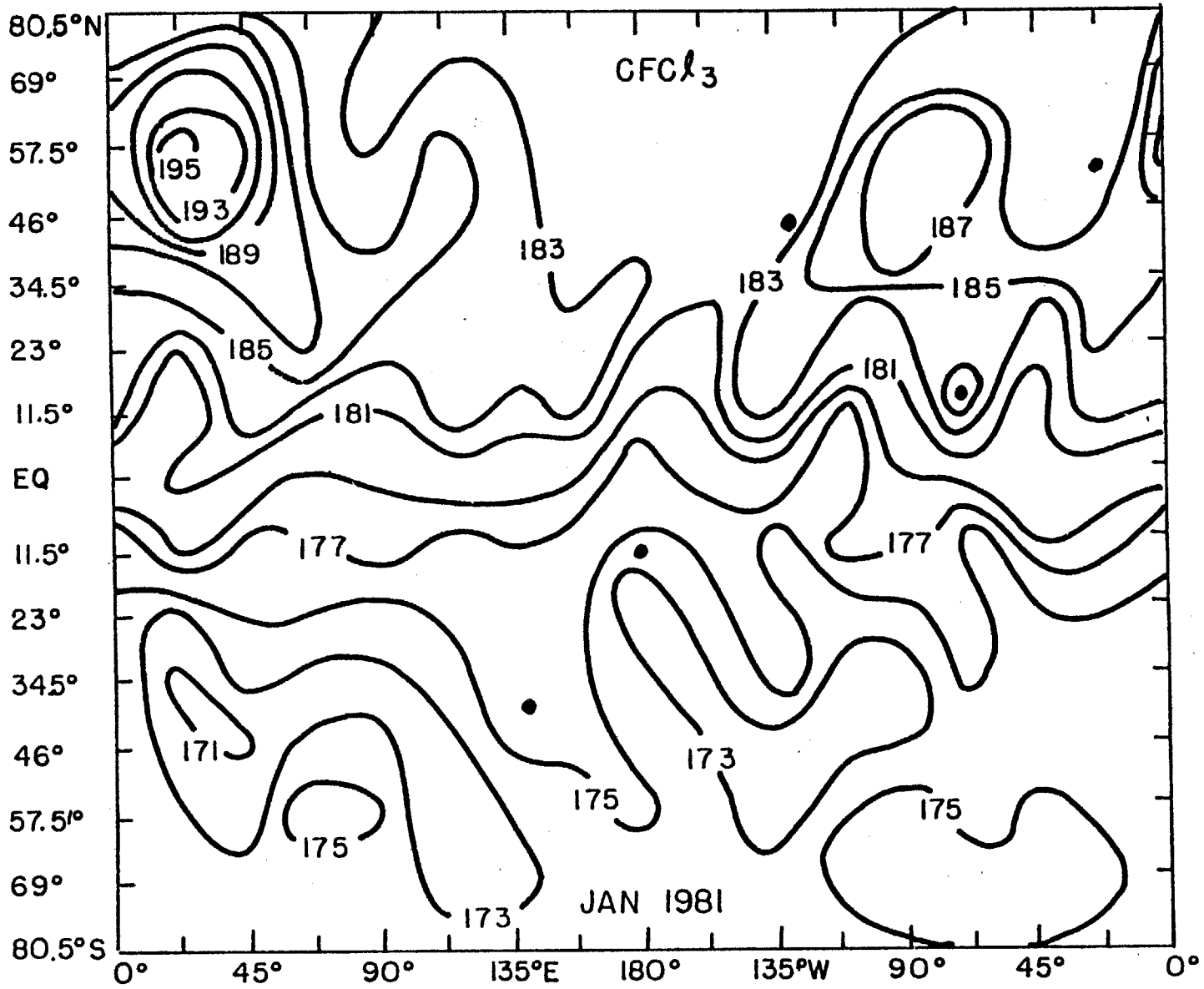


Figure 15 : The 2-D $CFCl_3$ Surface Distribution, January 1981 (pptv). Solid circles denote ALE sites.

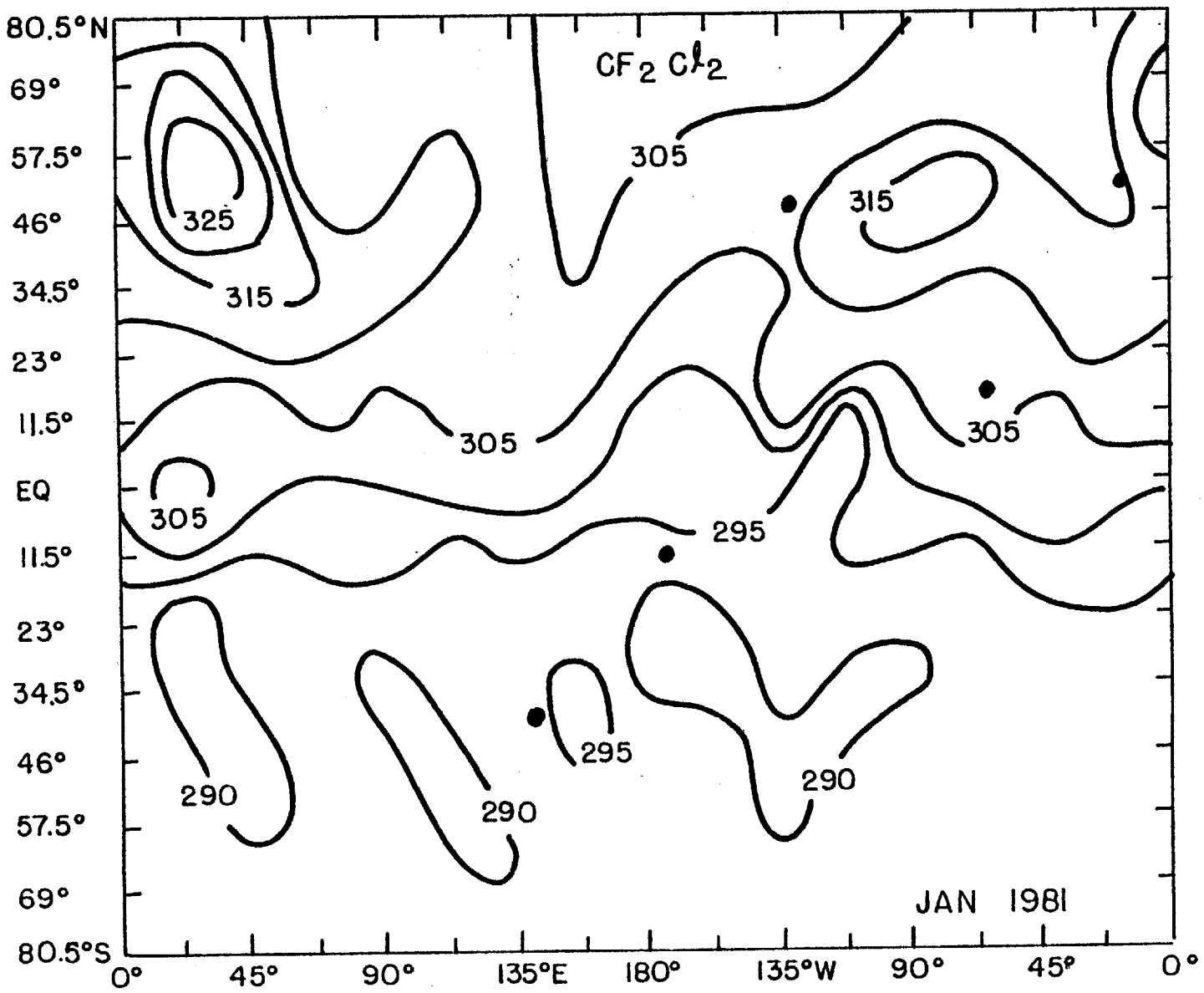


Figure 16 : The 2-D CF_2Cl_2 Surface Distribution, January 1981 (pptv). Solid circles denote ALE sites.

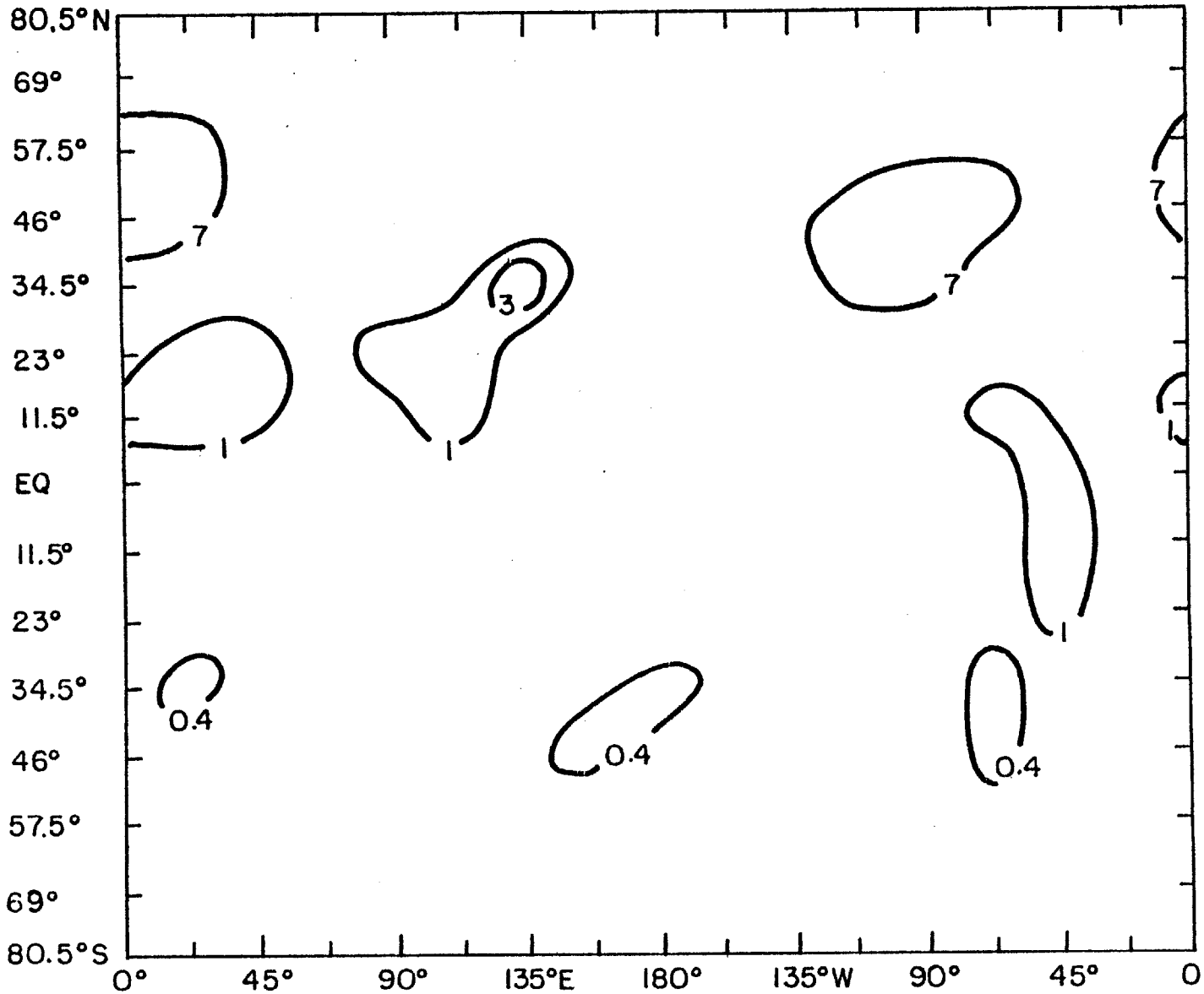


Figure 17: The 2-D source wighting factor distribution of $CFCl_3$. The units are percent of the total daily emission per one grid point area.

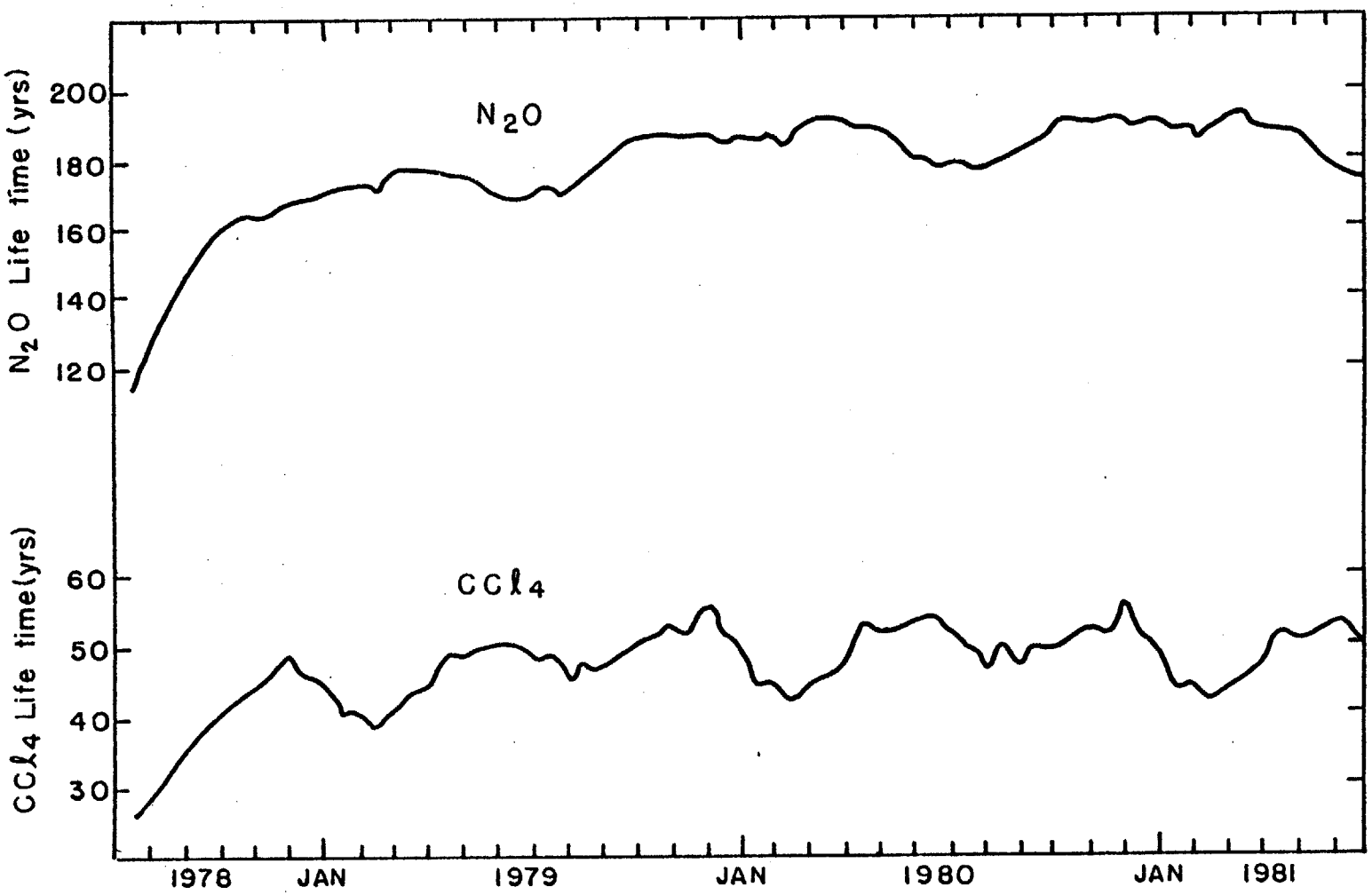


Figure 18 : CCl_4 and N_2O lifetime trends.

trends converge to an annual average value of ∿50 years for $CC\ell_4$ and of ∿180 years for N_2O. We are not aware of any previous estimates for the photochemical lifetime of $CC\ell_4$. For N_2O, values of 175, 150 and 159 were calculated respectively by Johnson *et al.* (1979) using a three-dimensional model, by Levy *et al.* (1979) using a three-dimensional model, and by Sze and Ko (1981), using a two-dimensional model. A strong semi-annual cycle in the lifetime of $CC\ell_4$ is found with minima in February and August, and maxima in June and December, very much like the lifetime oscillations calculated for $CFC\ell_3$. The nitrous oxide lifetime trend shows a semi-annual and also an annual cycle with a minimum in the northern hemisphere summer and a flat maximum in the northern hemisphere winter, similar to $CF_2C\ell_2$. The amplitude of this annual cycle for N_2O is small, due to the relatively small photochemical sink that this pollutant has in the stratosphere. for reasons discussed earlier, the short-lived tracers ($CC\ell_4$ and $CFC\ell_3$) we have a distinct semi-annual cycle in the lifetime trend, whereas for the longer lived tracers (N_2O and $CF_2C\ell_2$) the semi-annual cycle is weak or absent and replaced by a low amplitude annual cycle.

Trends of $CC\ell_4$ and N_2O in the five ALE station locations are given in Figure 19. Quantitative comparison of the trends in the five ALE station locations is given in Table 18. Again, the trends were obtained using weighted linear fits to the model and observed monthly-mean mixing ratios. Generally, the $CC\ell_4$ trends have much lower amplitude

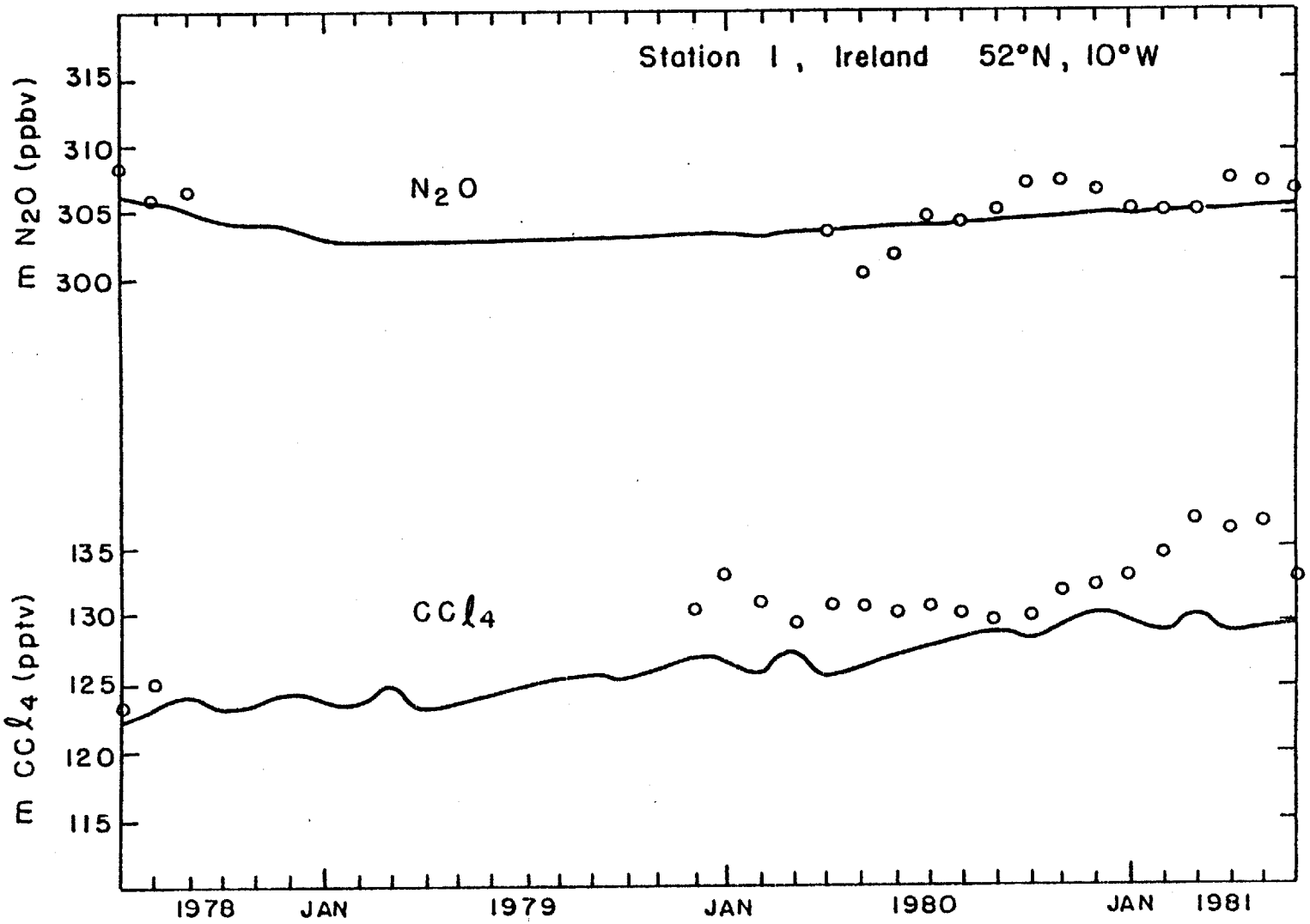


Figure 19a: CCl_4 and N_2O monthly-mean trends (calculated values are solid lines, and ALE measurements are open circles). Station 1, Ireland.

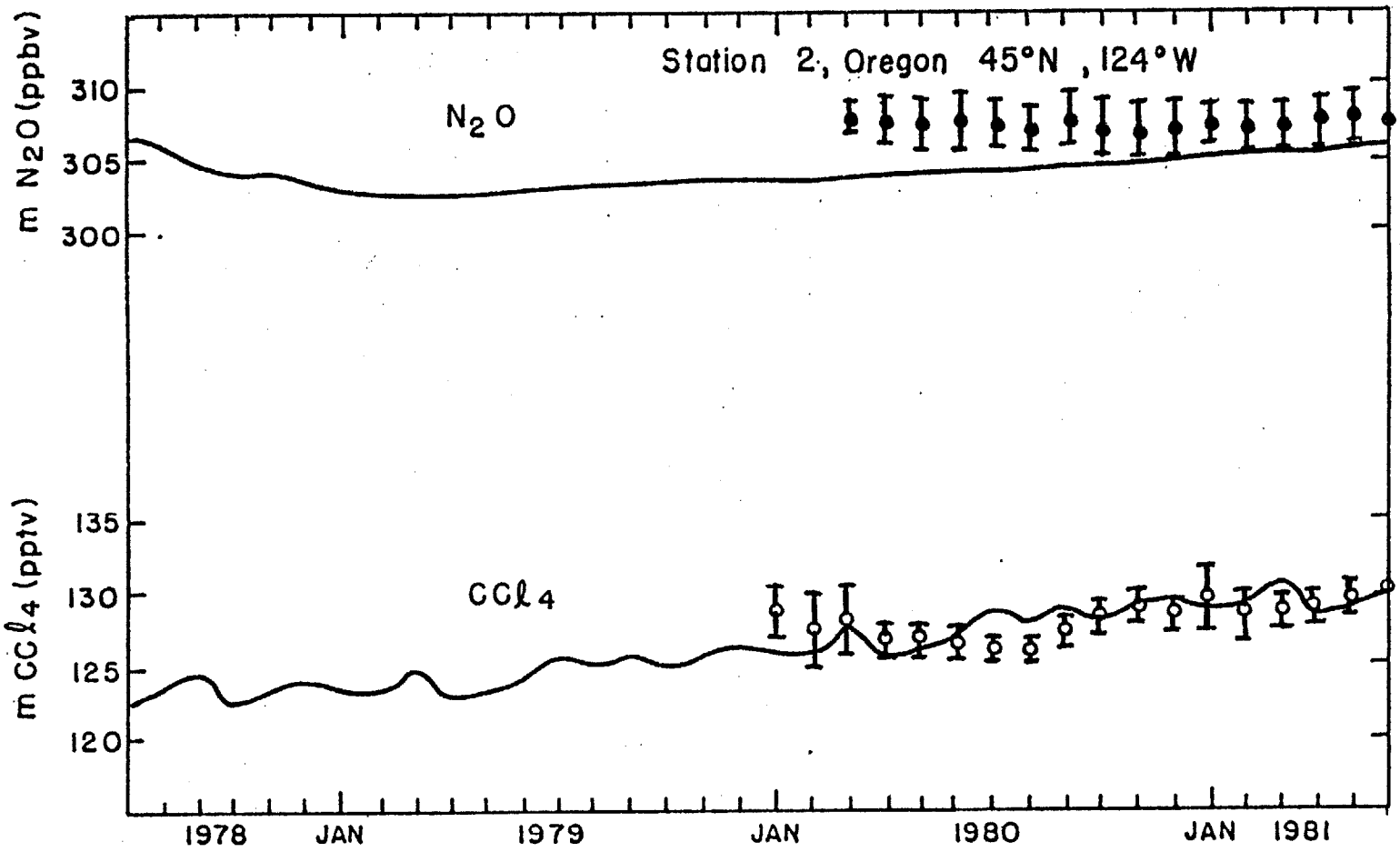


Figure 19b: Same as figure 19a, but for Station 2, Oregon.

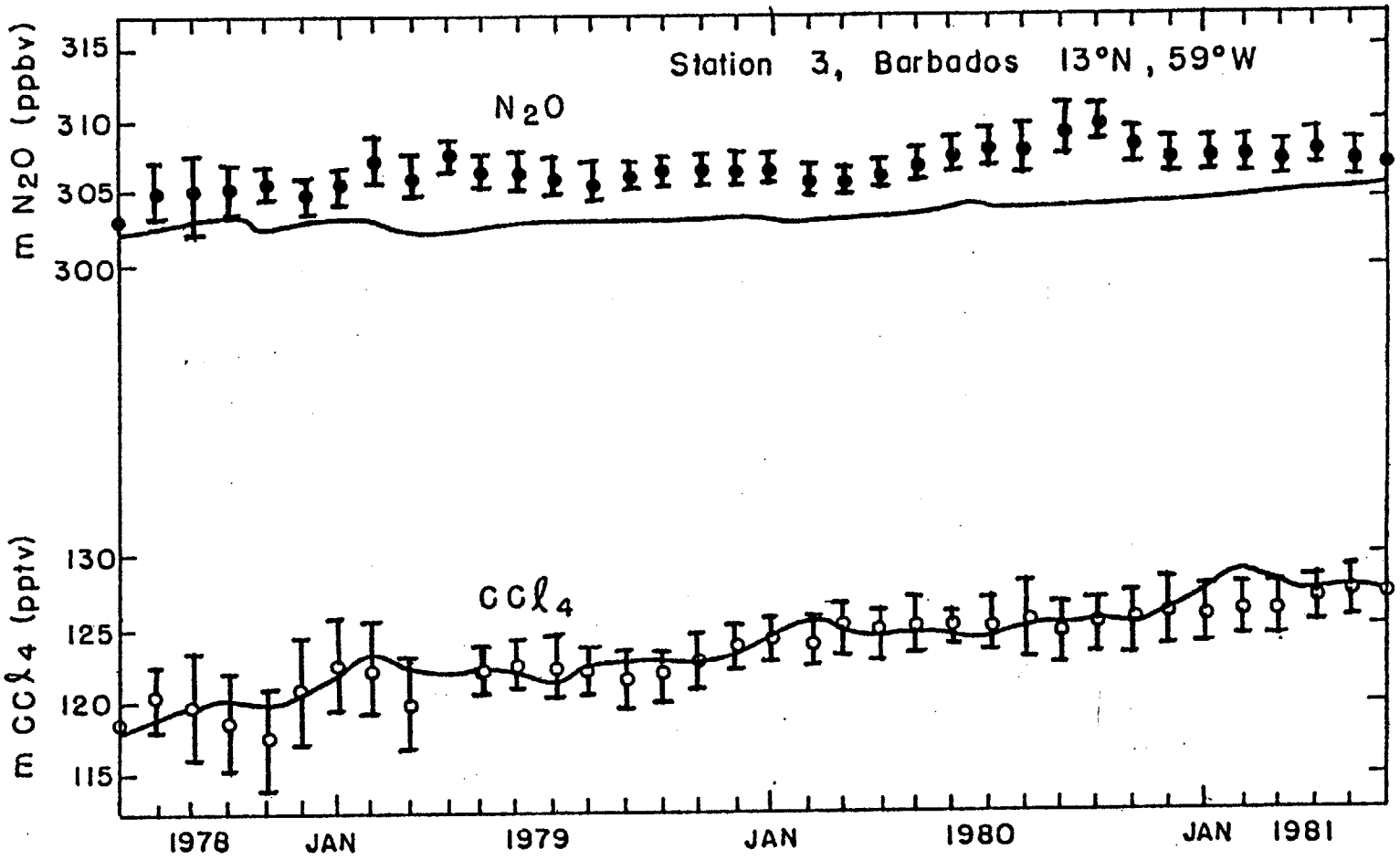


Figure 19c : Same as figure 19a , but for Station 3, Barbados.

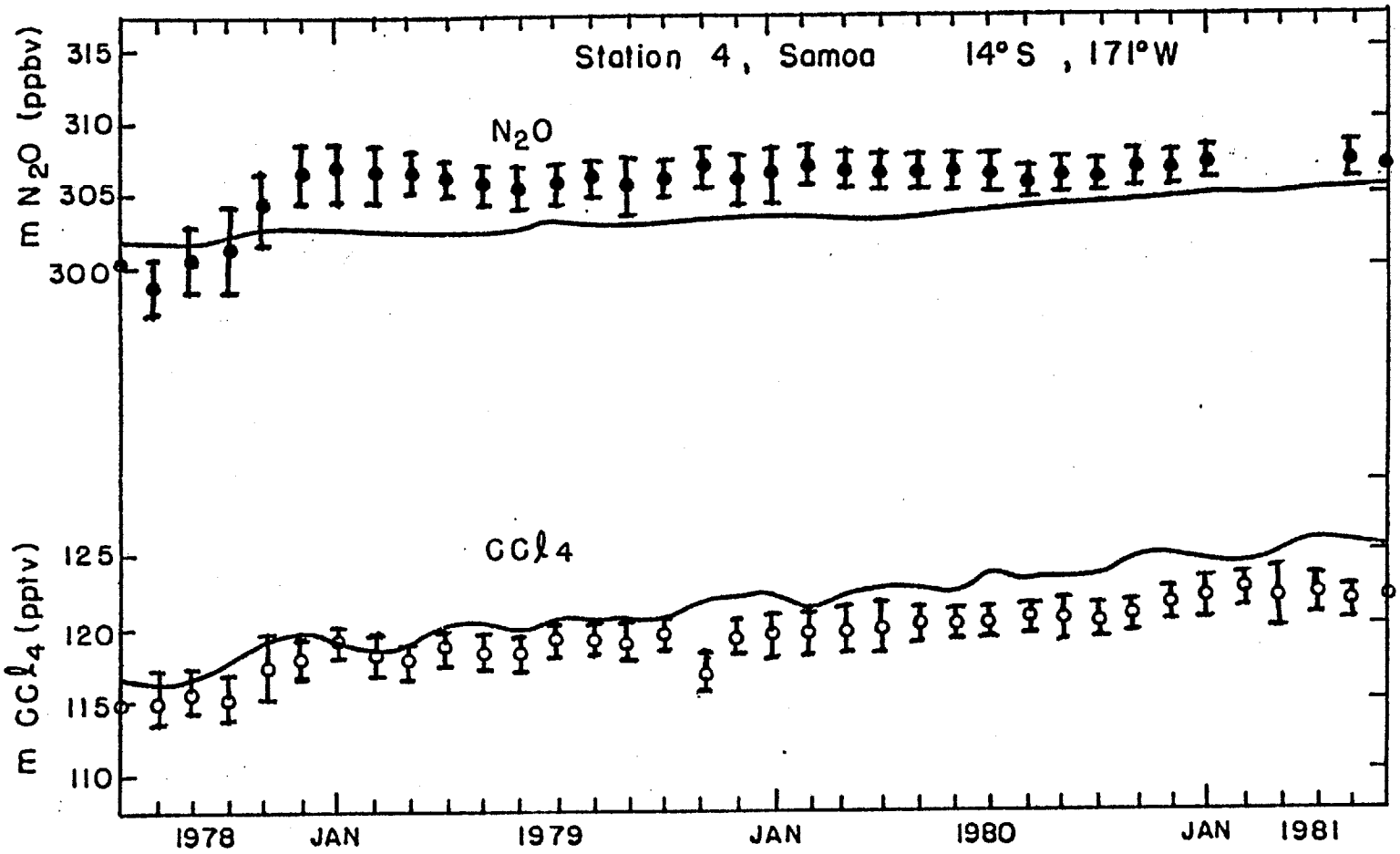


Figure 19d: Same as figure 19a, but for Station 4, Samoa.

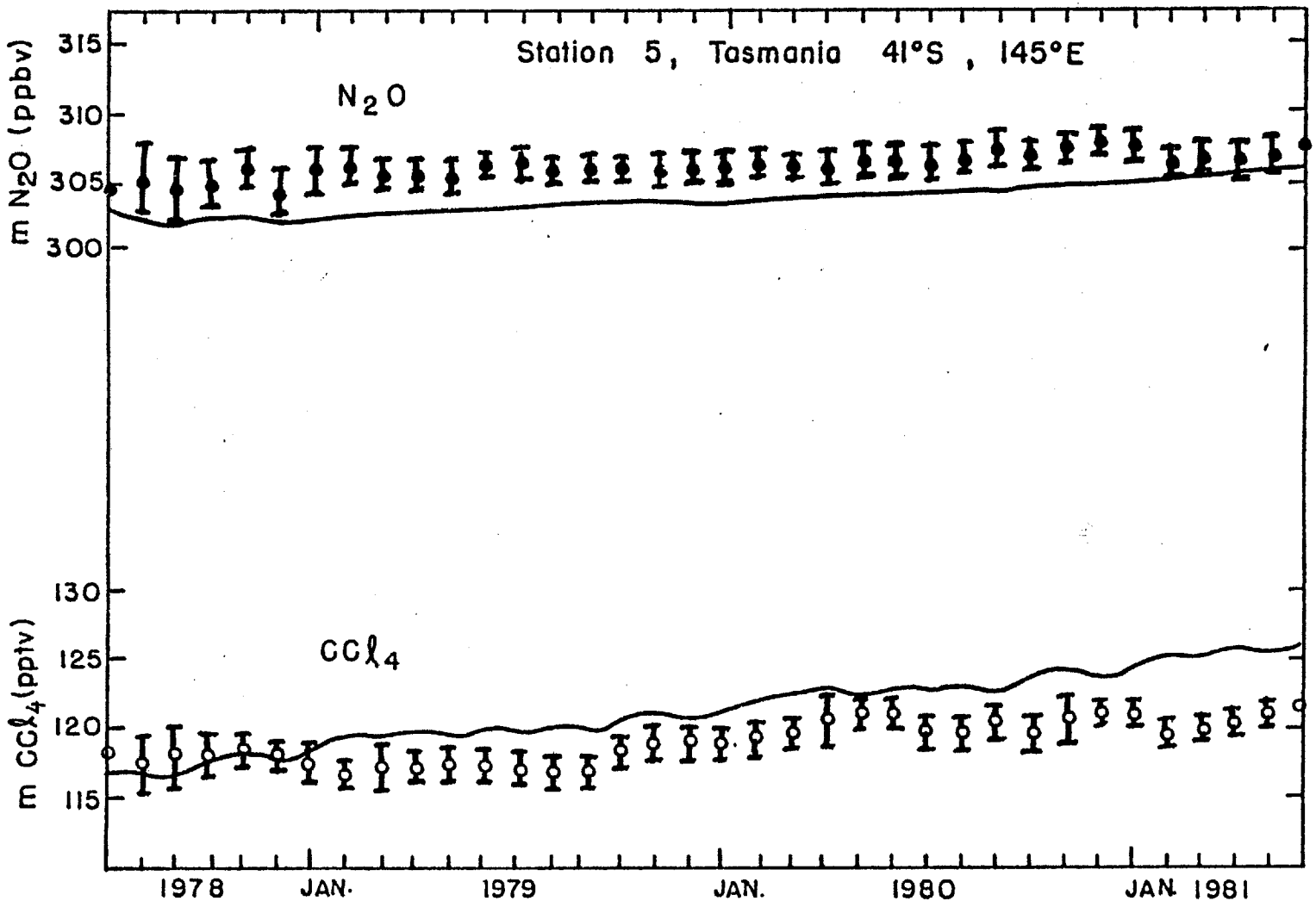


Figure 19e : Same as figure 19a , but for Station 5, Tasmania.

Table 18: CCl_4 and N_2O Experimental and Calculated Trends, based on Three Years of Data. Trends are in percent per year while mixing ratios m_0 and m_H are in pptv for CCl_4 and in ppbv for N_2O.

Station	Experimental			Calculated			
	trend	m_0	m_H	trend	m_0	m_H	
1	2.63±0.69*	129*	132*	2.03±0.12	122	126	
2	1.88±0.36*	126*	128*	1.96±0.13	122	126	
3	2.16±0.12	120	123	2.43±0.09	119	124	CCl_4
4	1.65±0.13	116	119	2.43±0.10	117	121	
5	1.22±0.14	117	119	2.57±0.08	117	121	
1	0.82±0.34*	304*	306*	0.29±0.04	302	304	
2	-*	-*	-*	0.27±0.05	303	304	
3	0.19±0.05	306	307	0.35±0.02	302	304	N_2O
4	0.24±0.06	305	306	0.41±0.02	302	303	
5	0.22±0.03	305	306	0.43±0.01	302	304	

* - not enough data.

fluctuations than those for $CFC\ell_3$ and $CF_2C\ell_2$ which appears to be due to the lower latitudinal gradient and much lower global trend for $CC\ell_4$.

The fit to the experimental trend of $CC\ell_4$ in ALE site 3, Barbados, is remarkably good. However, as for $CFC\ell_3$ and $CF_2C\ell_2$, we find a slight overestimate in the calculated southern-hemisphere trends of $CC\ell_4$, as compared to the experimental trends measured by ALE stations 4 and 5. Nitrous oxide trends are very smooth, due to the assumed homogeneous source. The comparison to the experimental trend for N_2O is influenced by the inhomogeneous initial experimental latitudinal N_2O distribution of July 1979, used to initialize the model integration (see also Figure 5b). The model tends to homogenize the N_2O surface distribution as integration is pursued because we have chosen a symetric N_2O source distribution over the surface of the globe between the latitudes 57.5°N and 57.5°S.

Nitrous oxide vertical profiles (zonally-averaged values) are compared to three sets of measurements in Figure 20. The general fit to measurements is good if we take into account the fact that the calculations are zonally averaged, and the measurements are single sets of measurements, corresponding to a specific time and location.

Zonally-averaged calculated surface distributions for $CC\ell_4$ and N_2O for June 30 and December 30, 1980 are given in Figure 21. The calculated latitudinal distribution is more

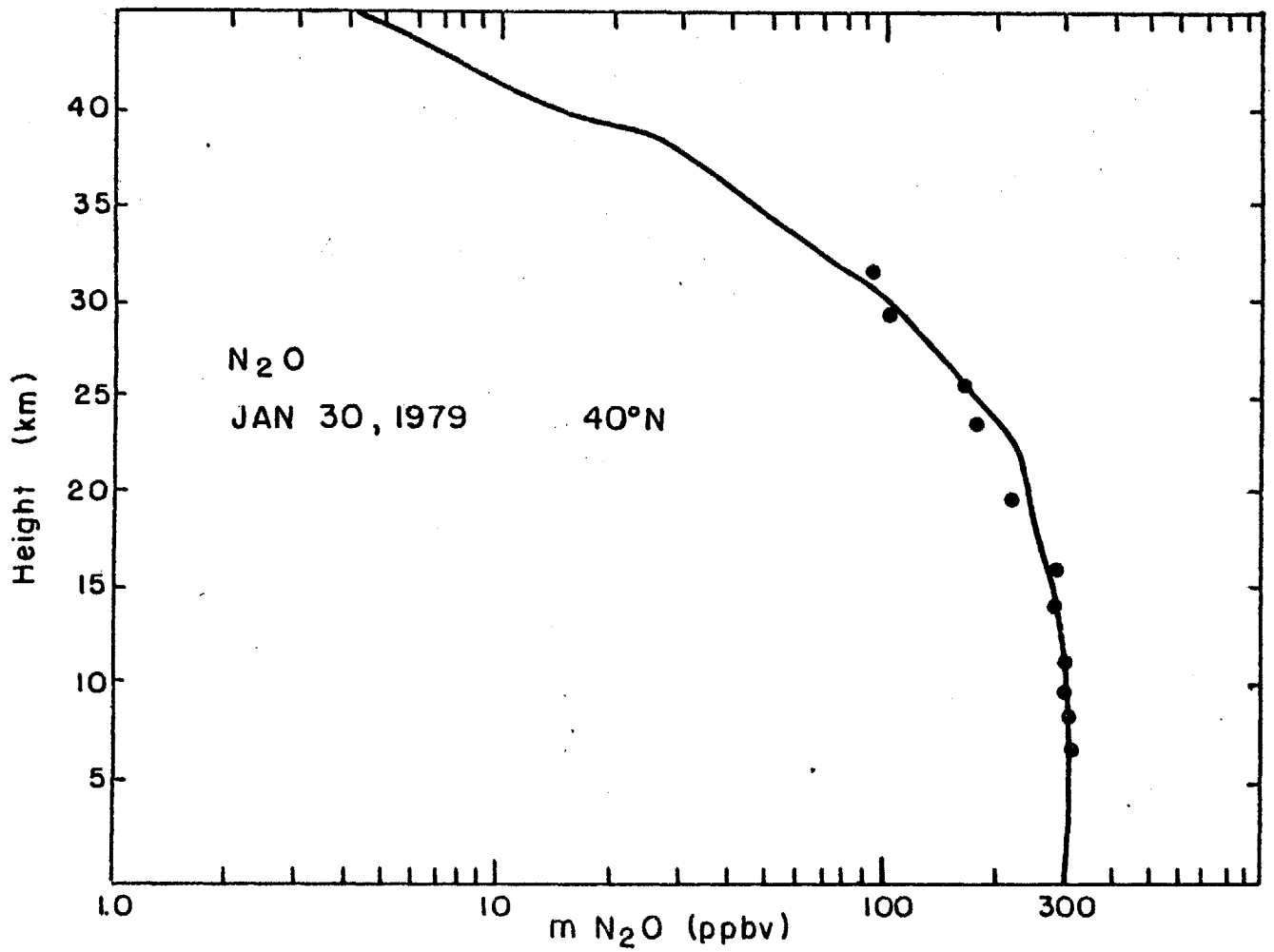


Figure20a : N_2O calculated vertical profile, solid line, for January 30, 1979 $40^{o}N$, zonally averaged, circles are measurements for February 1, 1979 $41^{o}N$, Goldan et al. (1980).

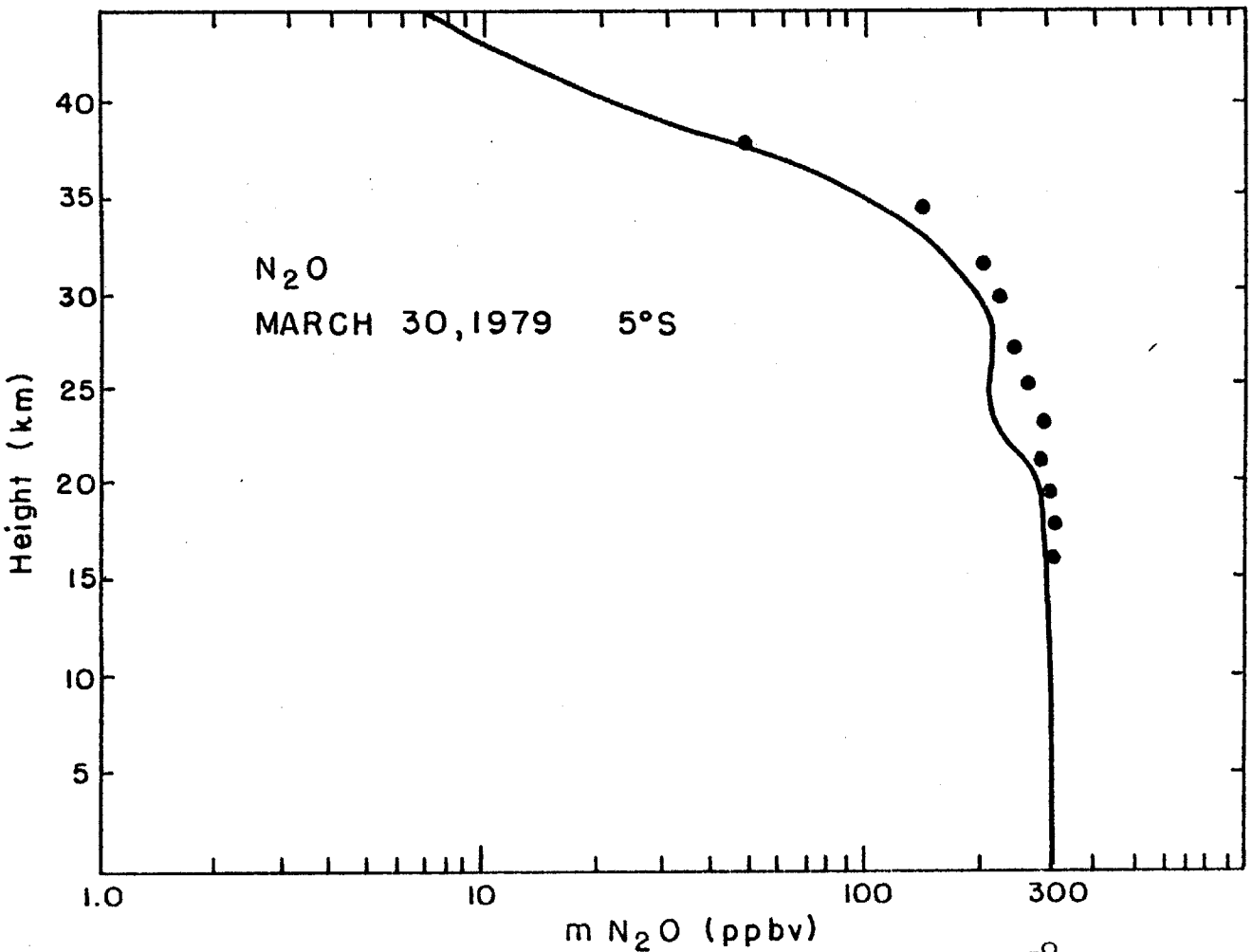


Figure 20b: Same as figure 20a, calculated line is for March 30, 1979 5°S, measurements were made on March 29, 1979 5°S, Goldan et al. (1980).

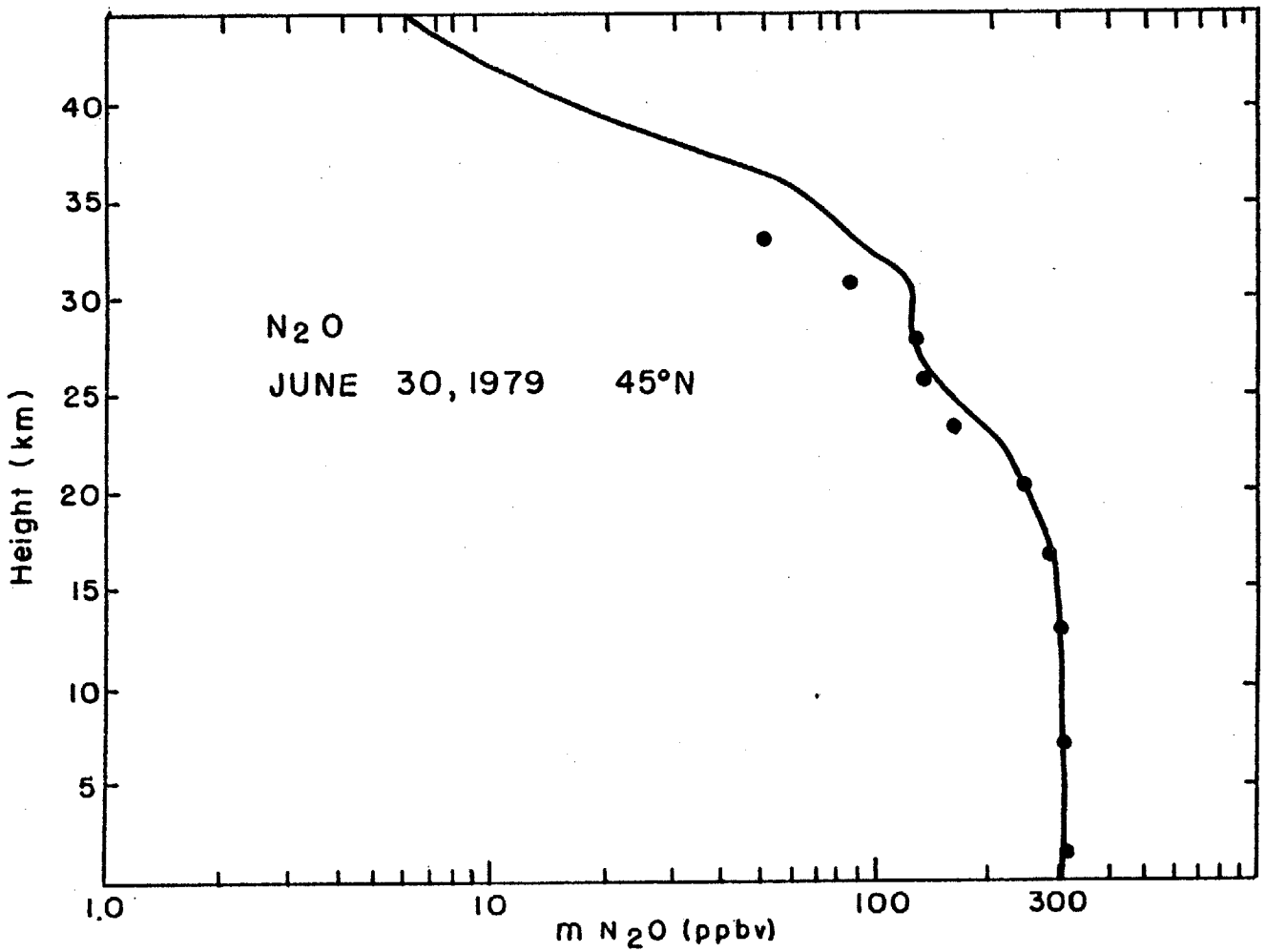


Figure 20c: Same as figure 20a , calculated line for June 30, 1979 45°N, measurements were made on June 28, 1979 44°N, Fabian et al. (1981).

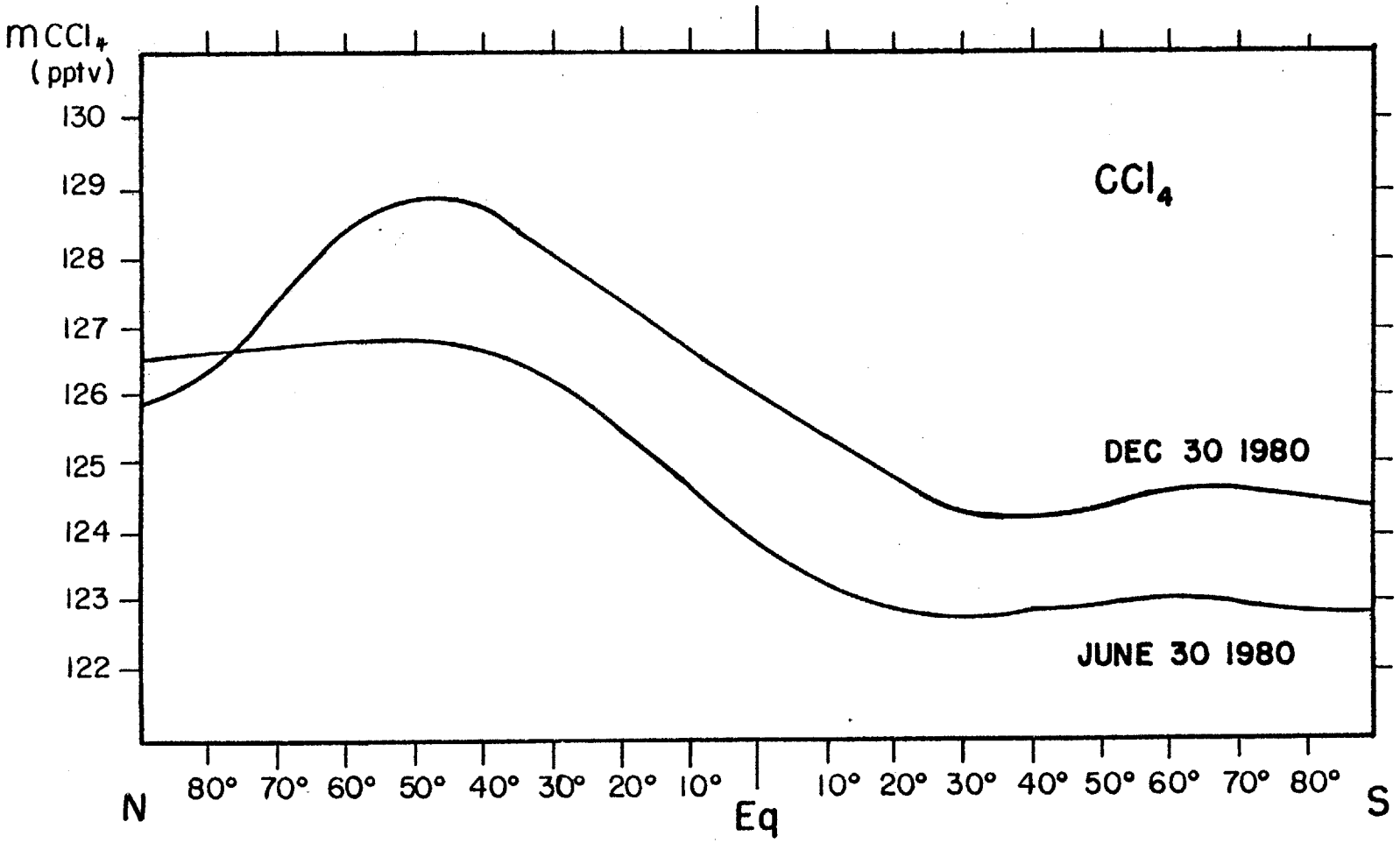


Figure 2la : CCl_4 zonally averaged calculated surface distribution, June 30 and December 30, 1980.

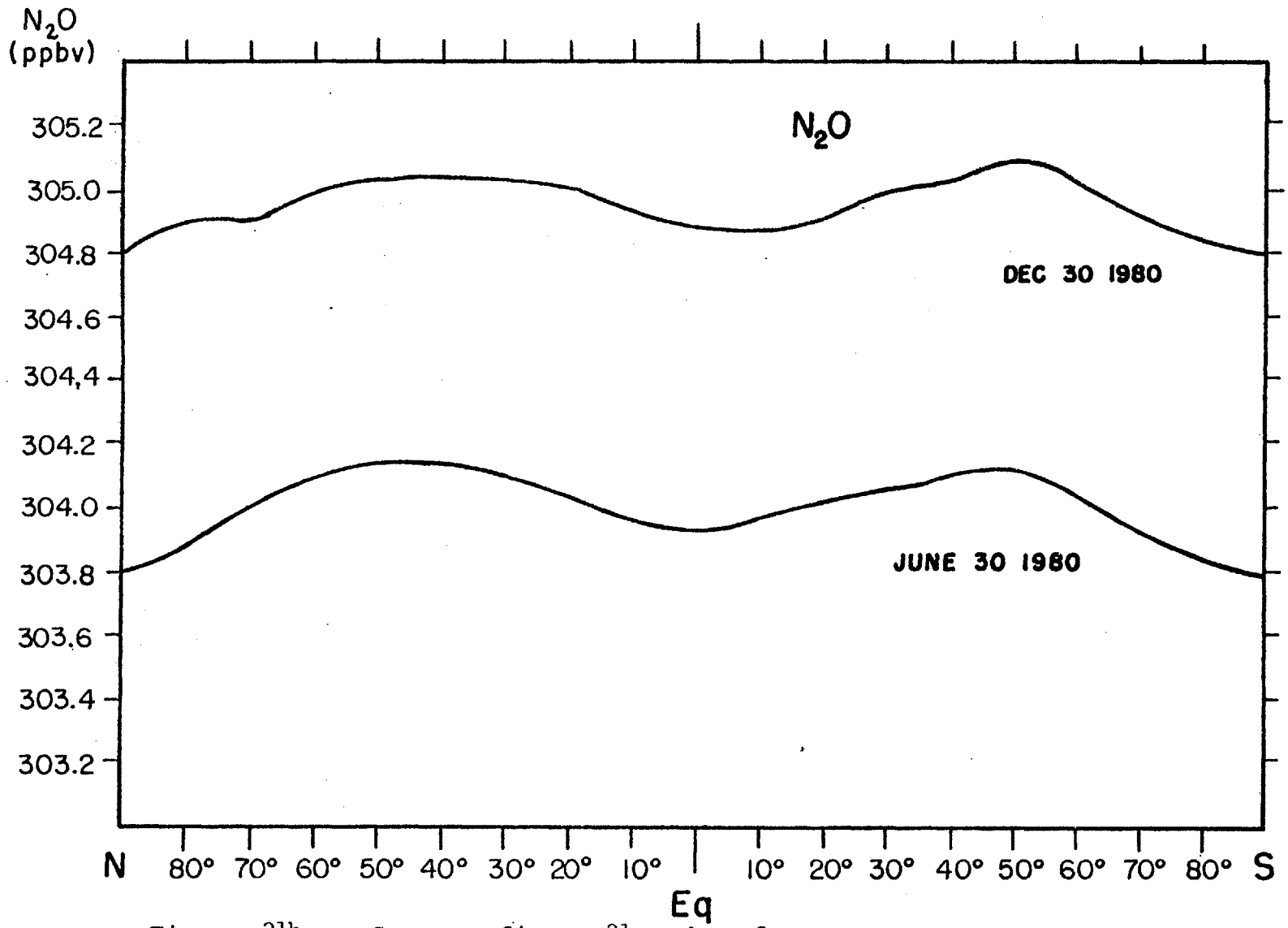


Figure 21b : Same as figure 21a , but for N_2O.

homogeneous than suggested by measurements (e.g., as published by Weiss (1981)). However, the disagreement is very small, since the measurements show the northern hemispheric N_2O concentration is only 0.8 ppb higher than the southern hemisphere.

Figures 22 and 23 show the zonally averaged calculated two-dimensional distribution of $CC\ell_4$ and N_2O respectively for December 30, 1980. The two-dimensional latitude-altitude distribution as calculated in our model, Figure 23 is similar to the results of the three-dimensional calculation of Levy *et al.* (1979) particularly in regard to the equator to pole gradients in the lower stratosphere.

Finally, in Figure 24 we show the calculated two-dimensional, latitude-longitude, $CC\ell_4$ surface distribution for the month of January 1981. This distribution, which is similar to those of $CFC\ell_3$ and $CF_2C\ell_2$, shows a persistent well-defined standing wave pattern in the northern hemisphere, corresponding to the location of the principal $CC\ell_4$ anthropogenic sources.

3.4 Discussion of the Results for $CFC\ell_3$, $CF_2C\ell_2$, $CC\ell_4$, and N_2O.

In order to compare the results for these four tracers some of the characteristic inputs for them will first be discussed. The source strength and distribution over the globe for $CFC\ell_3$ and $CF_2C\ell_2$ are rather accurately known due

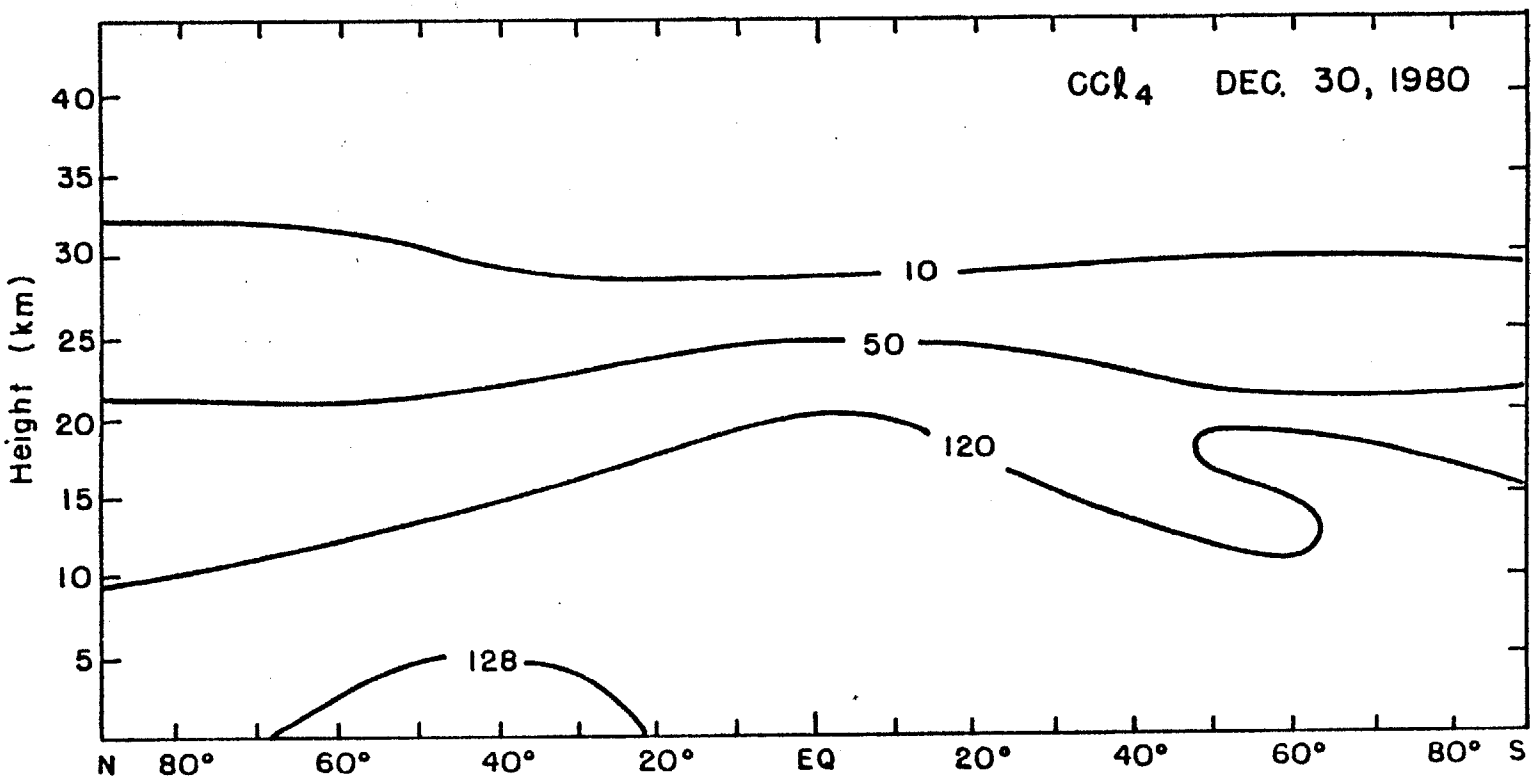


Figure 22 : Zonally averaged calculated 2-D CCl_4 distribution, December 30, 1980. (pptv).

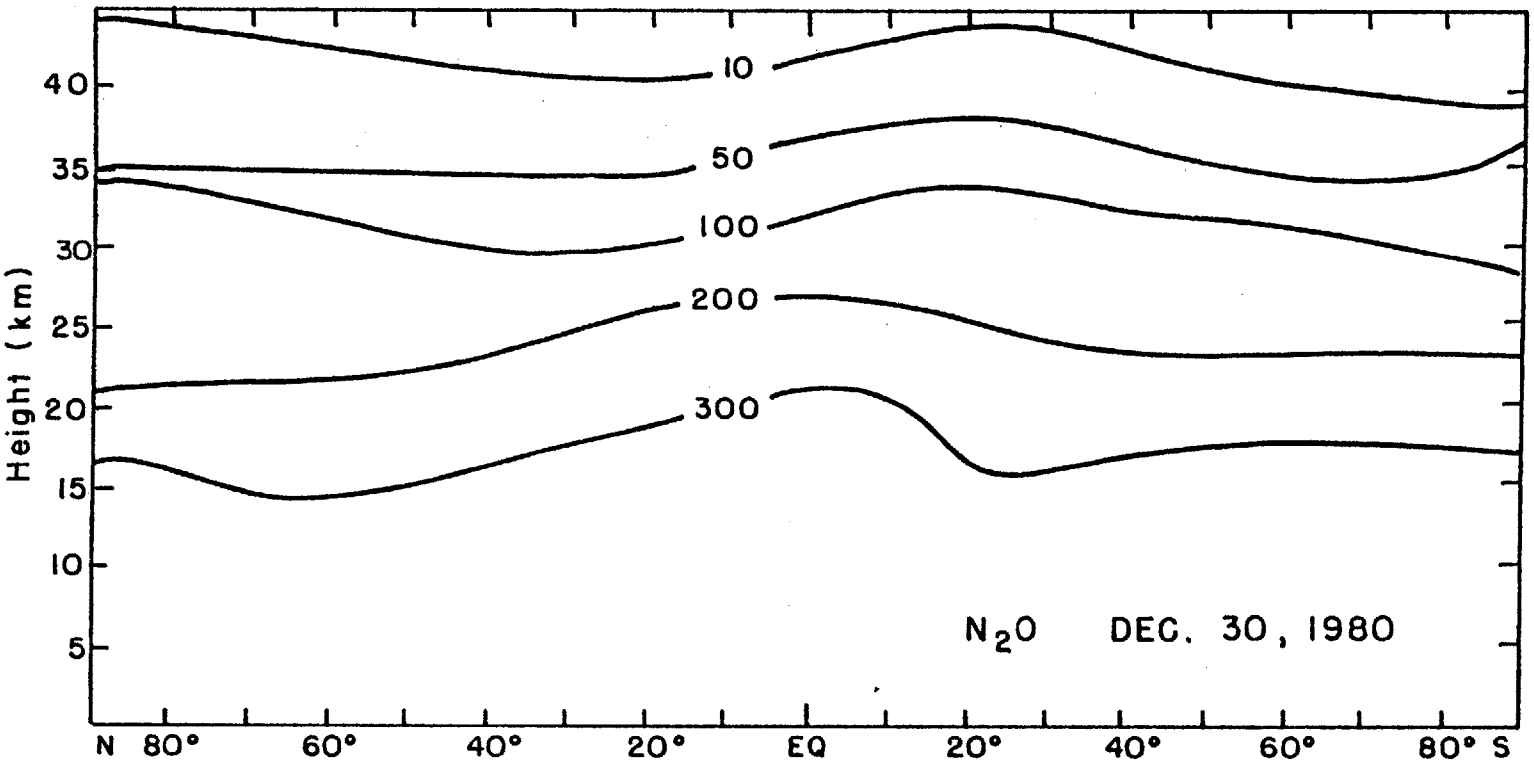


Figure 23 : Same as figure 22 , but for N_2O, (ppbv).

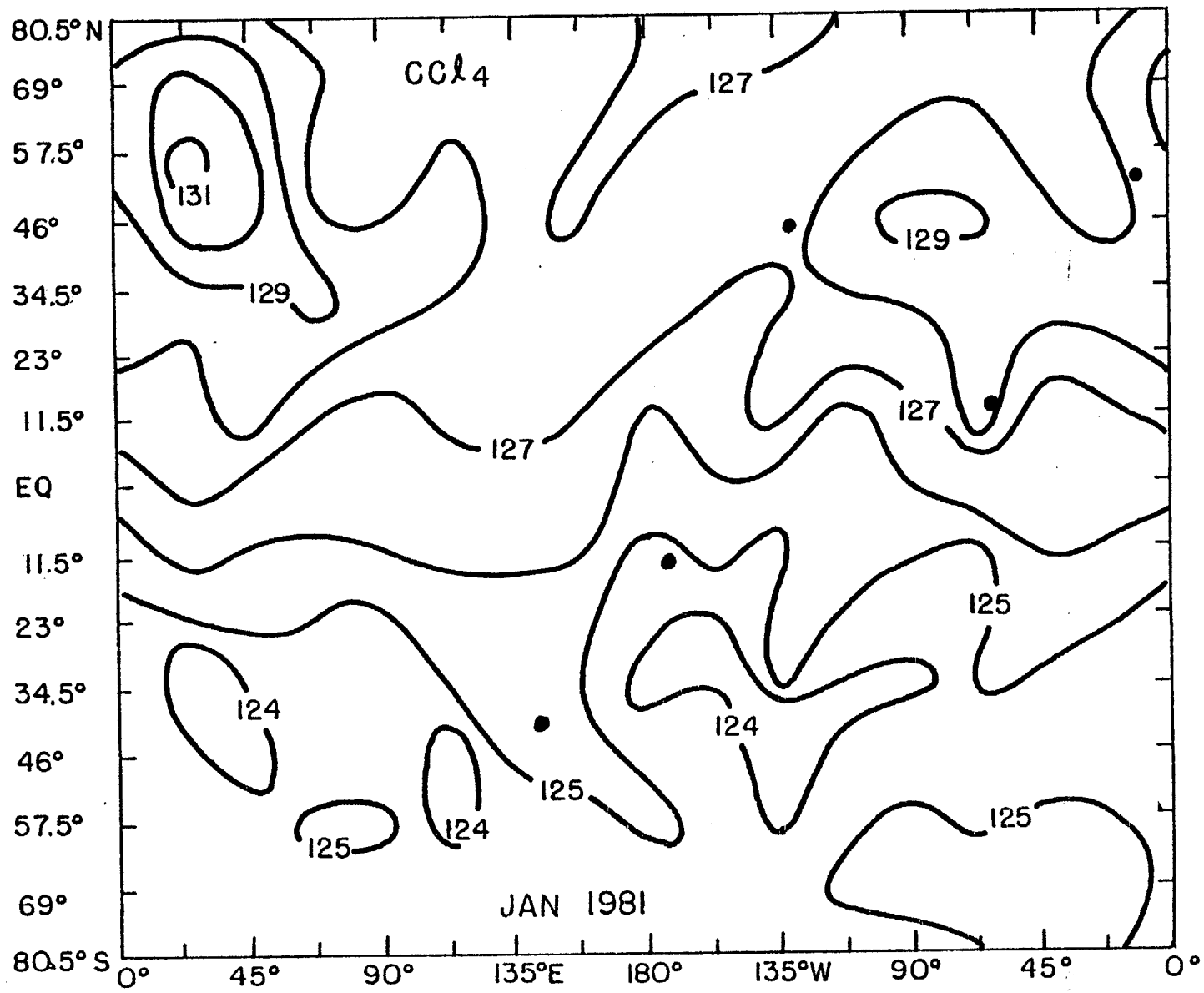


Figure 24: The 2-D CCl_4 surface distribution, January 1981 (pptv). Solid circles denote positions of ALE sites.

to the extensive studies made by the Chemical Manufacturers Association (CMA, 1981), and by Cunnold *et al.* (1982a, 1982b). The source strength and distribution for $CC\ell_4$ are much less accurately known (Simmonds *et al.*, 1982). The source strength for N_2O is currently only assessed so as to balance the photochemical dissociation in the stratosphere (Levy *et al.*, 1979), and an arbitrary homogeneous surface distribution is assumed between $\sim$57.5°N and 57.5°S. In spite of that, the general good fit of the model calculations to measurements by the ALE stations, implies that the chosen source strengths for $CC\ell_4$ and N_2O are not far from reality.

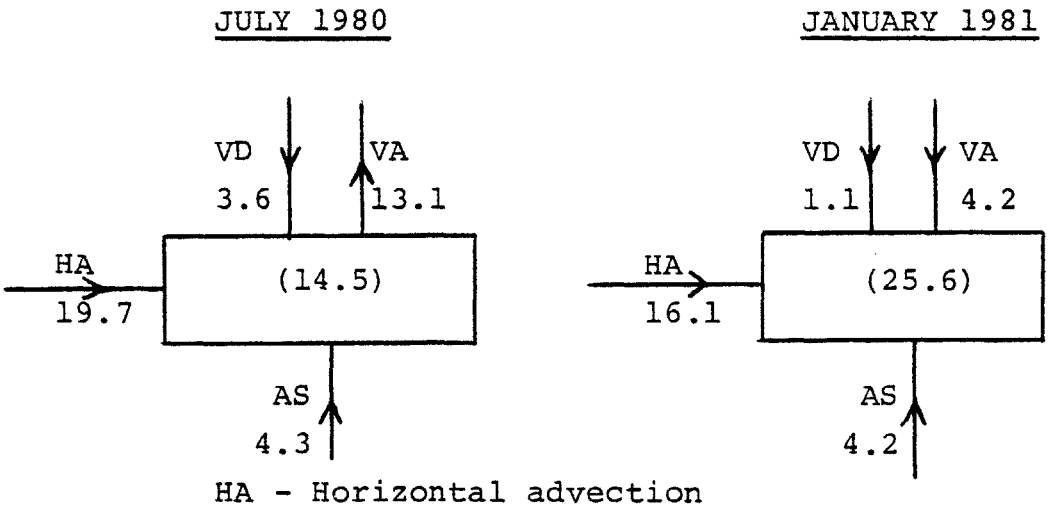
It seems that the model generally tends to slightly overpredict the trend in the southern hemisphere as judged by the model versus observed results for ALE sites 4 and 5 (Samoa and Tasmania). The calculated trends in the northern hamisphere are in contrast very close to the experimental trends.

There is reasonable agreement in the vertical profiles: there is a tendency for the model to overpredict stratospheric concentrations but some of the fits are, in contrast, very good. We can also compare absolute values of calculated mixing ratios to absolute values of measured mixing ratios. We find that along with the slight over-estimation of the trends in the southern hemisphere, the calculated values of the mixing ratios there, are also slightly too high when compared to measurements. Other than the slight overprediction

of trends and mixing ratios in the southern hemisphere we emphasize that the model is providing a remarkably good simulation of the spatial and temporal behaviour of $CFC\ell_3$, $CF_2C\ell_2$, $CC\ell_4$ and N_2O in the atmosphere. The success with these four compounds can therefore be regarded as a validation of the vorticities and vertical velocities used in the model for global-scale transport of trace species.

In order to illustrate this point and assess the possible sources of error leading to the over-prediction of trends in the southern hemisphere, we calculated the complete material flow in the model southern hemisphere bottom two layers (between levels 24 and 26). The calculation was done for the months of July 1980 and January 1981 (monthly averages) for $CFC\ell_3$ and is shown in Table 19. The net change in the southern hemisphere lower troposphere is governed by transport, and the ratio between transport and source terms is about 5:1 . If we look now at the error in estimating the southern hemisphere trends of $CFC\ell_3$ as compared to measurements (see Table 17), we find an overestimation of $\sim$14%. In order to produce this error for example during January 1981, the model transport is either 17% too large if there is no source error, or the southern hemisphere source term is 85% larger than reported by the CMA, if the model transport is perfect. In fact the CMA estimates of the southern hemisphere source are believed to be accurate to $\sim$10%. We conclude therefore that the model transport is $\sim$15% too large and this causes the effect found in the southern hemisphere.

Table 19: Material balance for $CFC\ell_3$ July 1980 and January 1981.
(units 10^6gm/time step of 2 hours)
The net change for the southern hemisphere 2 bottom layers is given in parentheses.



HA - Horizontal advection

VA - Vertical advection

VD - Vertical diffusion

AS - Anthropogenic source

In order to see the relative magnitudes of the various terms contributing to $\frac{\partial m}{\partial t}$ at each model layer we calculated them as horizontal averages for the same months, i.e. July 1980 and January 1981. We summarized the results of this calculation in Table 20. In this table we show the contribution to $\frac{\partial m}{\partial t}$ by vertical advection (the horizontally averaged horizontal advection is zero), vertical diffusion, chemistry (photochemical dissociation) and by sources (anthropogenic surface source) for $CFC\ell_3$ in model layers 12 - 25 (or between model levels 12 - 26). We expressed the contributions as 10^6 gm / time step (of two hours) in each of the layers and in the whole atmosphere. It is clear that vertical diffusion is unimportant in comparison to advection by the specified vertical winds throughout the stratosphere. Accuracy of the vertical transport in the model stratosphere, judging from comparison to measurements (see Figure 11) is good. For the troposphere where on the average the vertical eddy diffusion is comparable to vertical advection, the validity of the vertical transport is equally divided between estimates of K_d values and W values there.

The next compound we will discuss, methyl-chloroform is more complicated than these latter four compounds because its chemical lifetime is not much longer than the global transport time and it has a recognized tropospheric destruction

Table 20: Contribution to the mixing ratio prediction equation of $CFC\ell_3$ July 1980 and January 1981, monthly averages.
(units 10^6gm/time step of 2 hours)

Layer	Vertical diffusion		Vertical advection		Chemistry		Source	
	7/80	1/81	7/80	1/81	7/80	1/81	7/80	1/81
12	0.0001	0.0002	0.02	0.03	-0.05	-0.06	0.0	0.0
13	0.001	0.001	0.11	0.15	-0.12	-0.15	0.0	0.0
14	0.006	0.006	0.47	0.62	-0.50	-0.56	0.0	0.0
15	0.02	0.02	1.4	1.8	-1.5	-1.6	0.0	0.0
16	0.04	0.04	3.1	3.7	-2.7	-3.0	0.0	0.0
17	0.08	0.08	5.0	5.1	-2.9	-3.3	0.0	0.0
18	0.07	0.06	4.5	2.7	-2.1	-2.3	0.0	0.0
19	-0.03	-0.07	-0.9	-6.0	-1.0	-1.2	0.0	0.0
20	-0.1	-0.09	-5.4	-11.5	-0.31	-0.35	0.0	0.0
21	-0.03	0.01	-1.9	0.6	-0.06	-0.07	0.0	0.0
22	0.08	3.4	8.3	10.0	-0.01	-0.009	0.0	0.0
23	8.2	15.3	7.3	-0.7	0.0	0.0	0.0	0.0
24	7.1	6.9	-8.1	-4.8	0.0	0.0	15.0	14.4
25	-15.4	-25.6	-13.9	-15.4	0.0	0.0	45.0	43.2
Total	-0.01	-0.02	-0.01	-0.01	-11.4	-12.6	60.0	57.6

mechanism dependent on a presently very poorly known distribution of atmospheric OH radicals. Thus while our simulations of $CFC\ell_3$, $CF_2C\ell_2$, $CC\ell_4$, and N_2O are dependent largely on the model circulation and assumed source strengths, our simulation of $CH_3CC\ell_3$ will depend also on the OH tropospheric distribution. Thus $CH_3CC\ell_3$ is not by itself useful for validation of our model transport. This is the reason why we discuss its model runs last -- the validity of the transport in our model is determined by the simulation of the other four species.

3.5 Results for Methyl-chloroform

The main problem with $CH_3CC\ell_3$ is to find the correct OH distribution in the troposphere since reaction with OH is the dominant sink for $CH_3CC\ell_3$. An initial guess tropospheric OH distribution was chosen from Volz *et al.* (1981) who used the reaction with CO and measurements of ^{14}CO to indirectly

assess the OH concentrations. This distribution suggests only a small difference between hemispheres. In stratospheric levels, as mentioned earlier, the GIT/MIT stratospheric model run No. 34 OH distribution was used (see Table 14). At both stratospheric and tropospheric levels, a two-dimensional OH distribution was used (no longitudinal variation), and a seasonal dependence was included (simple sinusoidal time dependence between the winter and summer initial distributions). The initially guessed total OH tropospheric content which was obtained from Volz *et al.* (1981) was in general multiplied by an unknown dimensionless factor F of order unity. Using F values of 0.06, 2.0, and 5.0, the predicted $CH_3CC\ell_3$ trends at the locations of the five ALE stations are shown in Figure 25. An assymetric behavior is immediately observed for the two hemispheres in these runs (denoted as Run A). We apparently need a smaller F in the northern hemisphere than in the southern hemisphere. A run with such a tropospheric OH distribution (Run B), was performed where the original Volz *et al.* (1981) OH troposphere distribution was multiplied by a factor F = 0.5 in the northern hemisphere, F = 0.75 in the equator, and F = 1.0 in the southern hemisphere. The assumed OH distribution is plotted in Fig. 26a, b. The trends for this run are given graphically in Figure 27. and in tabular form in Table 21 It was found that in the northern hemisphere the calculated trends are lower than the experimental trends, while

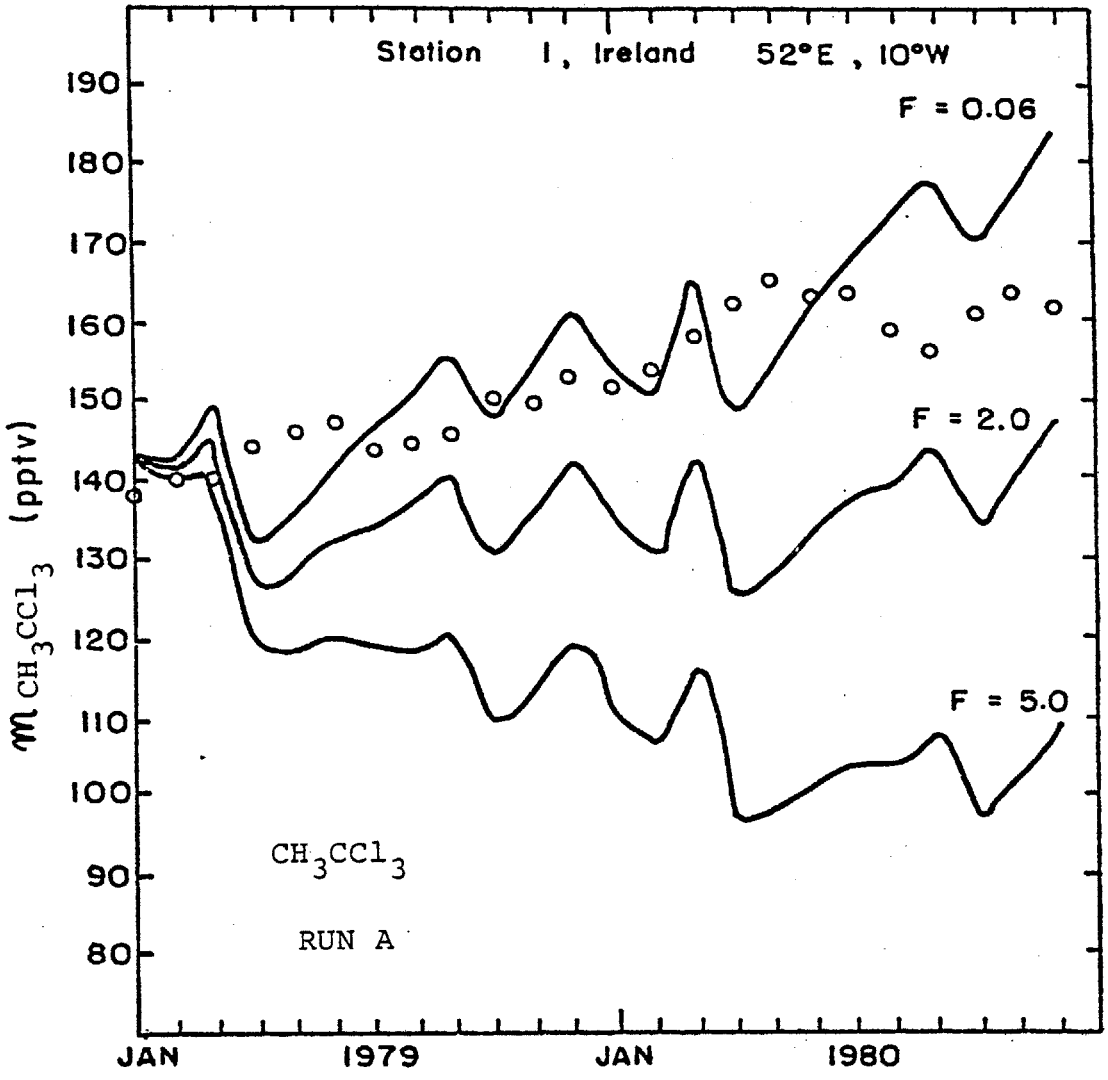


Figure 25a : CH_3CCl_3 monthly-mean trends, solid lines. F denotes factor multiplying the Tropospheric OH distribution. Open circles are ALE measurements. Station 1, Ireland.

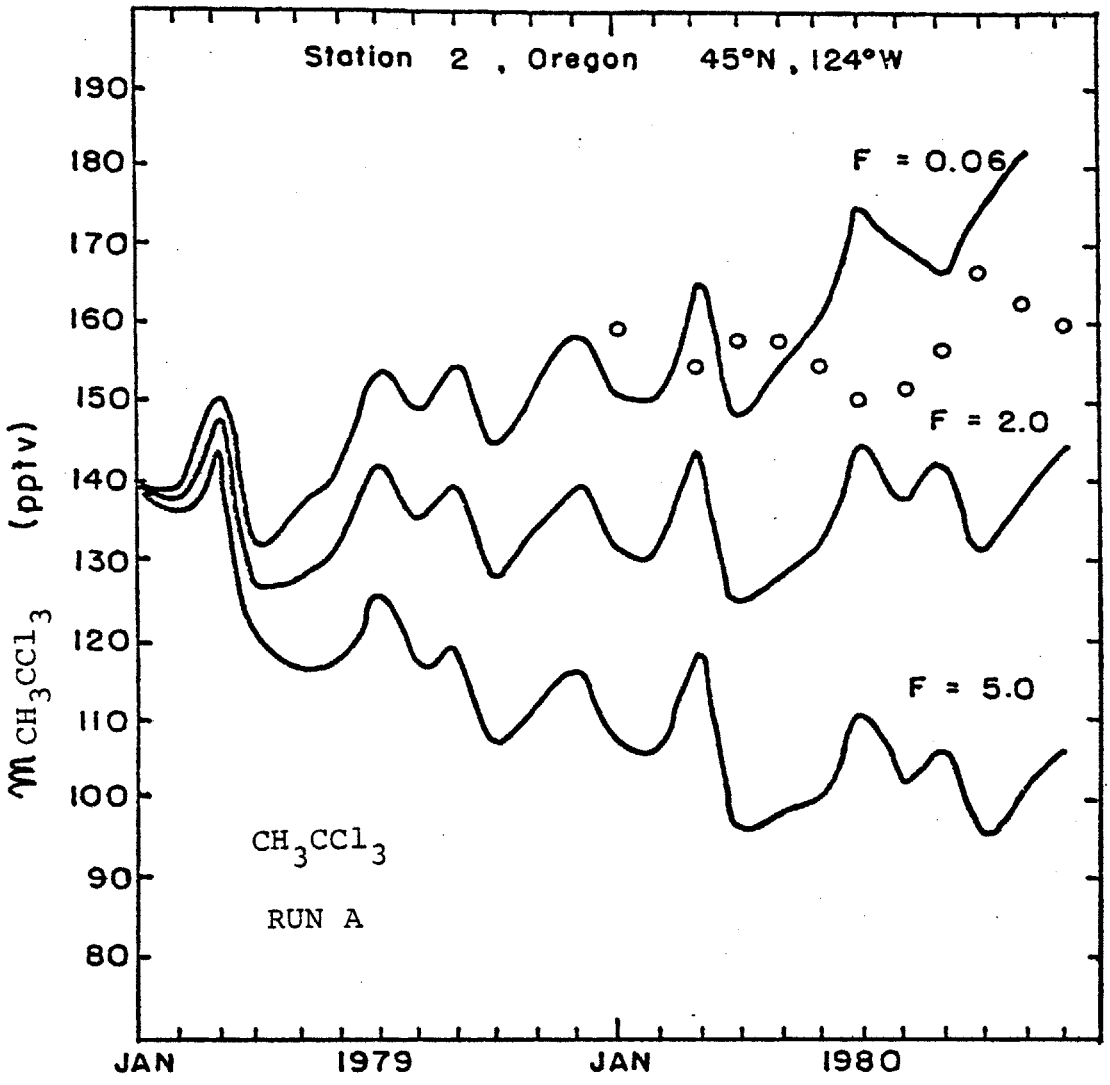


Figure 25b : Same as figure 25a, but for Station 2, Oregon.

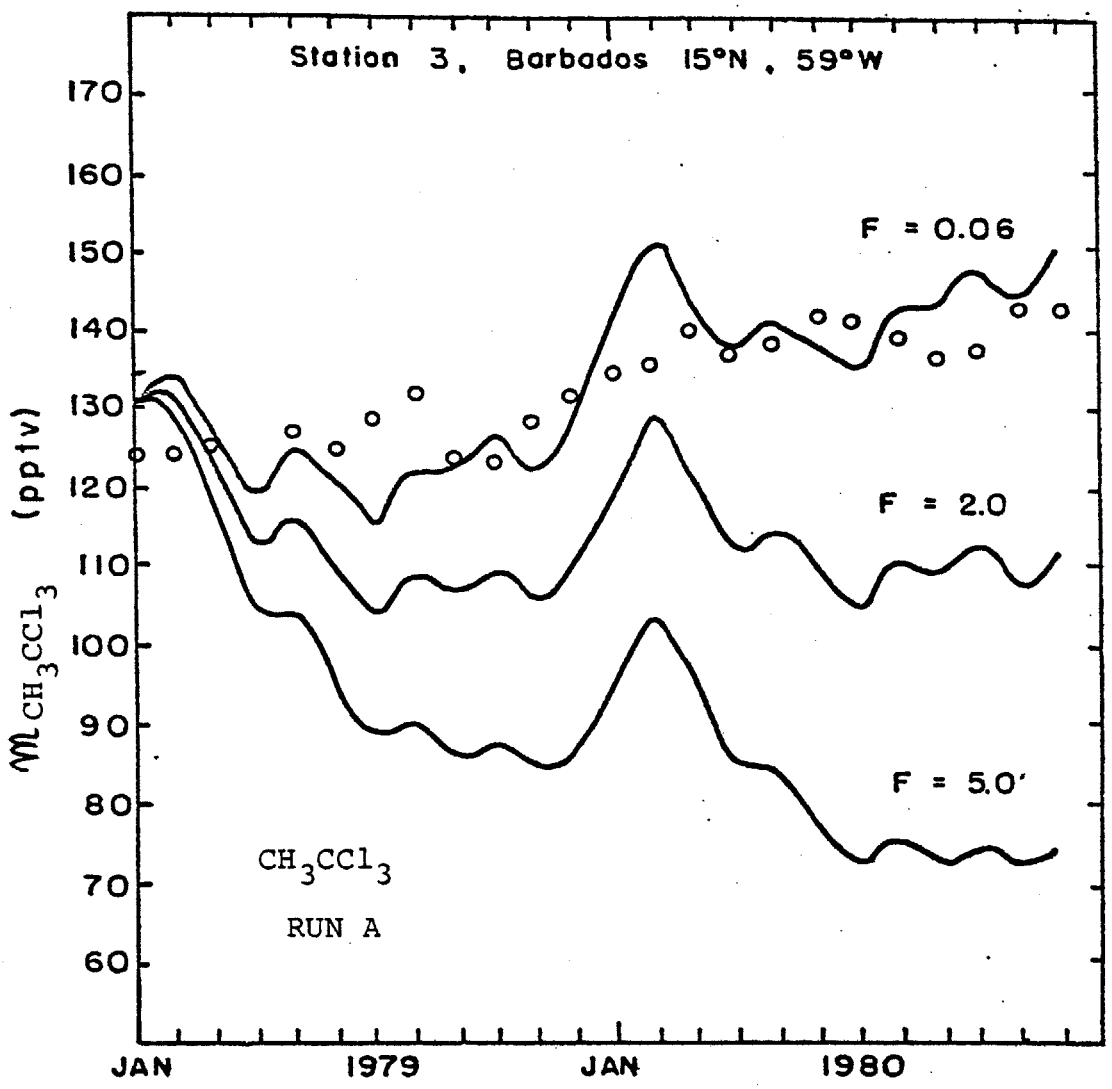


Figure 25c : Same as figure 25a , but for Station 3, Barbados.

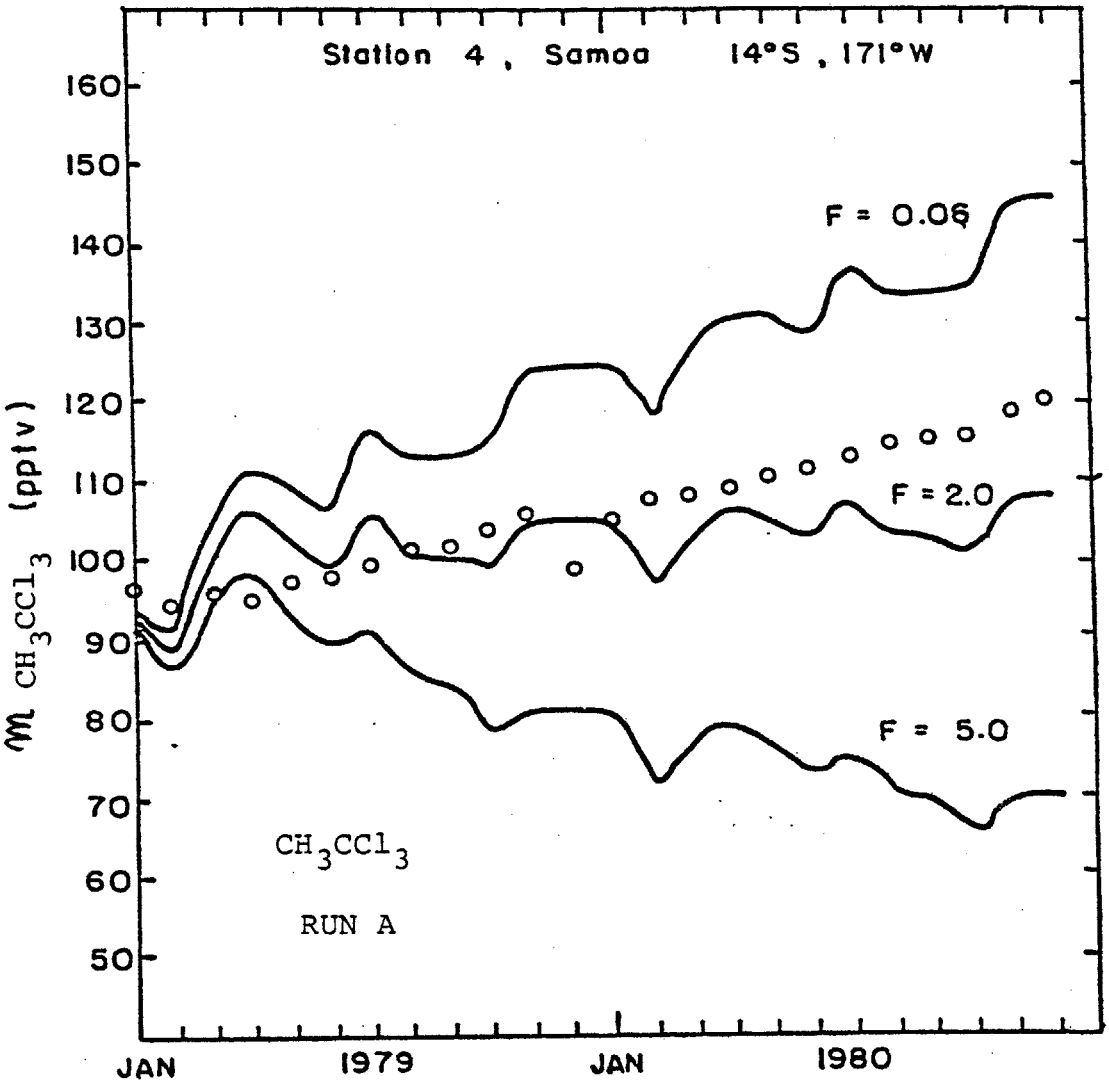


Figure 25d: Same as figure 25a , but for Station 4, Samoa.

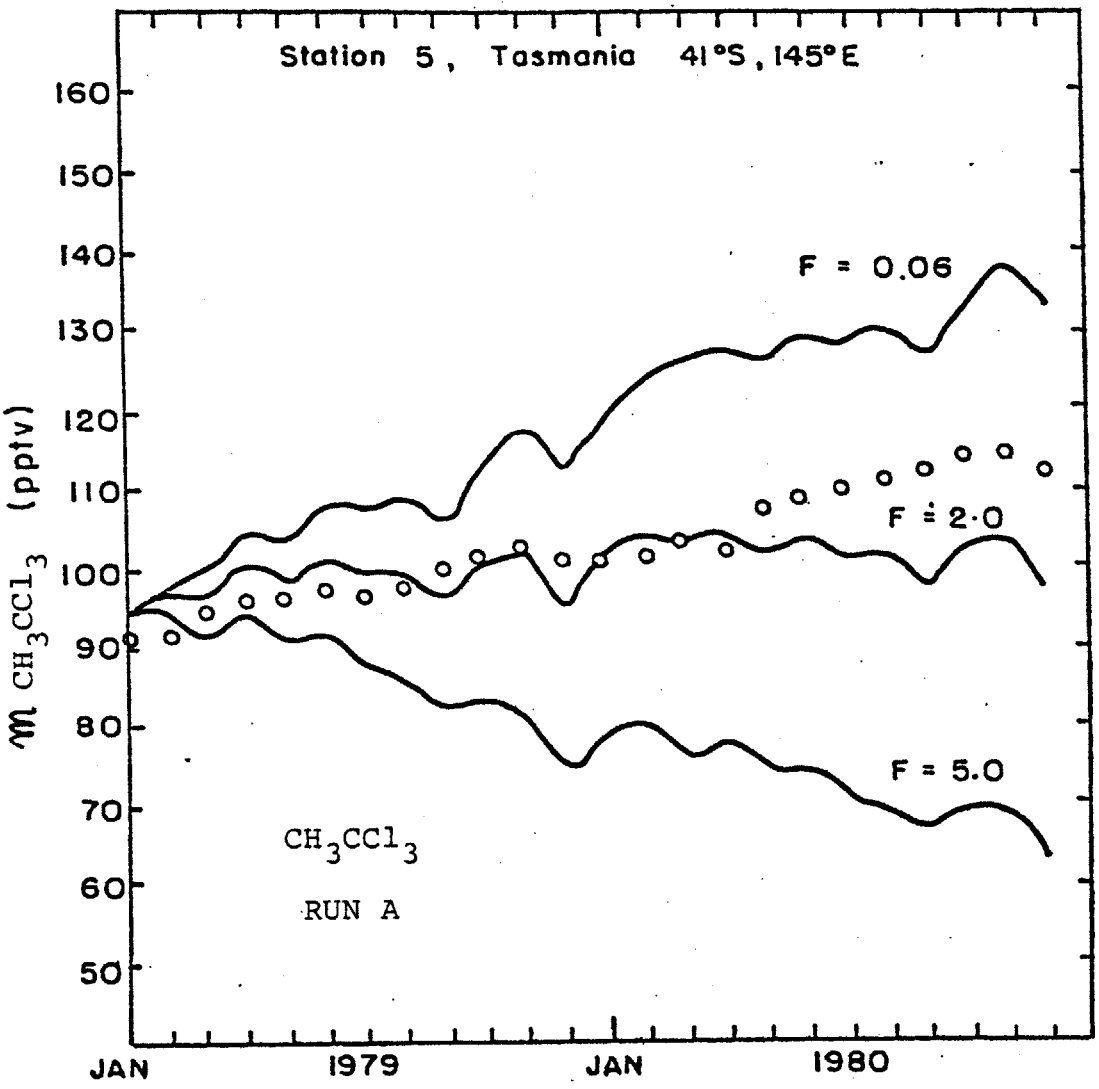


Figure 25e : Same as figure 25a, but for Station 5, Tasmania.

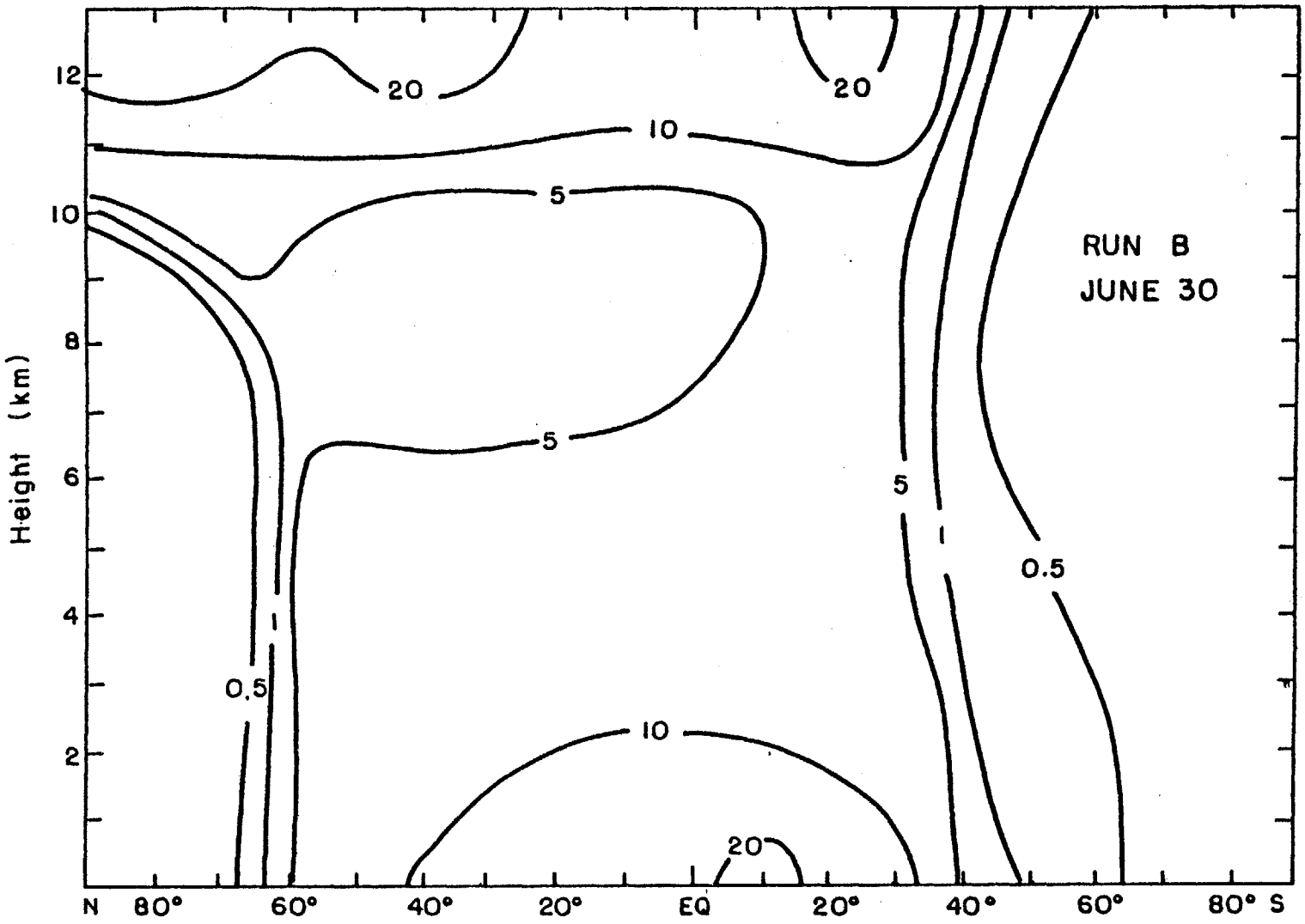


Figure 26a : Tropospheric OH distribution (daily averaged values) as used in RUN B, June 30, (10^5 molecules cm^{-3}).

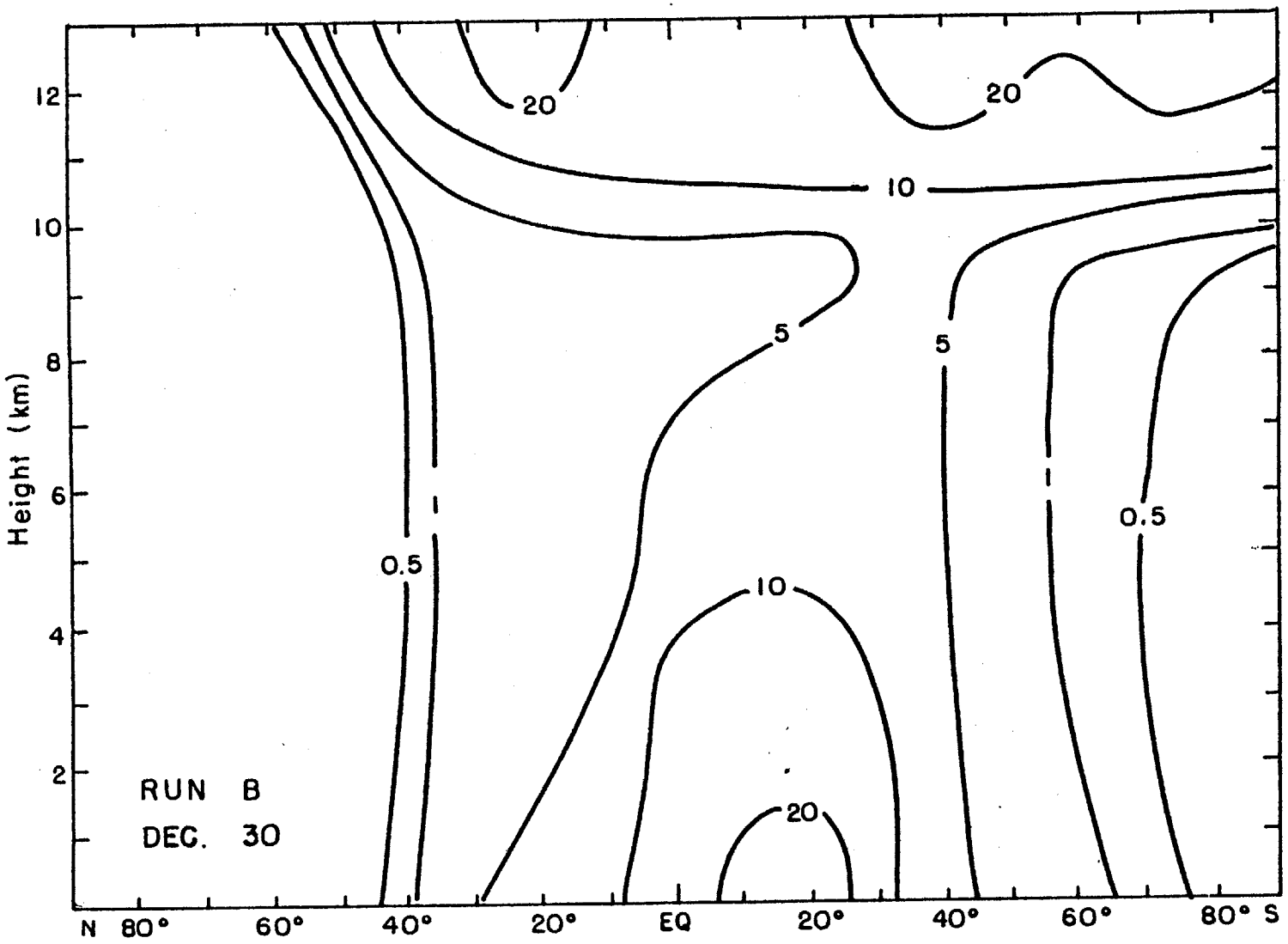


Figure 26b : Same as figure 26a , but for December 30.

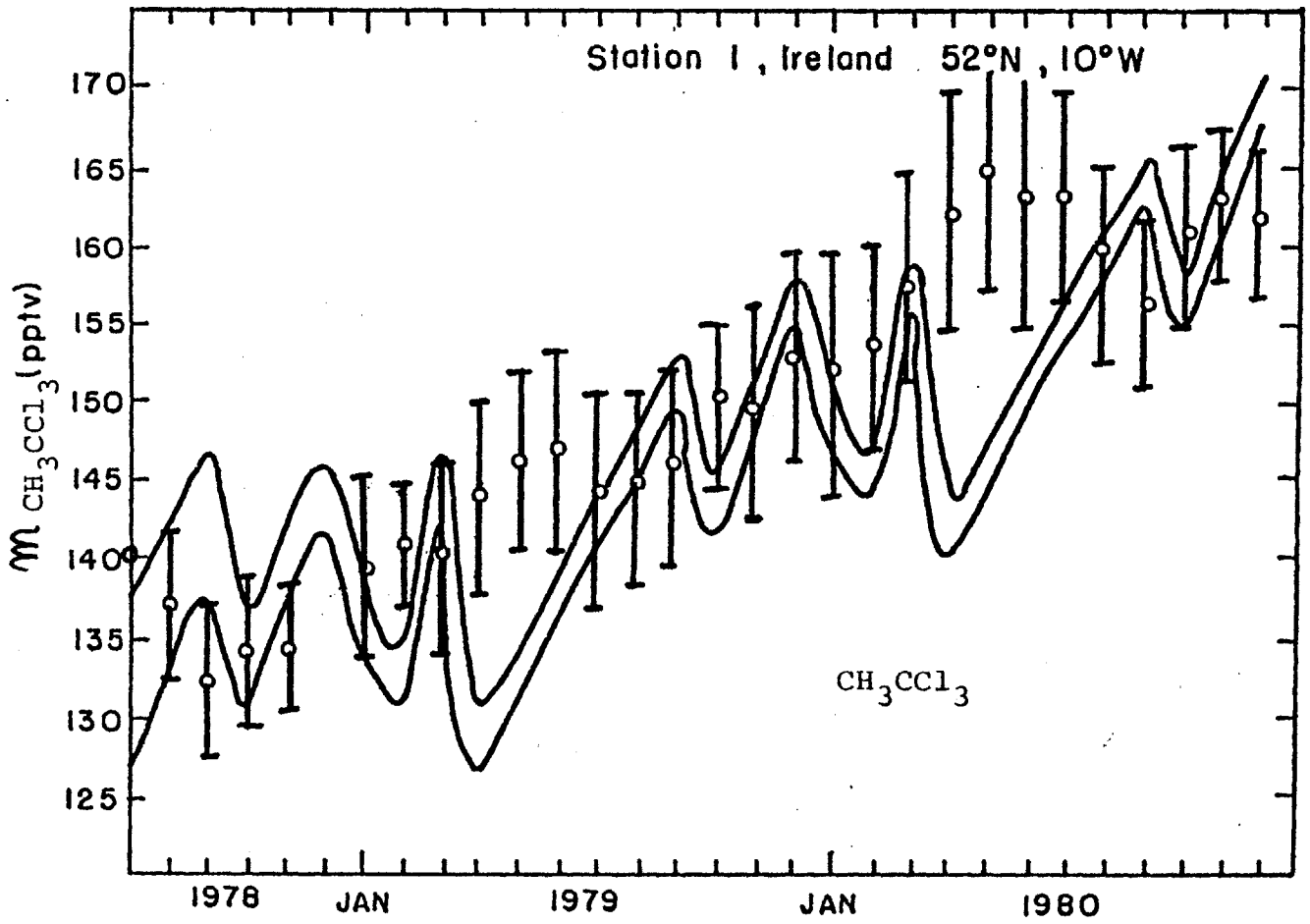


Figure 27a : CH_3CCl_3 RUN B and RUN F, calculated monthly-mean trends , solid lines (upper line is RUN B), open circles are ALE measurements, Station 1, Ireland.

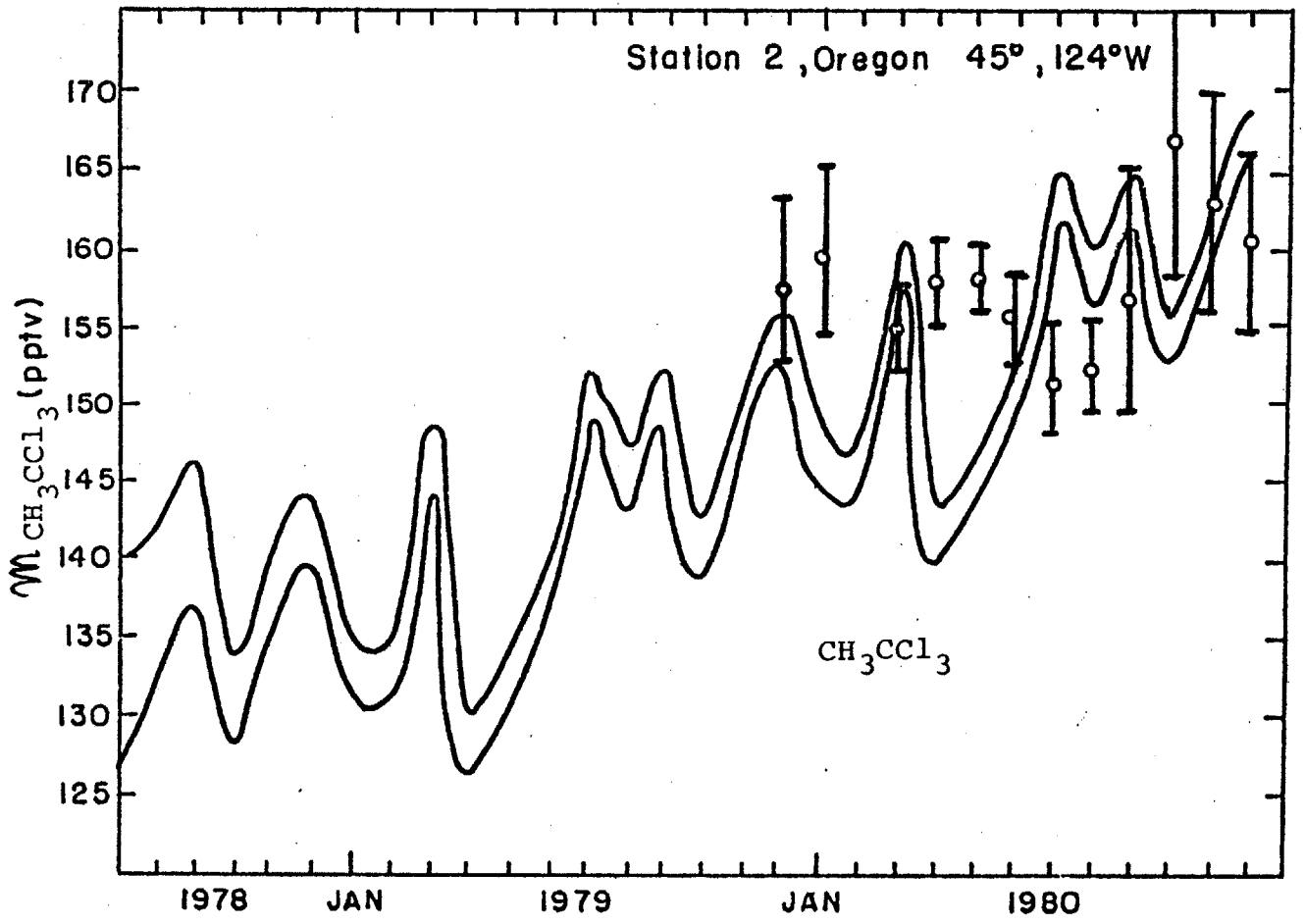


Figure 27b : Same as figure 27a , but for Station 2, Oregon.

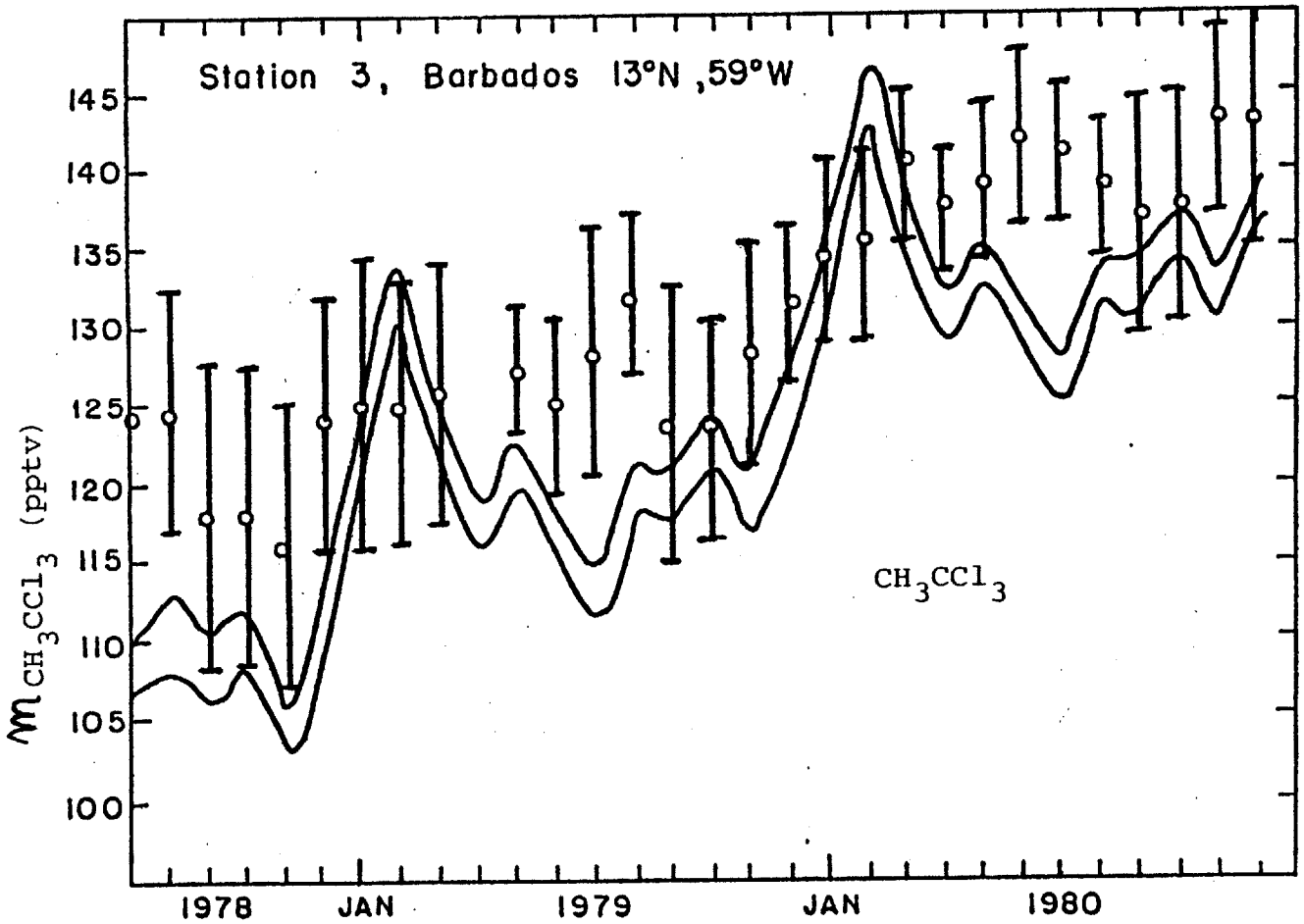


Figure 27c : Same as figure 27a , but for Station 3, Barbados.

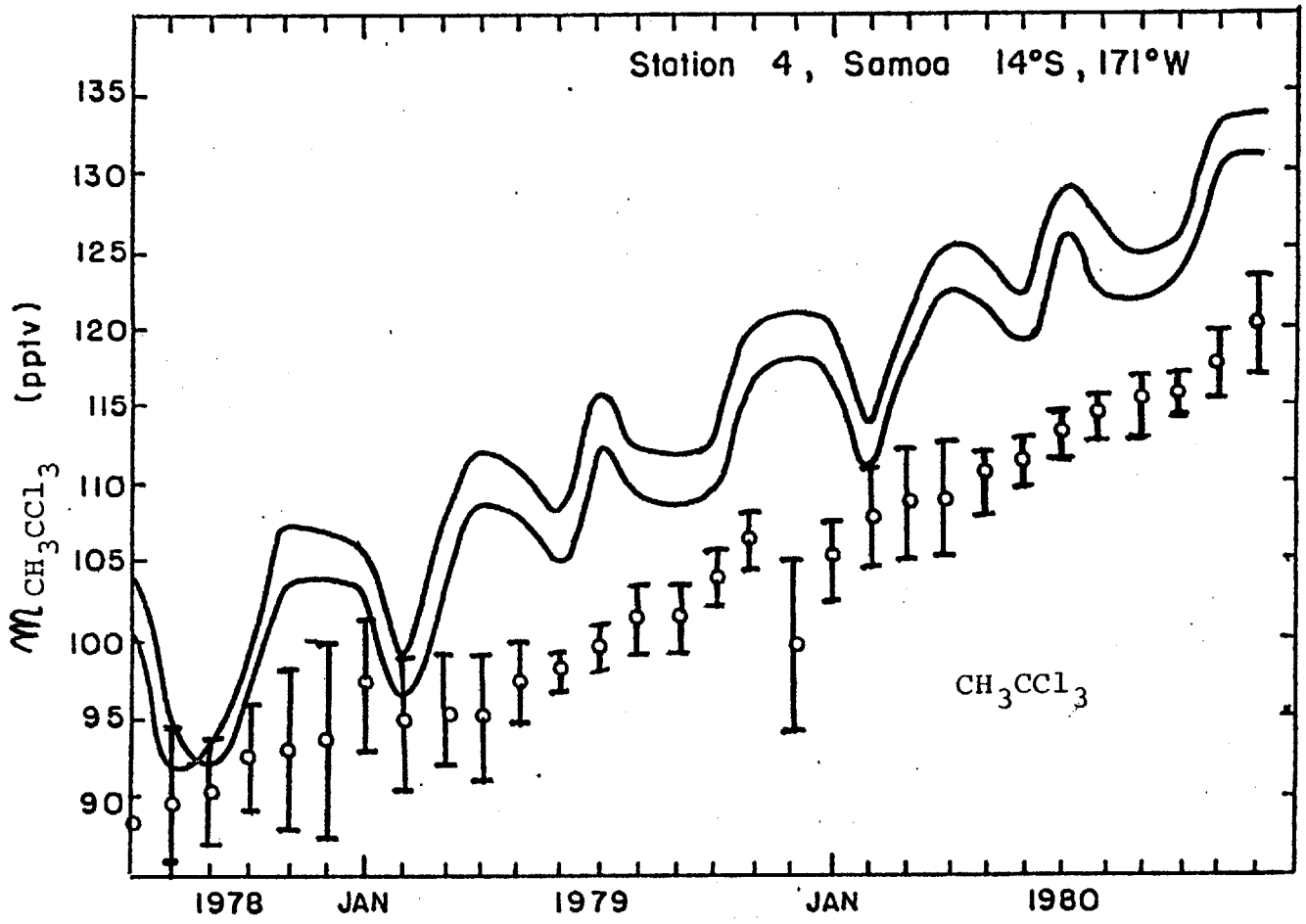


Figure 27d : Same as figure 27a , but for Station 4, Samoa.

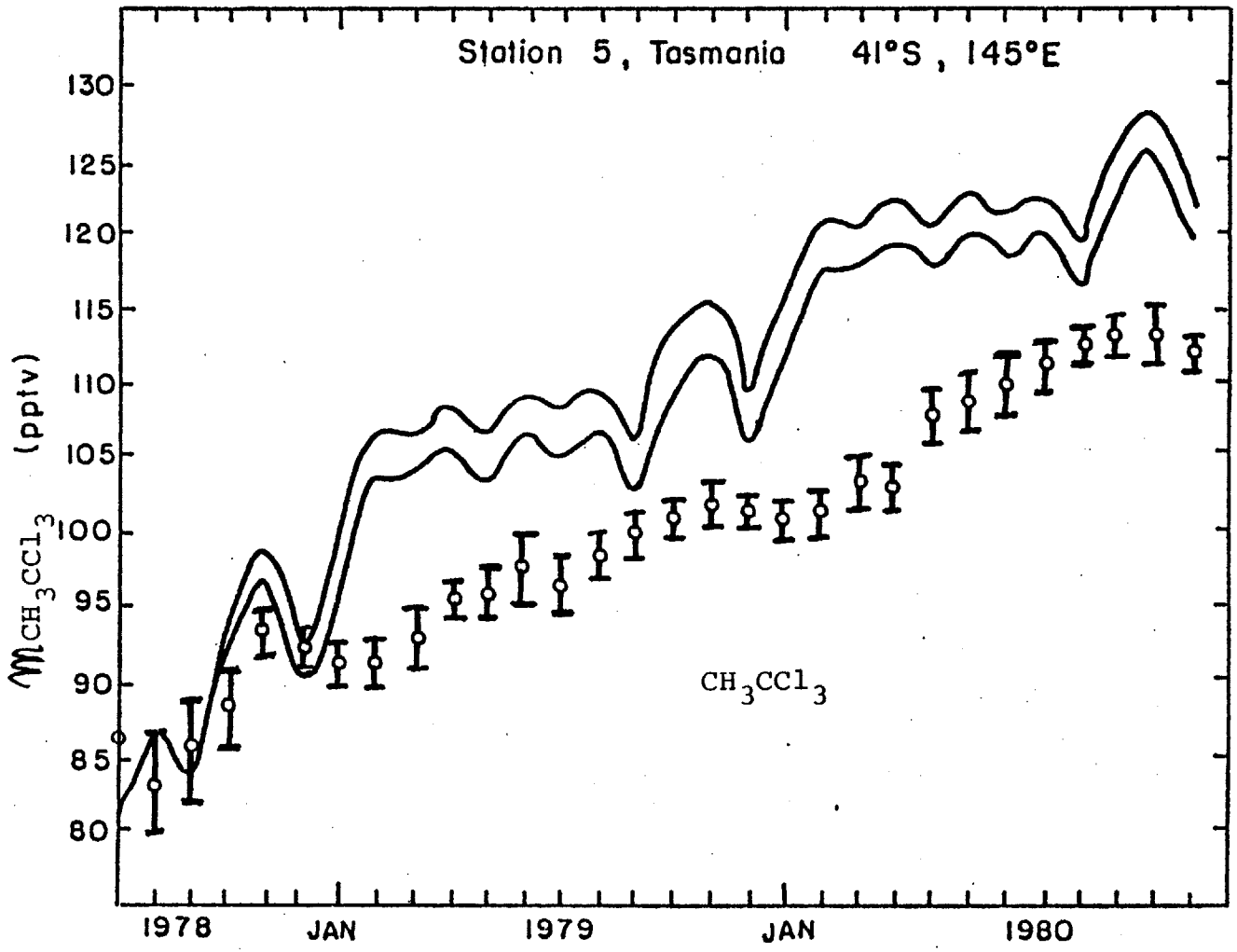


Figure 27e : Same as figure 27a , but for Station 5, Tasmania.

Table 21: CH_3CCl_3 Experimental and Calculated Trends based on Two and a Half Years of Data. Trends are in percent per year and mixing ratios m_0 and m_H are in pptv.

Station	Experimental			Calculated - RUN B		
	trend	m_0	m_H	trend	m_0	m_H
1	8.36±0.50	133	148	6.22±0.95	137	148
2	not enough data			5.75±0.91	138	149
3	7.88±0.66	119	131	9.44±0.83	110	124
4	12.23±0.26	87	102	11.88±1.36	97	113
5	9.63±0.69	88	99	14.6 ±1.06	91	109
	Calculated - RUN E			Calculated - RUN F		
1	4.54±0.98	138	146	8.23±1.00	129	143
2	4.22±0.92	139	147	8.58±1.06	129	143
3	7.36±0.84	111	122	10.2 ± 0.88	106	121
4	9.55±0.98	96	108	12.08±0.83	94	110
5	12.2 ±0.98	90	104	14.24±0.90	89	107

in the southern hemisphere they are higher. This implies that the assumed F assymetry is not enough, i.e., we need even less OH in the northern hemisphere, and more OH in the southern hemisphere. However, further runs with larger F (i.e., OH) assymetries did not improve the results. No matter how large an OH assymetry was chosen, no increase was achieved in the northern hemisphere trends, due to the apparent strong coupling between hemispheres. In particular, as more OH is put in the southern hemisphere to decrease the trend there, it also affects the northern hemisphere decreasing even further the trends calculated in this latter hemisphere. An example of such a run is Run E whose trends are also given in Table 21. In this latter run we increased sharply the OH concentration in the southern latitudes around 20°S, compared to the OH distribution of Run B (see Figure 28a, b for OH distribution in Run E). A strong coupling of the hemispheres of the type seen is expected when the $CH_3CC\ell_3$ lifetime significantly exceeds the interhemispheric mixing time.

The next thing that we tried was to alter the assumed initial $CH_3CC\ell_3$ distribution. In the runs reported above, a homogeneous $CH_3CC\ell_3$ distribution around each latitude circle defined using the observed latitudinal distribution of July 1978 from the five ALE stations was used. As an alternative a longitudinally-varying distribution calculated by our 3-D model was used. This was achieved by integrating the

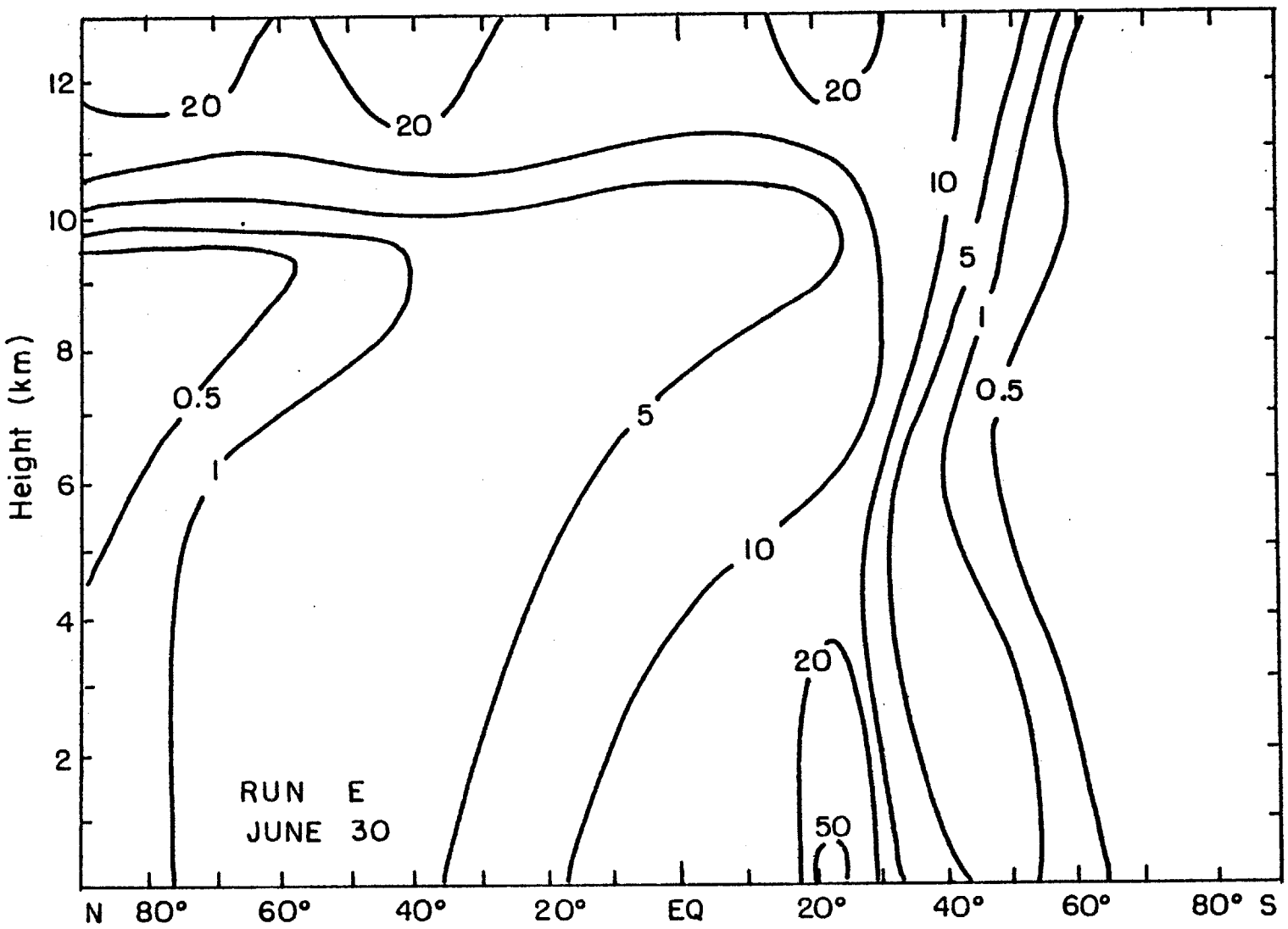


Figure 28a : Tropospheric OH distribution (daily averaged values) as used in RUN E, June 30 (10^5 molecules cm^{-3}).

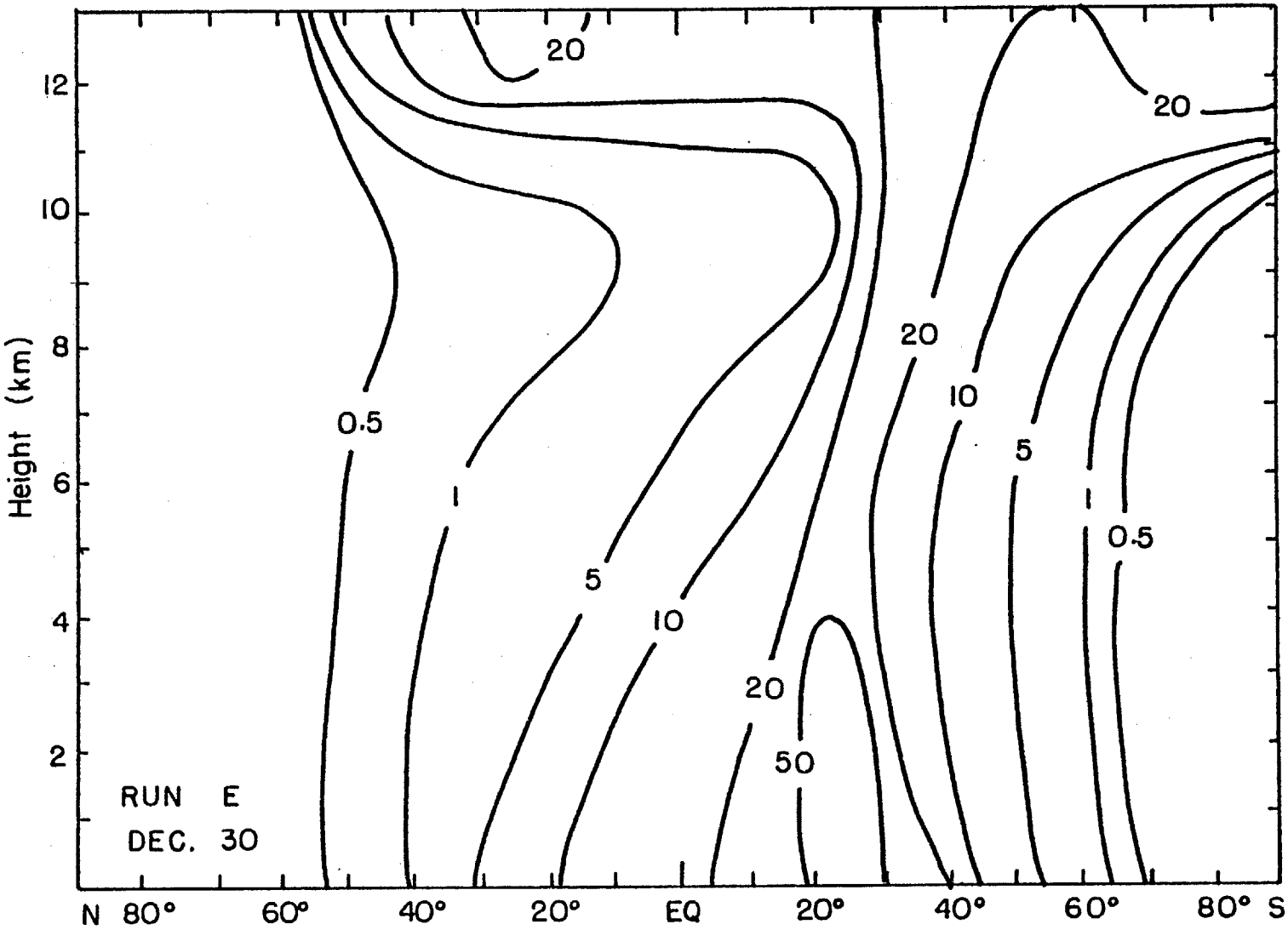


Figure 28b: Same as figure 28a , but for December 30.

model from July 16, 1978 to March 30, 1979. This three-dimensional distribution of March 30, 1979 was then adjusted so that at the ALE sites, it approximately fitted the monthly-average measurements of CH_3CCl_3 for July 1978 at these ALE stations. The monthly mean data from the ALE stations for July 1978, and the appropriate values used in the new initial CH_3CCl_3 distribution are given in Table 22.

The trends in the model run (Run F) using this initial distribution are also shown in Figure 27 and in Table 21. The agreement between model and observed trends is improved but the model trends are still too high in the southern hemisphere.

Model Runs B, E, and F when compared to the CH_3CCl_3 observations suggest that the limited resolution in the model (spectral save 6 truncation) affects the results. In particular, it does not allow a perfect fit to all five ALE station trends and mixing ratios. Methyl chloroform unlike $CFCl_3$, CF_2Cl_2, CCl_4 and N_2O, has a very pronounced observed gradient across the equator between the hemispheres. This behaviour of CH_3CCl_3 is similar to that of CO and probably of OH also. This sharp gradient is not reproduced successfully by the model since the truncation tends to smear this gradient across the equator, i.e., creating excess mixing ratio values in the model station 4, and deficient mixing ratio values in the model station 3, as compared to measurements.

Table 22: Initial CH_3CCl_3 Distribution in the Model Run F. The mixing ratios m are given in pptv.

ALE Station	1	3	4	5
$m_{CH_3CCl_3}$ Experimental July 1978 (monthly mean)	140.1	124.5	88.9	86.0
$m_{CH_3CCl_3}$ used in the Initialization of RUN F	138.6	126.5	89.7	85.3

In the CH_3CCl_3 model runs, this problem is added to the already existing problem of the slightly higher values calculated by the model, for trends and absolute mixing ratio values in the southern hemisphere as seen for $CFCl_3$, CF_2Cl_2, CCl_4 and N_2O. This makes it even harder to pin-point the correct OH radical distribution in the troposphere.

The instantaneous CH_3CCl_3 lifetime as given by the model Run B is shown in Figure 29. The CH_3CCl_3 lifetime suggested in this run is $\sim$12 years. The distinct annual cycle in the lifetime is related to the larger CH_3CCl_3 concentrations in the northern hemisphere which results in a larger CH_3CCl_3 destruction in northern hemisphere summer relative to southern hemisphere summer.

The CH_3CCl_3 latitude distribution at the surface expressed in the form of zonally-averaged mixing ratios, as calculated by the model Run B for June 30 and December 30, 1970 is given in Figure 30a. To compare this latitudinal distribution to existing sets of measurements, we prepared Figure 30b for December 1979 and Figure 30c for December 1980, where we plot model Run B results and measurements made at ALE sites as reported by Prinn *et al.* (1982b), and other measurements as reported by Rasmussen and Khalil (1981).

The two-dimensional (latitude, altitude) CH_3CCl_3 zonally-averaged distribution for December 30, 1980 as calculated by the model Run B is given in Figure 31. Unfortunately no observed vertical CH_3CCl_3 profiles have been

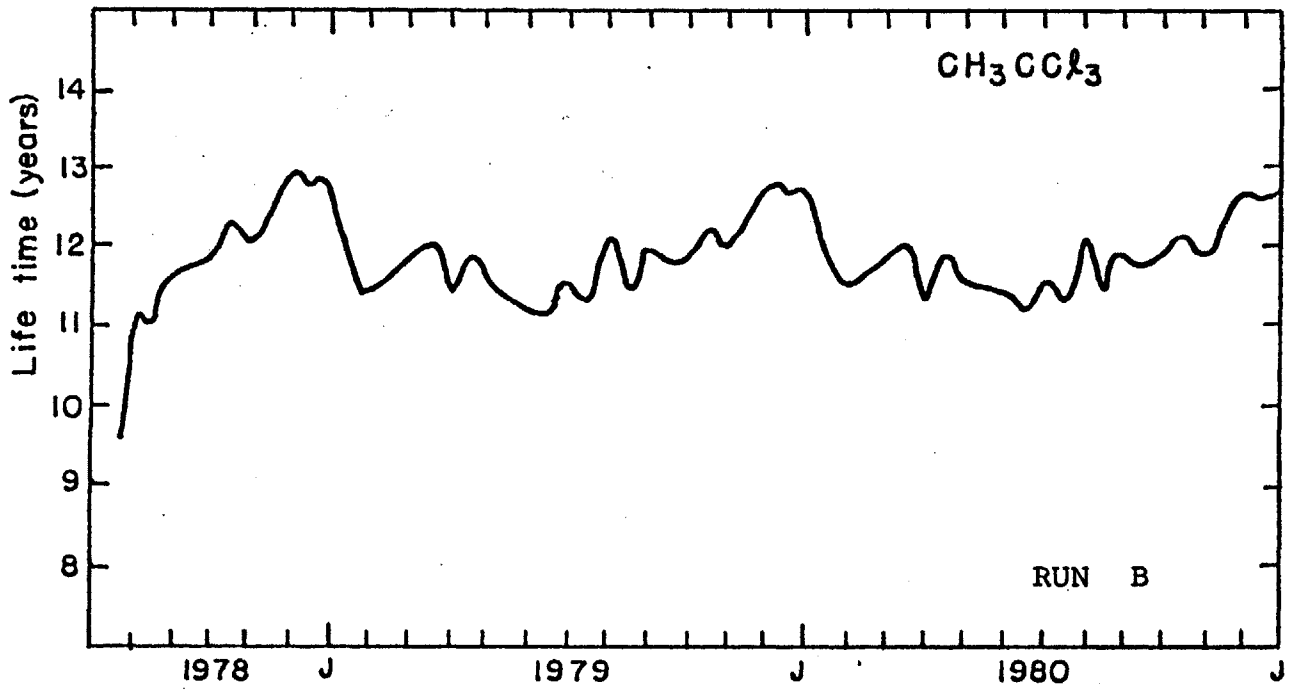


Figure 29 : CH_3CCl_3 lifetime trend.

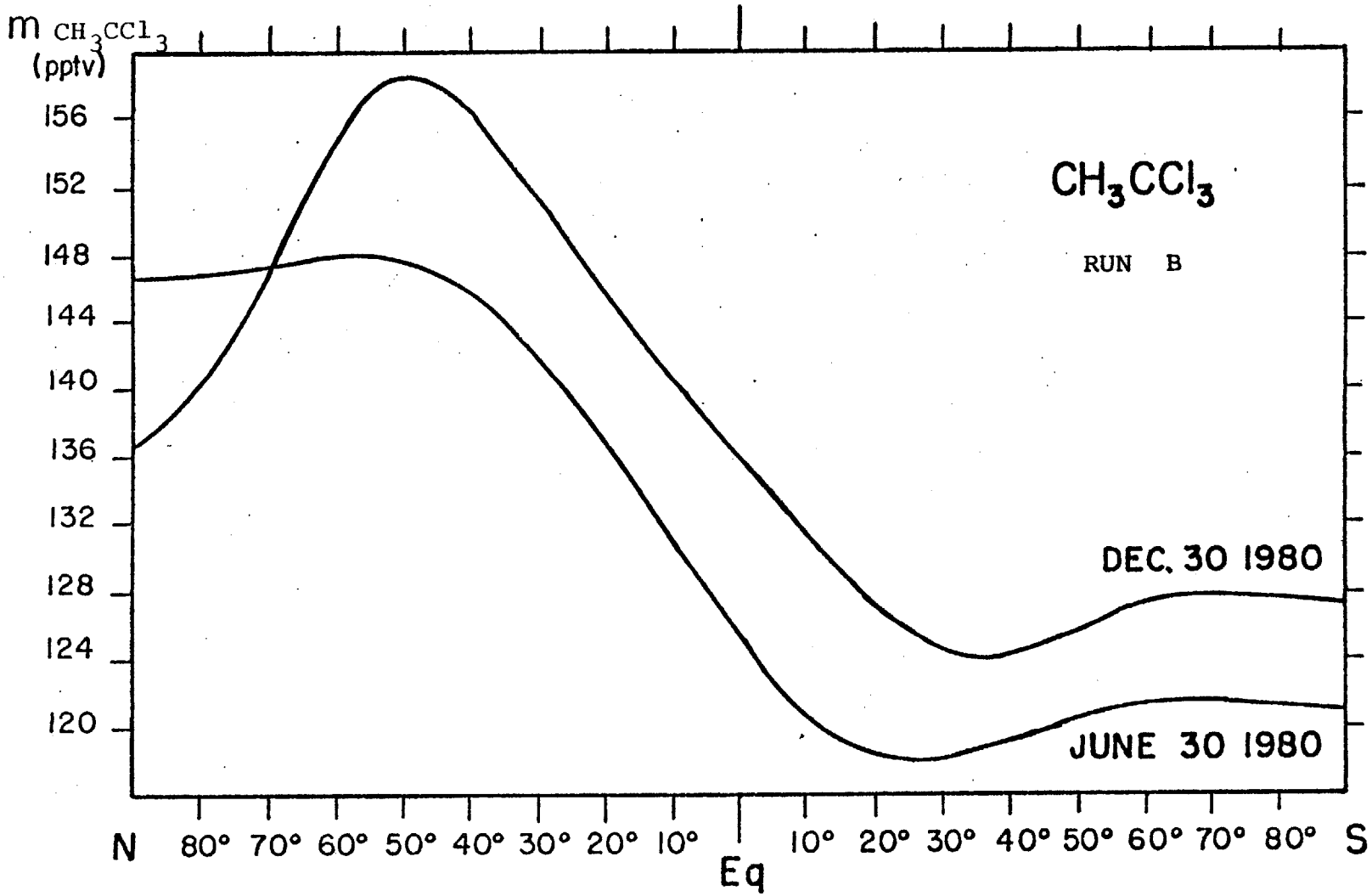


Figure 30a : Zonally averaged calculated CH_3CCl_3 Surface Distribution June 30 and December 30, 1980.

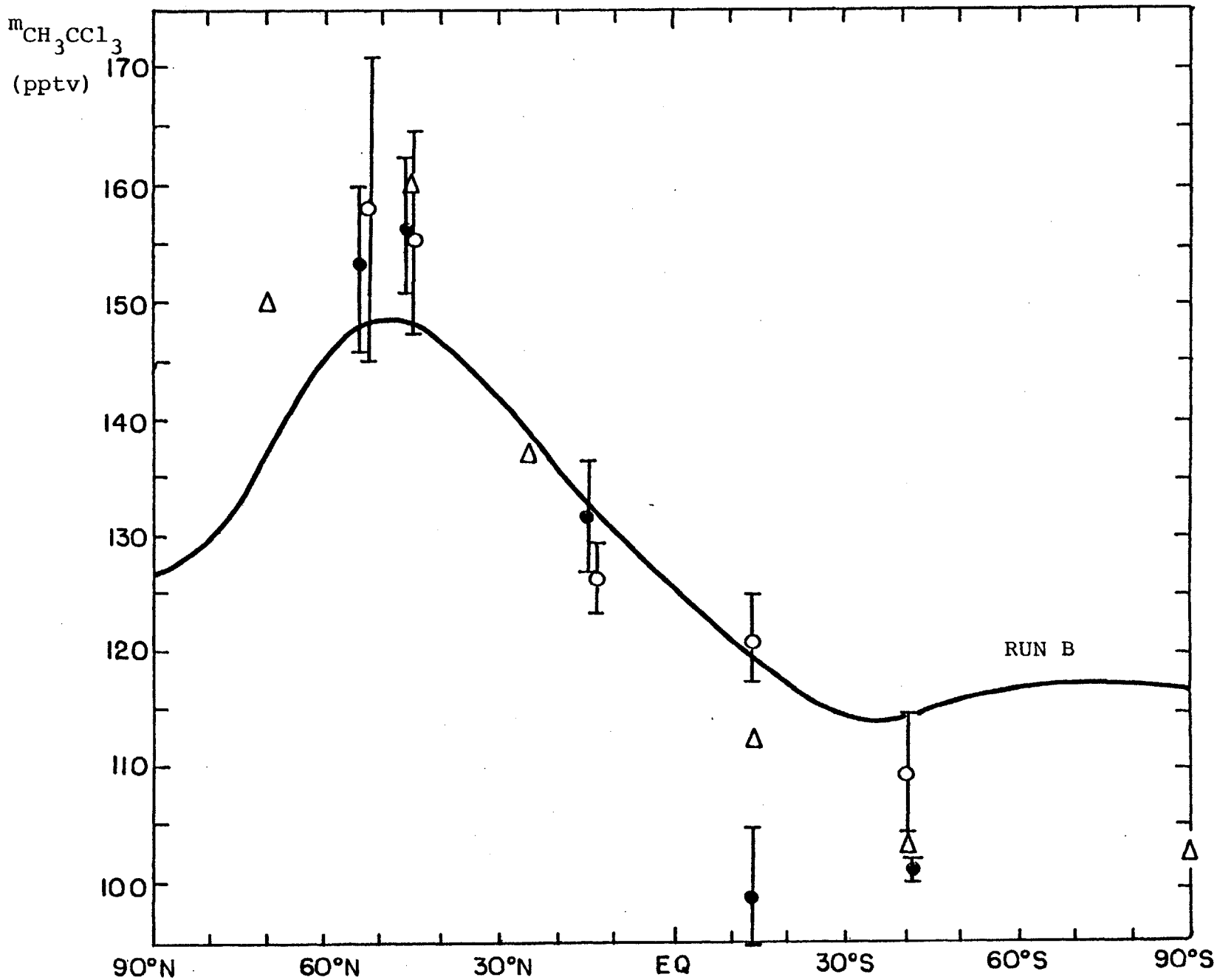


Figure 30b: CH_3CCl_3 Surface Distribution, December 30, 1979. Zonally-averaged calculated values - solid line, Dec. 79 monthly-mean calc. values - open circles, Dec. 79 monthly-mean measured values, Prinn et al.(1982b) - solid circles, Dec. 79-Jan.80 mean values, Rasmussen and Khalil (1981) - open triangles.

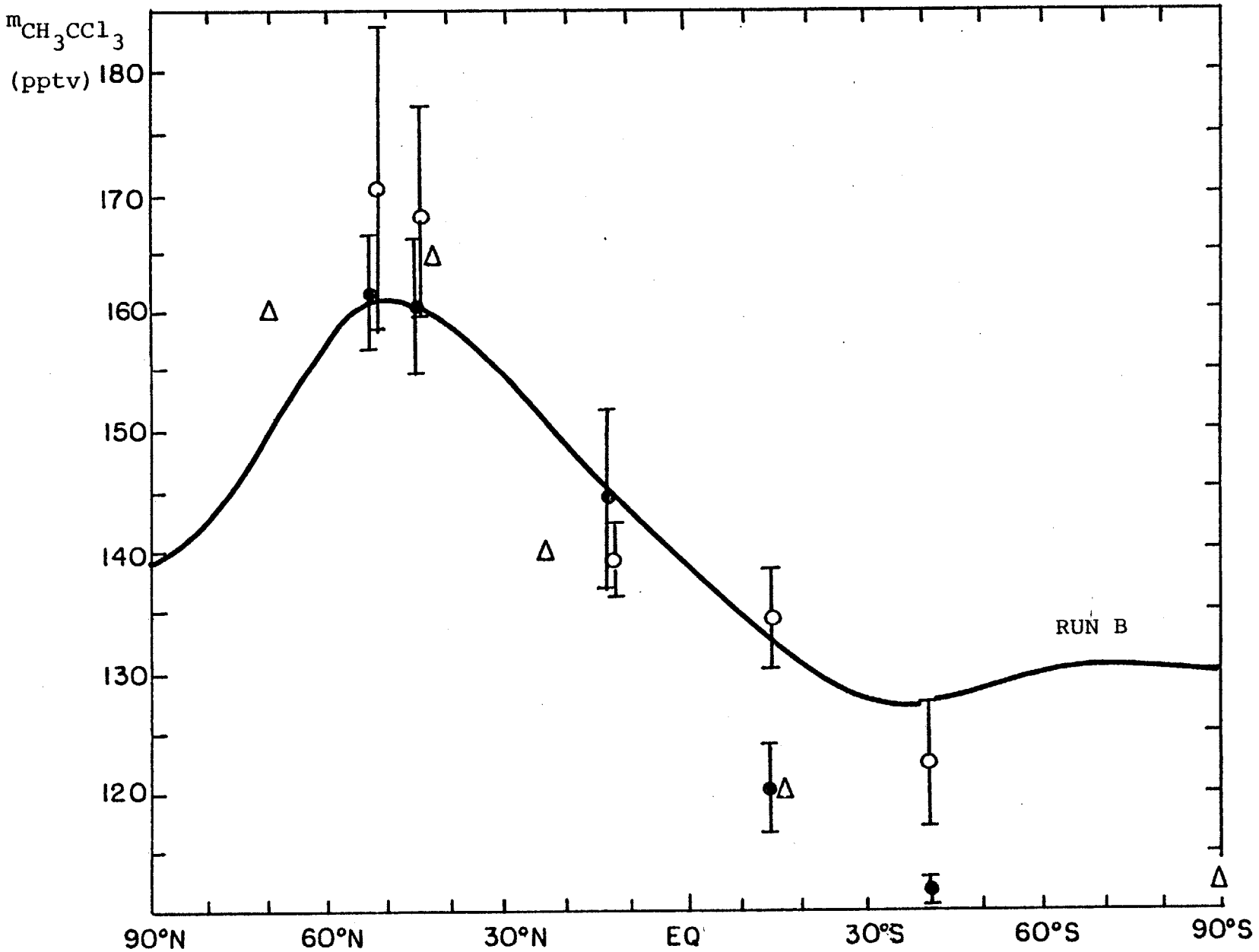


Figure 30c : Same as Figure 30b , but for December 1980.

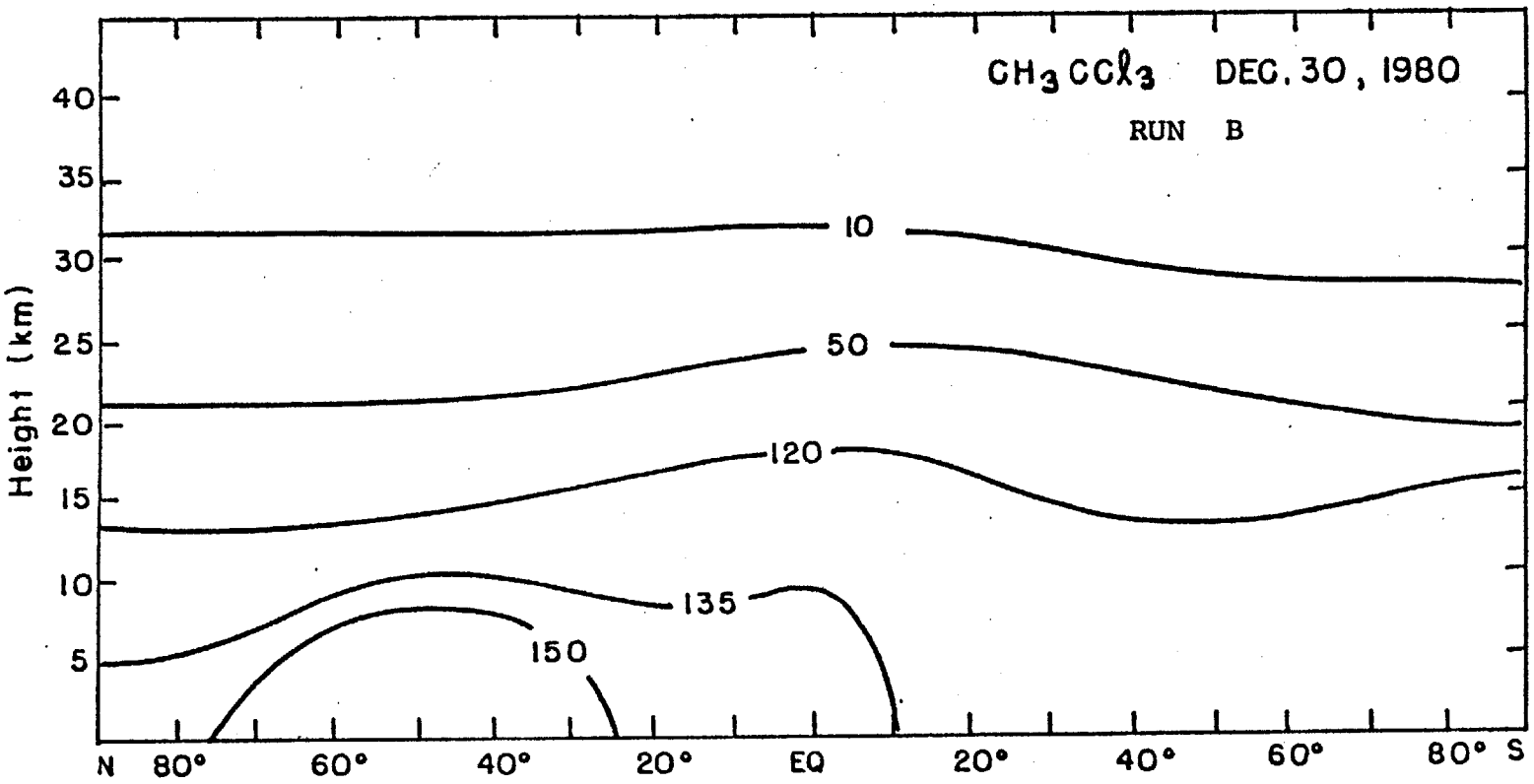


Figure 31 : Zonally averaged calculated CH_3CCl_3 2-D Distribution, December 30, 1980, (pptv).

published so far, and therefore we cannot compare our calculations to measured vertical CH_3CCl_3 distributions.

The two-dimensional (latitude, longitude) CH_3CCl_3 monthly-averaged surface distribution as calculated by model Run B for the month of January 1981, is shown in Figure 32. Here, as we have seen for $CFCl_3$, CF_2Cl_2 and CCl_4, we observe a strong persistent standing wave pattern in the northern hemisphere, caused by the distribution of the anthropogenic sources of CH_3CCl_3.

The OH two-dimensional (latitude, altitude) distribution in the troposphere, used by the model Run B was shown in Figure 26. For comparison the tropospheric OH distribution used in Run E was shown in Figure 28. This Run E OH distribution is artificial and perhaps unreasonable consisting as it does of high OH radical values around 20°S, in order to lower the trends in the southern hemisphere. The CH_3CCl_3 lifetime and the tropospheric average OH number densities predicted by CH_3CCl_3 Runs B and E are given in Table 23.

Some estimates for the OH distribution based on different studies, are given in Table 24. Singh (1977b, 1979), using a one-dimensional model of the study of CH_3CCl_3 budget, and its reaction with OH radicals, finds a global OH concentration of $(3\text{-}4)\times10^5$ molecules cm^{-3}. Neely and Plonka (1970) using a box model find a value of 3.3×10^5 molecules cm^{-3}. Two-dimensional models result in higher values. Crutzen and Fishman (1977), using a two-dimensional tropospheric-chemical

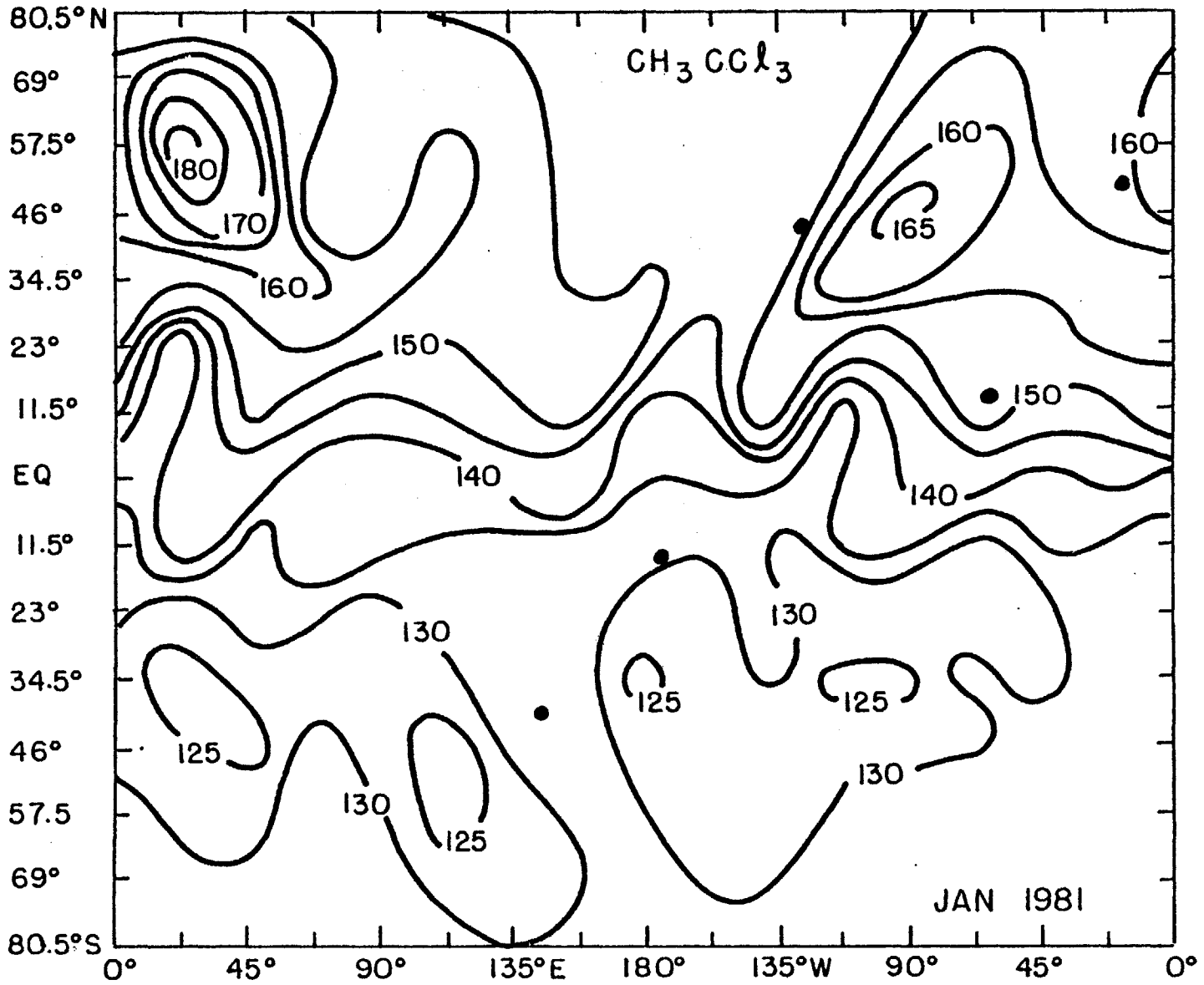


Figure 32 : The 2-D CH_3CCl_3 Surface Distribution, January 1981 (pptv). Solid circles denote ALE sites.

Table 23 : CH_3CCl_3 Lifetime and Tropospheric OH Number Density.

	CH_3CCl_3 Lifetime (years)		Tropospheric OH Number Density (10^5 molecule cm^{-3})		
	Seasonal average	Annual average	Global average	Northern Hemisphere average	Southern Hemisphere average
RUN B	DEC79-FEB80 12.0 JUNE-AUG 80 11.8	12.0	7.4 6.5	7.9 4.3	7.6 9.5
RUN E	DEC79-FEB80 8.4 JUNE-AUG 80 11.7	10.2	7.6 11.1	5.3 4.2	10.1 17.6

Table 24: Tropospheric Hydroxyl Radical Concentrations (Daily averages in 10^5 mol cm^{-3}).

Reference	Global	NH	SH	SH/NH
Singh(1977b,1979)	3-4	-	-	1.6
Crutzen and Fishman (1977)	5	2.5	7	2.8
Neely and Plonka (1978)	3.3	4.8	18	3.8
Derwent and Eggleton (1981) using Volz et al. (1981)	6.5	6.8	6.1	0.9
Logan et al. (1981)	-	10	-	-
Chameides and Tan (1981)	2.2-8	2.0-7.6	2.3-8.4	1.1
Pinto et al. (1982)	7.0	-	-	-
This study, RUN B	7.0	6.1	8.6	1.4
This study, RUN E	9.4	4.8	13.2	2.9

model including the budgets of CH_4, CO, and H_2 as well as $CH_3CC\ell_3$, find a global tropospheric value for OH of $5x10^5$ molecules cm^{-3}. Derwent and Eggleton (1981) using a two-dimensional model for $CH_3CC\ell_3$ and using the tropospheric OH distribution reported by Volz *et al.*, (1981), find an average tropospheric OH concentration of $6.5x10^5$ molecules cm^{-3}. The reported value for the northern-hemisphere OH concentration, as calculated by Logan *et al.* (1981) using a two-dimensional comprehensive tropospheric chemical model, is 10^6 molecules cm^{-3} with an uncertainty factor of 2. Chameides and Tan (1981), using a detailed diagnostic two-dimensional tropospheric chemical model and a careful uncertainty analysis, reported an OH daily averaged tropospheric concentration of $(2.2\text{-}8)x10^5$molecules cm^{-3}. Finally, Pinto *et al.* (1982), using a three-dimensional study of the distribution of ^{12}CO find a global-averaged value of the tropospheric OH concentration of $7x10^5$ molecules cm^{-3}.

The differences between these values are mainly due to the following reasons: the complexity of the mathematical models used (one-, two- or three-dimensional); different averaging techniques of values in the troposphere (definition of the height of the tropopause, vertical spacing of levels, horizontal spacing of grid points); different chemistry schemes with varying degrees of complexity; different top boundary conditions (assessment of the photochemical stratospheric sink); and finally, differences in reaction rate

constants, absorption cross-sections, vertical mixing coefficients, and anthropogenic emission estimates. The most recent estimates (Derwent and Eggleton (1981), Volz *et al.* (1981), Logan *et al.* (1981), Chameides and Tan (1981), Pinto *et al.* (1982), this thesis) all agree within a factor of two.

3.6 Oceanic Sink

As discussed earlier two versions of the oceanic sink were tested in CH_3CCl_3 Run B: *the perfect sink* (which assumes very rapid destruction of CH_3CCl_3 dissolved in the ocean thus causing an essentially zero CH_3CCl_3 concentration in the ocean at the beginning of each time step); and *the partial sink* (which assumes very long residence times for CH_3CCl_3 in the ocean, and rapid equilibration of CH_3CCl_3 between air and ocean water so that in each time step, any increase of CH_3CCl_3 in the air is immediately translated into an increase in its ocean water concentration).

These test runs were integrated for six months using Δt = 2 hours. The partial sink had no effect at all on the CH_3CCl_3 horizontally-averaged mixing ratios, even at the surface level, while the perfect sink slightly decreased them. We conclude that the oceanic sink has only a very small influence if at all on the CH_3CCl_3 atmospheric distribution, at least when compared to CH_3CCl_3 destruction by tropospheric OH radicals.

3.7 Sensitivity to O_2 Herzberg Continuum Cross-sections

Recently it was reported by Frederick and Mentall (1982) that the O_2 absorption cross-sections in the wave length range of 200-210nm as measured in the real atmosphere are significantly lower than those used so far in photochemical modelling. Froidevaux and Yung (1982), using the updated O_2 absorption cross-sections in a one-dimensional model, calculated the changes caused in the vertical profiles of $CFCl_3$, CF_2Cl_2, CH_4, N_2O and HNO_3, and found better agreement to experimental vertical profiles. We attempt here also to assess the changes is our model results, using the updated values of O_2 absorption cross-sections.

As suggested by Froidevaux and Yung (1982), we reduced the O_2 absorption cross-sections of our model in the wave length range of 200-220nm by 40% , and recalculated the J values of $CFCl_3$, CF_2Cl_2, CCl_4, N_2O and CH_3CCl_3 for January 1, 1981. In Table 25 we show the increase caused in the various J values.

Using the formulation by Prinn (1975), we can now assess the changes in stratospheric mixing ratios of the various tracers, caused by the update in the O_2 absorption cross-sections. In particular, we have

$$m = m_0 \exp\left(-\frac{z}{H_m}\right) \quad ,$$

Table 25: Correction in J Values.

LEVEL	$CFCl_3$	CF_2Cl_2	CCl_4	N_2O	CH_3CCl_3
2	1.00	1.00	1.00	1.00	1.00
3	1.00	1.00	1.00	1.00	1.00
4	1.00	1.00	1.00	1.00	1.00
5	1.01	1.00	1.01	1.01	1.01
6	1.01	1.01	1.01	1.01	1.01
7	1.01	1.01	1.02	1.01	1.02
8	1.02	1.01	1.02	1.02	1.02
9	1.04	1.02	1.03	1.03	1.04
10	1.05	1.03	1.05	1.05	1.05
11	1.08	1.05	1.07	1.07	1.08
12	1.11	1.08	1.11	1.11	1.11
13	1.17	1.13	1.16	1.16	1.17
14	1.24	1.20	1.23	1.23	1.24
15	1.36	1.30	1.33	1.33	1.35
16	1.54	1.45	1.50	1.50	1.53
17	1.87	1.69	1.80	1.77	1.85
18	2.48	2.06	2.34	2.23	2.43
19	3.66	2.62	3.42	3.03	3.56
20	6.27	3.30	5.86	4.37	6.07
21	10.33	2.26	10.9	3.66	10.0
22	10.8	1.69	14.9	2.60	10.4

reported here are the values of the ratio,

$$\frac{\text{updated J}}{\text{former J}}$$

$$H_m = -\{ \frac{1}{2H_0} + (\frac{1}{4H_0^2} + \frac{J}{K_d})^{1/2} \}^{-1} \quad .$$

Here H_m is the tracer volume mixing ratio scale height. We chose to investigate the changes caused in m at z=33 km (or level 14 of our model). At this height in our model $K_d = 7.33 \times 10^4$ cm^2/sec. We specifically compute updated values of H_m and the ratio of the former mixing ratios to the updated mixing ratios at this height level. The results are shown in Table 26, along with the results published by Froidevaux and Yung (1982) for 30km. The agreement between our assessment and their correciton factor is very good. For the two fluorocarbons and N_2O (for which we have measured vertical profiles), the largest effect will be for $CFC\ell_3$ mixing ratios in the stratosphere (reduction by a factor of $\sim$5). For $CF_2C\ell_2$ and N_2O the correction is much smaller (reduction by factors of 1.4 and 1.3, respectively). These corrections are in good agreement with the conclusions from our model runs reported earlier in this thesis. Namely that a comparison between our model runs and observations suggests the need for additional sinks for $CFC\ell_3$ and $CC\ell_4$ (e.g., increased photodissociation rates) but not for the other three tracers we have modelled.

We can also approximately assess the changes caused in the calculated surface trends of the various tracers by this update in the O_2 absorption cross-sections. The "corrected"

Table 26: Updated Mixing Ratios at 33 Km.

	$CFCl_3$	CF_2Cl_2	CCl_4	N_2O	CH_3CCl_3
former J (sec^{-1})	1.33E-6	1.17E-7	3.06E-6	6.67E-8	2.03E-6
updated J (sec^{-1})	1.65E-6	1.40E-7	3.76E-6	8.20E-8	2.52E-6
former H_m (Km)	2.77	13.5	1.73	20.9	2.18
updated H_m (Km)	2.44	11.8	1.54	17.8	1.93
m_{old}/m_{new} (a)	5	1.4	10.5	1.3	7.1
m_{old}/m_{new} (b)	5.3	1.6	-	1.4	-

References: (a) - this study

(b) - Froidevaux and Yung (1982)

instantaneous global lifetimes for January 1, 1981 are shown in Table 27, beside the former values. These "corrected" values are however a lower limit for the lifetimes since the updated calculation is based on a single step computation as of January 1, 1981 using the existing calculated vertical profiles (which are given by the model integration prior to January 1, 1981 without the update of the O_2 absorption cross-sections). Since the instantaneous calculation is not based on a new model run (starting for example in July 1978) using the updated O_2 absorption cross-sections, the correct updated lifetime values should be larger than the "corrected" values given in Table 27. This is because stratospheric concentrations achieved by a full model run using the updated O_2 absorption cross-sections should be lower than the presently calculated concentrations. The effect of increasing stratospheric J values is somewhat compensated by lower stratospheric mixing ratios.

In order to assess the maximum possible changes in the surface trends resulting from these maximum possible changes in lifetime, we use the global tracer continuity equation in trend form

$$\frac{1}{C}\frac{dC}{dt} = \frac{I - L}{C} = \eta \cong \frac{1}{m_s}\frac{dm_s}{dt}$$

where C is the tracer's atmospheric content, I its anthropogenic source, L its total loss rate due to all sinks,

Table 27: Updated Lifetimes and Correlation Factors (January 1, 1981 values).

	$CFCl_3$	CF_2Cl_2	CCl_4	N_2O	CH_3CCl_3
former τ (years)	79.7	242.4	48.7	190.2	12.6
new τ (years)	32.4	137.5	18.8	134.0	10.0
daily input (10^6gm/day)	721.8	1107	270	41670	1417
former loss (10^6gm/day)	144.5	71.1	187.7	34320	680
new loss (10^6gm/day)	355.0	125.3	486.8	48730	855
former net input (10^6gm/day)	577.3	1036	82.2	7350	737
new net input (10^6gm/day)	366.8	982	-216.8	-7060	562
atmospheric content (10^6gm)	.415E7	.620E7	.329E7	.235E10	.308E7
former η (10^4/day)	1.39	1.67	0.25	0.031	2.39
new η (10^4/day)	0.88	1.58	-0.66	-0.03	1.82
experimental trend (%/year)	5.93	6.23	1.79	0.36	9.36
former calc. trend (%/year)	6.45	6.51	2.37	0.32	10.84
predicted change in calc. trend (%/year)	-2.7	-0.35	-3.5	-0.24	-2.2

and m_s is the tracer's globally averaged surface mixing ratio. The correlation between the calculated surface trend and η for all five tracers is shown in Figure 33. By updating the O_2 absorption cross-sections (i.e., L or η values) we now find the expected changes in the surface trends using this correlation. The results are also summarized in Table 27. We find that indeed the changes are too large when compared to observations, but at least for $CFC\ell_3$, $CF_2C\ell_2$ and $CH_3CC\ell_3$ (for which we have good estimates of the source terms) the corrections are in the right direction. In particular, we get smaller trends for $CFC\ell_3$, $CFC\ell_2$ and $CH_3CC\ell_3$. Therefore, our results are quite sensitive to the O_2 Herzberg continuum cross-sections.

The exact effect on the surface global trends can only be determined by a full rerun of the model itegrations starting July 1978. A complete three years run with the new values for O_2 absorption cross-sections in the wavelength range of 200-210nm, was performed for $CFC\ell_3$ only. The new vertical profile for November 10, 1979 at 45°N is compared to the formerly calculated vertical profile in Figure 34. The change in the vertical profile (namely a lowering of $CFC\ell_3$ stratospheric mixing ratios by a factor of two) has a significant effect on the stratospheric and total lifetime of $CFC\ell_3$, but only a small effect on the surface trend of this species. The new and old results for these parameters are given in Table 28. We note that the computed global $CFC\ell_3$

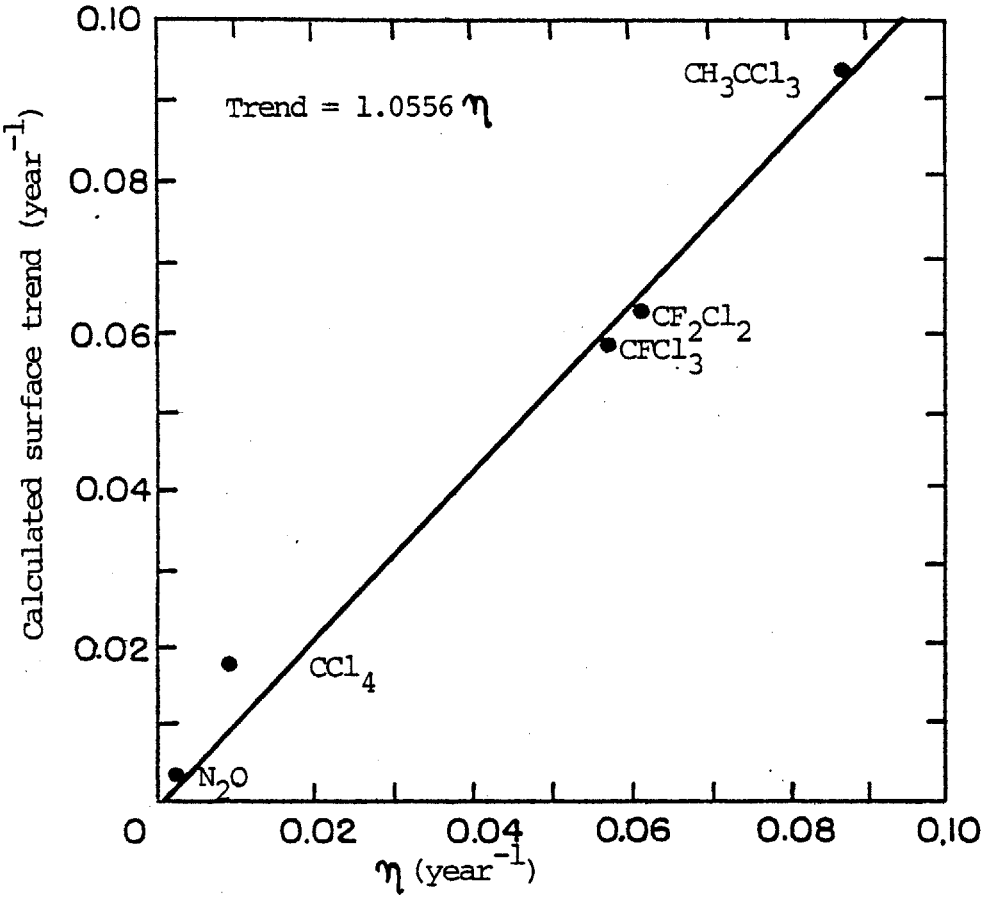


Figure 33: Surface trend and η correlation.

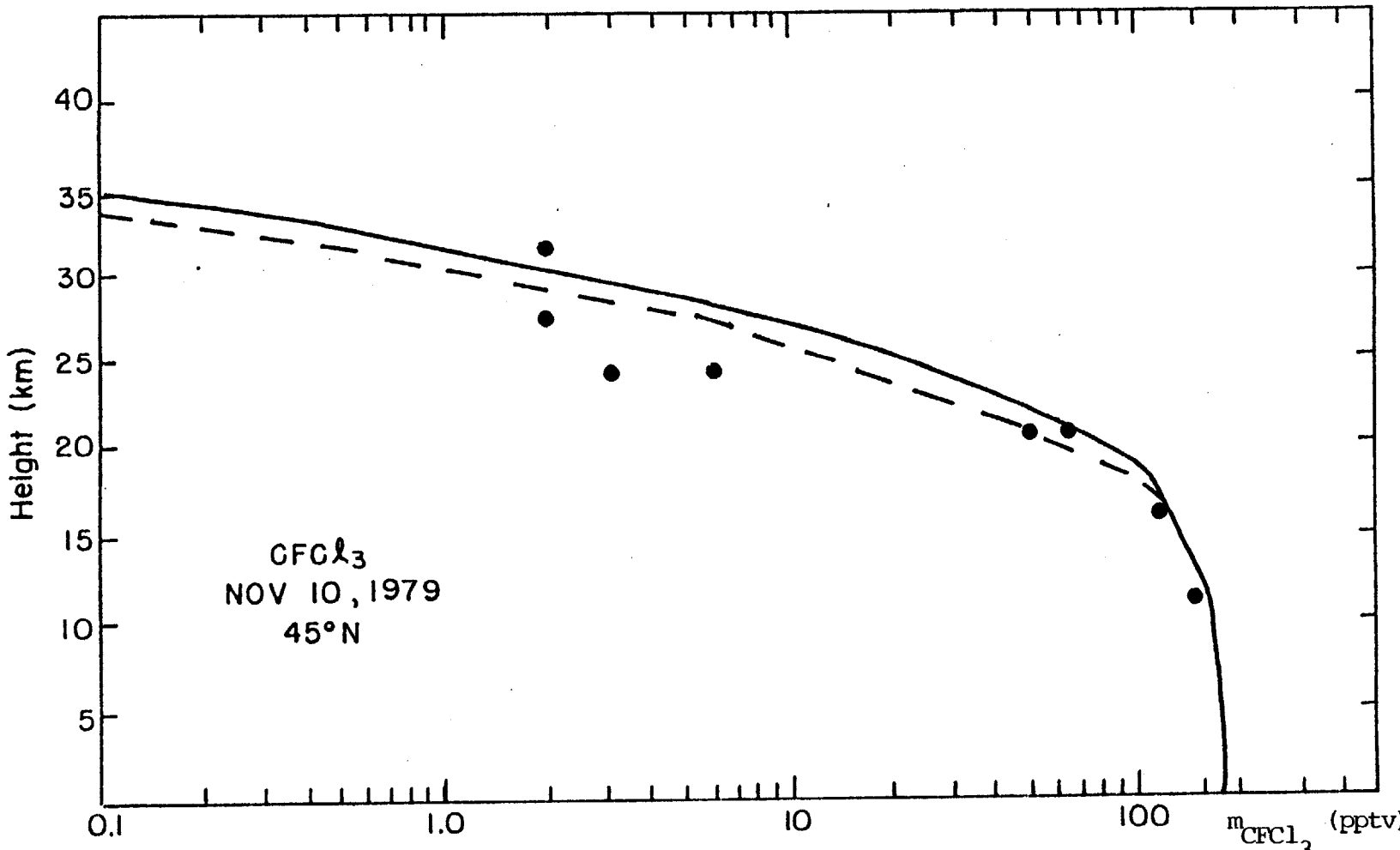


Figure 34: $CFCl_3$ vertical profiles, dashed line is the updated calculation, solid line is the former calculated profile (same as in figure 11c), circles denote measurements by Goldan et al. (1980).

Table 28: Updated Lifetimes and Trends for $CFCl_3$(Fabian), based on a three years run.

	Experimental	Calculated	
		Former	Updated
Station 1, surface trend (%/year)	4.95± 0.13	4.76± 0.26	4.39± 0.37
Station 2, surface trend (%/year)	*5.47± 0.33	4.67± 0.26	4.32± 0.36
Station 3, surface ternd (%/year)	6.33± 0.15	6.26± 0.19	5.66± 0.25
Station 4, surface trend (%/year)	6.10± 0.15	6.63± 0.23	6.43± 0.37
Station 5, surface trend (%/year)	6.43± 0.17	7.68± 0.24	7.67± 0.37
Global total mass trend (%/year)	-	7.57± 0.06	6.81± 0.07
Global surface trend (%/year)	-	6.45± 0.05	6.04± 0.05
Weighted average surface tend, Stations 1,3,4,5 (%/year)	5.93± 0.15	6.42± 0.23	6.13± 0.34
τ above 198mb, Jan. 1,1981(years)	-	12.2	6.4
τ global, Jan. 1,1981(years)	-	79.7	43.8
Photochemical destruction rate, Jan. 1,1981 (10^8 gm/day)	-	1.44	2.58
τ July 1980-June 1981 (years)	-	78	44.8

* - not enough data.

trend in the updated compensation is now much closer to the observed experimental trend. We also note that we do not get a factor of 5 change in $CFC\ell_3$ mixing ratio in the updated calculations which was seen in the 1-D model of Froidevaux and Yung (1982). This updated calculation using the new values for O_2 absorption cross-sections, is given here in order to show how sensitive our model is to such changes. These experimental measurements of O_2 absorption cross-sections should be further verified before final conclusions can be drawn about this effect.

4. GENERAL SUMMARY AND CONCLUSIONS

4.1 Global Averages

Now that we have seen the detailed results of the model runs for five different tracers and compared them to ALE and other atmospheric measurements, it is interesting to look at globally-averaged trends. Two specific globally-averaged trends were computed. The first was obtained by fitting the increase in the globally-averaged calculated surface mixing ratio of the tracer to a simple linear fit, yielding the globally-averaged tracer surface trend. The second was obtained by doing the same thing with the calculated total atmospheric mass of the tracer, yielding the globally-averaged trend in the atmospheric content of the tracer. To compare the surface trends with the experimental results, we calculated a weighted surface experimental global trend, by averaging

the experimental trends at each of the four ALE stations (Ireland, Barbados, Samoa and Tasmania) for which a full three years of data are available. Each of these stations represents almost the same area of the globe and therefore the weighting functions associated with each are very similar. The various calculated and experimental values are summarized in Table 29.

It seems from this table that $CFC\ell_3$ needs a sink in addition to the calculated photodissociation sink, since its calculated global surface trend is slightly less than the experimental value. This conclusion is in agreement with a detailed trend analysis of the ALE data suggesting a true present lifetime for $CFC\ell_3$ of 67 years (Cunnold *et al.*, 1982a) compared to the lifetime of 78 years computed in this thesis. The $CF_2C\ell_2$, $CH_3CC\ell_3$ and N_2O global surface experimental trends show good agreement with our model values and additional sources or sinks other than those in our model are not suggested. Carbon tetrachloride like $CFC\ell_3$ needs either a sink in addition to the calculated photodissociation sink, or a smaller source strength than assumed here in order to allow agreement between observed and calculated trends. However we did find that using updated O_2 absorption cross-sections in the Herzberg continuum eliminates the need for an additional sink for $CFC\ell_3$.

Table 29 : Global Trends (percent per year).

	Global Total-Mass Trend	Global Surface Trend	Weighted* Average Trend of 4 Stations (1, 3, 4, 5)
EX $CFCl_3$	-	-	5.93±0.15
$CFCl_3$ FAB	7.57±0.06	6.45±0.05	6.42±0.23
$CFCl_3$ CRU	7.06±0.04	6.71±0.07	6.72±0.24
$CFCl_3$ updated	6.81±0.07	6.04±0.05	6.13±0.34
EX CF_2Cl_2	-	-	6.23±0.19
CF_2Cl_2 FAB	7.56±0.02	6.51±0.04	6.44±0.20
CF_2Cl_2 CRU	7.08±0.01	6.69±0.04	6.64±0.20
EX CH_3CCl_3	-	-	9.36±0.56
RUN B	11.37±0.12	10.84±0.2	10.75±1.03
RUN E	N.A.	N.A.	8.61±0.94
RUN F	N.A.	N.A.	11.35±0.90
EX CCl_4	-	-	1.79±0.26
CCl_4	2.40±0.03	2.37±0.02	2.38±0.10
EX N_2O	-	-	0.36±0.12
N_2O	0.79±0.04	0.32±0.03	0.37±0.02

* Weighting (by area) for each Station was:

Station 1 - 0.9254 Station 3 - 1.0746

Station 4 - 0.7654 Station 5 - 1.2346

N.A.-was not calculated.

4.2 Seasonal Averages

In order to compare absolute calculated mixing ratios with the experimental values, the seasonal mean for the three-month period November 1980-January 1981 was computed and compared in Table 30 , for all five tracers and at the five ALE sites.

Small discrepancies between model and observation occur for $CC\ell_4$ and $CH_3CC\ell_3$ in the southern hemisphere, and for N_2O in stations 2, 3, 4 and 5. For the tracers $CFC\ell_3$, $CF_2C\ell_2$, $CC\ell_4$, and N_2O which have no OH sink, discrepancies can arrise from errors in estimating the sources or sinks, from initialization errors (e.g., errors in the July-1978 inital monthly mean values), from model truncation errors, and from problems in the model transport formulation (3-dimensional advection plus vertical diffusion). It seems that for $CFC\ell_3$ we have a very small source or sink error. For $CF_2C\ell_2$ the fit is good and no serious errors are apparent. We note that the updated $CFC\ell_3$ calculation gives excellent agreement to measurements.

Nitrous oxide has a clear initialization problem, if the initial (July-1978) surface concentrations were slightly larger and more homogeneous with latitude than suggested by ALE, we would have achieved a much better fit between calculations and measurements. Carbon tetrachloride has either a small source or sink error or for some reason the model transport inadequacies seem to be more pronounced

Table 30 : Mixing Ratios, November 1980 - January 1981.
units: $CFCl_3$, CF_2Cl_2, CCl_4, CH_3CCl_3 (pptv),
N_2O (ppbv).

Tracer	Station 1 Ireland	Station 2 Oregon	Station 3 Barbados	Station 4 Samoa	Station 5 Tasmania
$CFCl_3$ EX	187.0 ± 2.2	186.2±2.4	181.3±2.1	173.1±1.7	170.7±1.4
$CFCl_3$ CALC	188.8 ± 4.7	187.6±3.9	179.8±2.5	175.7±1.9	172.1±2.0
$CFCl_3$ updated	187.3 ± 4.8	186.1±4.0	178.4±2.5	174.2±1.9	170.5±2.0
CF_2Cl_2 EX	319.0 ± 2.9	313.9±2.8	307.0±2.2	291.6±2.1	287.6±1.3
CF_2Cl_2 CALC	316.7 ± 8.0	314.7±6.6	301.5±4.1	294.7±3.2	289.0±3.4
CCl_4 EX	132.3 ± 2.1	129.0±1.5	126.0±1.8	121.6±1.1	120.8±0.9
CCl_4 CALC	129.4 ± 1.5	129.1±1.3	126.6±0.8	125.2±0.7	125.1±0.7
N_2O EX	306.5 ± 2.3	307.2±1.4	307.6±0.8	306.8±0.8	307.4±0.6
N_2O CALC	304.9 ± 0.4	304.9±0.3	304.8±0.3	304.8±0.3	304.9±0.3
CH_3CCl_3 EX	161.2 ± 5.7	161.5±5.9	143.7±6.4	119.6±3.3	109.7±1.2
RUN B	164.1±10.1	161.8±8.3	136.5±3.7	131.0±3.1	125.6±3.4
RUN E	158.9±10.2	156.6±8.4	130.2±4.1	123.4±3.2	116.6±3.5

for $CC\ell_4$.

Methylchloroform which has an OH sink, can suffer from errors in the estimated tropospheric two-dimensional OH distribution in addition to all the previous errors. We find disagreement in the southern hemisphere, which can be interpreted either as a model transport problem, an initialization problem, a truncation problem, a sink/source problem or an OH problem. It is difficult to separate all these effects from one another. In studying the model runs for $CFC\ell_3$, $CF_2C\ell_2$, $CC\ell_4$, and N_2O where no OH sink was involved, we either had no apparent transport-related problems, or transport-related problems which had the same effect as we find with $CH_3CC\ell_3$, i.e., overestimation of the trends in the southern hemisphere. If we assume that the model runs for $CH_3CC\ell_3$ have transport-related problems no larger than those that we had for the other tracers, then the final fit to the experimental results must be attempted by altering only the assumed OH distribution. This implies that the true OH tropospheric distribution is somewhere near the distribution used in $CH_3CC\ell_3$ Run B, since the globally-averaged trend for $CH_3CC\ell_3$ as calculated by Run B is slightly larger than the experimental globally-averaged $CH_3CC\ell_3$ trend (as measured by the ALE stations). This slight overprediction is similar to the results we had with the other tracers (see Table 29).

At this point we would like to note that the model transport problem might be caused by the fact that we are

using the same vorticity fields for each of the model years, i.e., when we start a new year of integration, we still use the same vorticities, vertical velocities and ozone fields that we used in the previous year. In this way we do not take into consideration any significant year-to-year fluctuations in such phenomena as the Hadley-cell circulation which would obviously affect the interhemispheric exchange rate.

4.3 Atmospheric Lifetimes

To summarize our results for the global budgets of the various tracers we give in Table 31 the values of the globally-averaged lifetime above 198 mb (i.e., stratospheric lifetime), the globally-averaged total atmospheric lifetime, and the global rate of photochemical destruction for all five tracers for January 1, 1981. Recommended current lifetimes for all five tracers are also summarized in Table 31, as well as the recommended average tropospheric OH number density derived from the model run B for $CH_3CC\ell_3$. For $CFC\ell_3$ we give the results obtained using currently accepted O_2 cross-sections and also using modified cross-sections as suggested by recent stratospheric studies (Frederick and Mentall, 1982; Froidevaux and Yung, 1982).

Table 31: Summarized Results.

January 1, 1981 values	τ above 198mb (years)	τ global (years)	Photochemical destruction rate (10^8 gm/day)	Tracer atmospheric content (gm)
$CFCl_3$ FAB	12.2	79.7	1.44	4.15E12
$CFCl_3$ FAB updated	6.4	43.8	2.58	4.07E12
$CFCl_3$ CRU	11.6	75.2	1.56	4.22E12
CF_2Cl_2 FAB	39.5	242.4	0.71	6.20E12
CF_2Cl_2 CRU	33.9	204.5	0.85	6.28E12
CH_3CCl_3 RUN B	5.9	12.6	6.80	3.08E12
CH_3CCl_3 RUN E	5.9	8.6	9.34	2.90E12
CCl_4	7.5	48.7	1.88	3.29E12
N_2O	33.7	190.2	343	2.35E15

The model Atmospheric Mass: 5.188E21 gm.

Globally and Annually averaged present-day Lifetimes (years) ($CFCl_3$, CF_2Cl_2, CCl_4, N_2O averaged on July 80-June 81, CH_3CCl_3 averaged on Jan - Dec 1980).

$CFCl_3$	$CFCl_3$ updated	CF_2Cl_2	CH_3CCl_3	CCl_4	N_2O
78	45	232	12	49	185

Recommended Tropospheric OH free radical Distribution, Number Density, Daily-averaged values (10^5 mol cm^{-3}).

	NH	SH	Global average
NH Summer	7.9	7.6	7.0
NH Winter	4.3	9.5	

4.4 Accomplishments of the Thesis

We have developed a unique, efficient, low resolution spectral model for studying the circulation, photochemistry and chemistry of some long-lived atmospheric species in the troposphere and lower stratosphere. The integration time for one model day for a single advected species is about 8 seconds on a CDC 7600 computer and this time can, we believe, be decreased even further by further improvements in code efficiency. This model therefore has a high potential for future use in studying complex chemical cycles in the atmosphere. The method adopted here, of using precalculated vorticities, vertical velocities, temperatures, and ozone fields, will enable us to ultimately incorporate into the model the chemistry of many more species, thus providing a means for studying more complex interactive chemistry in the troposphere and lower stratosphere. Future uses of the model include either a many-species chemical scheme including cycles for different elements, an isolated study of one family of chemical species, or as done so far, for only one particular chemical species which has a current interest which justifies its unique and individual study.

Our model transport has been successfully validated by comparison with $CFC\ell_3$, $CF_2C\ell_2$, $CC\ell_4$ and N_2O data. Such a validation is necessary since our assumption of low horizontal resolution is in effect a "parameterization" of the true atmospheric circulation. Evidently, even though the model is

a spectral model truncated at wave number 6, it is still able to predict the behaviour of inert species in the troposphere to a high degree of accuracy. Earlier studies of the atmospheric energy budget (e.g., Wiin-Nielsen, 1967) have already shown that most of the atmospheric eddy kinetic energy is concentrated in waves with wave numbers less than 7. This might explain why the present model is able to reproduce the correct global if not smaller-scale transport mechanisms in the atmosphere.

Our model is reasonably successful in simulating the observed global spectral and temporal behaviour of $CFC\ell_3$, $CF_2C\ell_2$, $CC\ell_4$, N_2O and $CH_3CC\ell_3$. Our three-dimensional study of the budgets of all these five species, including their present-day lifetime calculation is the first such study ever done. We have already stated the importance of evaluating the lifetime of these pollutants with respect to the ozone-depletion problem. The three-dimensional study is more accurate than the existing lower dimensional model studies since it does not make any averaging assumptions for the third dimension (or the second and third dimensions as in one-dimensional studies). This three-dimensional study enables us to present the longitude-latitude distribution of the tracers in each height level. This is very important since as we have shown the various anthropogenic pollutants have a strong permanent standing wave pattern, at least in the northern hemisphere troposphere.

In the study of CH_3CCl_3 we have found the OH radical tropospheric distribution which is apparently necessary to approximately simulate CH_3CCl_3 observational data. This OH distribution is in good agreement with those predicted using CO is a similar way (Volz *et al.*, 1981; Pinto *et al.*, 1982).

The OH distributions computed using a priori models of tropospheric chemistry (Logan *et al.*, 1981; Chameides and Tan, 1981) have large stated uncertainty limits of a factor of 2-4 which include the values computed in this thesis. The OH distribution computed in this thesis is we believe, the most accurate one to date based on the CH_3CCl_3 indirect assessment technique, since it uses three-dimensional as opposed to one- or two-dimensional modelling.

We have also computed atmospheric lifetimes for $CFCl_3$, CF_2Cl_2, CCl_4, CH_3CCl_3, and N_2O taking into account all known sinks. We have shown for the first time that semi-annual and annual cycles in these lifetimes are expected. Our lifetime calculations for $CFCl_3$, CF_2Cl_2, CCl_4 and CH_3CCl_3 are the first ever reported using a three-dimensional model. We have also shown that decreasing the O_2 cross-sections in the Herzberg continuum from presently accepted values tends to bring our model into better agreement with observations.

5. References

Ackerman, M., 1971; UV solar radiation related to mesospheric processes, G. Fioco editor, Riedel, p. 149-159.

Anderson, J.G., 1971a; Rocket-borne ultraviolet spectrometer measurement of OH resonance fluorescence with a diffusive transport model for mesospheric photochemistry, J. Geophys. Res. 76, 4634-4652.

Anderson, J.G., 1971b; Rocket measurement of OH in the mesosphere, J. Geophys. Res. 76, 7820-7824.

Anderson, J.G., 1976; The absolute concentration of $OH(X^2\Pi)$ in the Earth's stratosphere, Geophys. Res. Lett. 3, 165-168.

Anderson, J.G., 1980; Free radicals in the Earth's stratosphere: A review of recent results. Proceeding of the NATO advanced study institute on atmospheric ozone, A.C. Aikin editor, FAA-EE-80-20, 233-251.

Allam, R.J., K.S. Groves, and F.A. Tuck, 1981; Global OH distribution derived from general circulation model fields of ozone and water vapor, J. Geophys. Res. 86, 5303-5320.

Alyea, F.N., D.M. Cunnold, and R.G. Prinn, 1978; Meteorological constraints on tropospheric halocarbon and nitrous oxide destruction by siliceous land surfaces, Atmos. Environ. 12, 1009-1011.

Broecker, W.S. and T.H. Peng, 1974; Gas exchange rates between air and sea, Tellus 26, 21-35.

Burnett, C.R., 1976; Terrestrial OH abundance measurement by spectroscopic observation of resonance absorption of sunlight, Geophys. Res. Lett. 3, 319-322.

Burnett, C.R., 1977; Spectroscopic measurement of atmospheric OH abundance, Bull. Am. Phys. Soc. 22, 539.

Burnette, C.R. and E.B. Burnette, 1981; Spectroscopic measurement of the vertical column abundance of hydroxyl (OH) in the Earth's atmosphere, J. Geophys. Res. 86, 5185-5202.

Campbell, M.J., J.C. Sheppard, and B.F. Au, 1979; Measurement of hydroxyl concentration in boundary layer air by monitoring CO oxidation, Geophys. Res. Lett. 6, 175-178.

Chameides, W.L. and A. Tan, 1981; The two-dimensional diagnostic model for tropospheric OH: An uncertainty analysis, J. Geophys. Res. 86, 5209-5223.

Chang, J.S. and K. Kaufman, 1977; Kinetics of the reactions of hydroxyl radicals with some halocarbons: $CHFCl_2$, CHF_2Cl, CH_3CCl_3, C_2Cl_4, J. Chem. Phys. 66, 4989-4994.

Chang, J. and J. Penner, 1978; Analysis of global budgets of halocarbons, Atmos. Environ. 12, 1867-1873.

Chemical Manufacturers Association, 1981; World production and release of chloroflurocarbons 11 and 12 through 1980: An update. Report of the Fluorocarbon Program Panel, July 29, 1981.

Clyne, M.A.A. and P.M. Holt, 1979; Reactions kinetics involving ground X^2 and excited $A^2\Sigma^+$ hydroxyl radicals, part I: Quenching kinetics of OH $A^2\Sigma^+$ and rate constants for reactions of OH $X^2\Pi$ with CH_3CCl_3 and CO, J. Chem. Soc. Faraday II 75, 569-581.

Cox, R., R. Derwent, A. Eggleton, and J. Lovelock, 1976; Photochemical oxidation of halocarbons in the troposphere, Atmos. Environ. 10, 305-308.

Crutzen, P.J., 1974; Photochemical reactions initiated by and influencing ozone in unpolluted tropospheric air, Tellus 26, 47-56.

Crutzen, P.J. and J. Fishman, 1977; Average concentrations of OH in the troposphere, and the budgets of CH_4, CO, H_2 and CH_3CCl_3, Geophys. Res. Lett. 4, 321-324.

Crutzen, P.J., I.S.A. Isaksen, and J.R. McAfee, 1978; The impact of the chlorocarbon industry on the ozone layer, J. Geophys. Res. 83, 345-363.

Cunnold, D., F. Alyea, N. Phillips, and R. Prinn, 1975; A three-dimensional dynamical-chemical model of atmospheric ozone, J. Atm. Sci. 32, 170-194.

Cunnold, D., F. Alyea, and R. Prinn, 1978; A methodology for determining the atmospheric lifetime of fluorocarbons, J. Geophys. Res. 83, 5493-5500.

Cunnold, D.M., F.N. Alyea, and R.G. Prinn, 1980; Preliminary calculations concerning the maintainance of the zonal mean ozone distribution in the northern hemisphere, Pageoph 118, 329-354.

Cunnold, D.M., R.G. Prinn, R.A. Rasmussen, P.G. Simmonds, F.N. Alyea, C.A. Cardelino, A.J. Crawford, P.J. Fraser, and R. Rosen, 1982a; The Atmospheric Lifetime Experiment IV: Methodology and application to results for three years of $CFCl_3$ data. Submitted to J. Geophys. Res.

Cunnold, D.M., R.G. Prinn, R.A. Rasmussen, P.G. Simmonds, F.N. Alyea, C.A. Cardelino, and A.J. Crawford, 1982b; The Atmospheric Lifetime Experiment, V: Results for CF_2Cl_2 based on three years data. Submitted to J. Geophys. Res.

Davis, D.D., W. Heaps, and T. McGee, 1976; Direct measurements of natural tropospheric levels of OH via an aircraft borne tunable dye laser, Geophys. Res. Lett. 3, 331-333.

Davis, D.D., 1980; Project GAMETAG: An overview, J. Geophys. Res. 85, 7285-7292.

Derwent, R.G. and A.E.J. Eggleton, 1978; Halocarbon lifetimes and concentration distributions calculated using a two-dimensional tropospheric model, Atmos. Environ. 12, 1261-1269.

Derwent, R. and A. Eggleton, 1981; Two-dimensional model studies of methylchloroform in the troposphere, Quart. J. Rol. Met. Soc. 107, 231-242.

Fabian, P., 1981; Atmospheric sampling, Adv. Space Res. 1, 17-27.

Fabian, P., R. Borchers, G. Flentje, W.A. Matthews, W. Seiler, H. Giehl, K. Bunse, F. Muller, U. Schmidt, A. Volz, A. Khedim, and F.J. Johnen, 1981; The vertical disrtibution of stable gases at mid-latitudes, J. Geophys. Res. 86, 5179-5184.

Frederick, J.E. and J.E. Mentall, 1982; Solar irradiance in the stratosphere: Implications for Herzberg continuum absorption of O_2, Geophys. Res. Lett. 9, 461-464.

Froidevaux, L. and Y.L. Yung, 1982; Radiation and chemistry in the stratosphere: Sensitivity to O_2 absorption cross-sections in the Herzberg continuum, In preparation.

Goldan, P.D., W.C. Kuster, D.L. Albritton, and A.L. Schmeltekopf, 1980; Stratospheric $CFCl_3$, CF_2Cl_2, and N_2O height profile measurements at several latitudes, J. Geophys. Res. 85, 413-423.

Hanabusa, M., C.C. Wang, S. Japar, D.K. Killinger, and W. Fisher, 1977; Pulse width dependence of ozone interference in the laser fluorescence measurement of OH in the stratosphere, J. Chem. Phys. 66, 2118-2120.

Heaps, Wm.S. and T.J. McGee, 1981; Balloon borne lidar measurement of stratospheric hydroxyl radical, J. Geophys. Res., submitted.

Howard, C.J. and K.M. Evenson, 1977; Rate constants for the reactions of OH with ethane and some halogen substituted ethanes at 296°K, J. Chem. Phys. 64, 4303-4306.

Jeong, K.M. and F. Kaufman, 1979; Rates of the reactions of 1,1,1-trichloroethane with OH, Geophys. Res. Lett. 6, 757-759.

Jesson, J., P. Meakim, and L. Glasgow, 1977; The fluorocarbon - ozone theory II: Tropospheric lifetimes - an estimate of tropospheric lifetime of $CFCl_3$, Atmos. Environ. 11, 449-508.

Johnson, H.S., O. Searang, and J. Podolske, 1979; Instantaneous global nitrous oxide phtochemical rates, J. Geophys. Res. 84, 5077-5082.

Killinger, D.K. and C.C. Wang, 1977; Absorption measurements of OH using a cw tunable laser, Chem. Phys. Lett. 52, 374-376.

Kurylo, M.J., P.C. Anderson, and O. Klais, 1979; A flash photolysis resonance fluorescence investigation of the reaction $OH + CH_3CCl_3 \rightarrow H_2O + CH_2CCl_3$, Geophys. Res. Lett. 6, 760-762.

Levy, H., 1971; Normal atmosphere: Large radical and formaldehyde concentration predicted, Science 173, 141-143.

Levy, H., 1972; Photochemistry of the lower stratosphere, Planet. Space Res. 20, 919-935.

Levy II, H., J.D. Mahlman, and W.J. Moxim, 1979; A preiminary report on the numerical simulation of the three-dimensional structure and variability of atmospheric N_2O, Geophys. Res. Lett. 6, 155-158.

Liss, P.S. and Slater, 1974; Flux of gases across the air-sea interface, Nature 247, 181-184.

Logan, J.A., M.J. Prather, S.C. Wofsy, and M.M. McElroy, 1981; Tropospheric chemistry: A global prespective, J. Geophys. Res. 86, 7210-7254.

Lorenz, E.N., 1960; Energy and numerical weather prediction, Tellus 12, 364-373.

Lorenz, E.N., 1971; An N-cycle time differencing scheme for stepwise numerical integration, Mon. Weath. Rev. 99, 644-648.

Lovelock, J.E., 1977; Methyl chloroform in the troposphere as an indicator of OH radical abundance, Nature 267, 32.

Makide, Y., and S. Rowland, 1981; Tropospheric concentrations of methylchloroform, CH_3CCl_3, in January 1978 and estimates of the atmospheric residence time for hydrocarbons, Proc. Nat. Acad. Sci. USA 78, 5933-5973.

McConnell, J.C. and H.I. Schiff, 1978; Methylchloroform: Impact on stratospheric ozone, Science 199, 174-177.

McElroy, M.B., J.W. Elkins, S.C. Wofsy, and Y.L.Yung, 1976; Sources and sinks for atmospheric N_2O, Rev. Geophys. Space Phys. 14, 143-150.

Molina, M.J. and F.S. Rowland, 1974a; Stratospheric sink for fluorochloromethanes: Chlorine atom-catalyzed destruction of ozone, Nature 249, 810-812.

Molina, M. and Rowland, 1974b; Predicted present stratospheric abundance of chlorine spesies from photodissociation of carbon tetrachloride, Geophys. Res. Lett. 1, 309-312.

National Academy of Science (NAS), 1979; Stratospheric ozone depletion by halocarbons: Chemistry and Transport.

NASA reference publication 1049, 1979; The stratosphere: Present and future, R.D. Hudson and E.I. Reed, Editors.

Neely, W.B. and J.H. Plonka, 1978; Estimation of time-averaged hydroxyl radical concentration in the troposphere, Environ. Sci. and Technol. 12, 317-321.

Newell, R., 1969; Radioactive contamination of the upper atmosphere, Progress in Nuclear Energy - series XII, Health Physics, Vol. 2, A.M. Francis Duhamel, editor, Pergamon, 535-550.

Ohta, T., M. Morita, I. Mizoguchi, and T. Toda, 1977; Washout effect and diurnal variation for chlorinated hydrocarbons in ambient air. Atmos. Environ. 11, 985-987.

Pack, D., J. Lovelock, G. Cotton, and C. Curthoys, 1977; Halocarbon behaviour from a long time series, Atmos. Environ. 11, 329-344.

Pearson, C.R. and G. McConnell, 1975; Chlorinated C_1 and C_2 hydrocarbons in the marine environment, Proc. Roy. Soc. Lond. B 189, 305-322.

Peng, T.H., W.S. Broecker, G.G. Mathieu, and Y.H. Li, 1979; Radon evasion rates in the Atlantic and Pacific oceans as determined during the GEOSECS program, J. Geophys. Res. 84, 2471-2486.

Perner, D., D.H. Ehhalt, H.W. Patz, U. Platt, E.P. Roth, and A. Volz, 1976; OH - radicals in tje lower troposphere, Geophys. Res. Lett. 3, 466-468.

Pierotti, D., L.E. Rasmussen, and R.A. Rasmussen, 1978; The Sahara as a possible sink for trace gases, Geophys. Res. Lett. 5, 1001-1004.

Pinto, J.P., Y.L. Yung, D. Rind, G.L. Russell, T.A. Lerner, J.E. Hansen, and S. Hameed, 1981; A general circulation model study of atmospheric carbon monoxide, J. Geophys. Res., submitted.

Prinn, R.G., 1975; Venus: Chemical and dynamical processes in the stratosphere and mesosphere, J. Atm. Sci. 32, 1237-1247.

Prinn, R.G., F.N. Alyea, and D.M. Cunnold, 1975; Stratospheric distribution of odd nitrogen and odd hydrogen in a two-dimensional model, J. Geophys. Res. 80, 4997-5004.

Prinn, R.G., F.N. Alyea, and D.M. Cunnold, 1978; Photochemistry and dynamics of the ozone layer, Ann. Rev. Earth and Planet. Sci. 6, 43-74.

Prinn, R.G., R.A. Rasmussen, R.D. Rosen, P.G. Simmonds, F.N. Alyea, C.A. Cardelino, S. Crawford, D. Cunnold, P. Fraser, and J. Lovelock, 1982a; The Atmospheric Lifetime Experiment, I: Introduction and overview. Submitted to J. Geophys. Res.

Prinn, R.G., R.A. Rasmussen, P.G. Simmonds, F.N. Alyea, and D. M. Cunnold, 1982b; The Atmospheric Lifetime Experiment, VI: Results for CH_3CCl_3 based on three years of data. Submitted to J. Geophys. Res.

Ramanathan, V., 1975; Greenhouse effect due to chlorofluorocarbons: Climatic implications, Science 190, 50-52.

Rasmussen, R. and M. Khalil, 1981; Global atmospheric distribution and trend of methyl-chloroform, Geophys. Res. Lett. 8, 1005-1007.

Rasmussen, R., P. Simmonds, F. Alyea, S. Crawford, D. Cunnold, and R. Prinn, 1982; The Atmospheric Lifetime Experiment VIII: Results for N_2O based on three years of data. To be submitted to J. Geophys. Res.

Rowland, F. and M. Molina, 1976; Estimated future atmospheric concentrations of $CFCl_3$ (fluorocarbon 11) for various hypothetical tropospheric removal rates, J. Phys. Chem. 80, 2049-2051.

Seiler, W. and J. Fishman, 1981; The distribution of carbon monoxide and ozone in the free atmosphere, J. Geophys. Res. 86, 7255-7265.

Simmonds, P.G., F.N. Alyea, D.M. Cunnold, J.E. Lovelock, R.G. Prinn, A.J. Crawford, C.A. Cardelino, and R.A. Rasmussen, 1982; The Atmospheric Lifetime Experiment VIII: Results for carbon tetrachloride based on three years of data. Submitted to J. Geophys. Res.

Singh, H.B., 1977a; Atmospheric halocarbons: Evidence in favor of reduced hydroxyl radical concentrations in the troposphere, Geophys. Res. Lett. 4, 101-104.

Singh, H.B., 1977b; Preliminary estimation of average tropospheric OH concentrations in the Northern and Southern hemispheres, Geophys. Res. Lett. 4, 453-456.

Singh, H.B., L.T. Salas, H. Shigeishi, and E. Scribner, 1979; Atmospheric halocarbons, hydrocarbons and sulfur hexafluoride: Global distribution, sources and sinks, Science 203, 899-903.

Singh, H.B., 1981; Private communication.

Slinn, W.G.N., L. Hasse, B.B. Hicks, A.W. Hogan, D. Lal, P.S. Liss, K.O. Munnick, G.A. Sehmel, and O. Vittori, 1978; Some aspects of the transfer of atmospheric trace constituents past the air-sea interface, Atmos. Environ. 12, 2055-2078.

Sze, N.D. and M.K.W. Ko, 1981; Private communication.

Sze, N. and M. Wu, 1976; Measurement of fluorocarbons 11 and 12 and model validation: An assessment. Atmos. Environ. 10, 1117-1125.

Turco, R.P., R.C. Whitten, O.B. Toon, E.C.Y. Ynn, and P. Hamill, 1981; Stratospheric hydroxyl radical concentrations: New limitations suggested by observations of gaseous and particulate sulfur, J. Geophys. Res. 86, 1129-1139.

Vanlaethem, M.N., J. Wisemberg, and P.C. Simon, 1979; Ultraviolet absorption spectrum of methyl-chloroform in the vapor phase, Geophys. Res. Lett. 6, 451-454.

Volz, A., D.H. Ehhalt, and R.G. Derwent, 1981; Seasonal and latitudinal variation of ^{14}CO and the tropospheric concentration of OH radicals, J. Geophys. Res. 86, 5163-5171.

Wang, C.C. and L.I. Davis, Jr., 1974a; Measurement of hydroxyl concentration in air using a tunable uv laser beam, Phys. Rev. Lett. 32, 349-352.

Wang, C.C. and L.I. Davis, Jr., 1974; Ground state population distribution of OH determined with a tunable uv laser, Appl. Phys. Lett. 25, 34-35.

Wang, C.C., L.I. Davis Jr., P.M. Selzer, and R. Munoz, 1981; Improved airborne measurements of OH in the atmosphere using a technique of laser-induced fluorescence, J. Geophys. Res. 86, 1181-1186.

Wang, W.C., Y.L. Yung, A.A. Lacis, T. Mo, and J.E. Hansen, 1976; Greenhouse effects due to anthropogenic perturbations of trace constituents in the atmosphere, Science 194, 685-690.

Watson, R.T., G. Machado, B.C. Conaway, S. Wagner, and D.D. Davis, 1977; A temperature dependent kinetics study of the reaction of OH with CH_2ClF, $CHCl_2F$, $CHClF_2$, CH_3CCl_3, CH_3CF_2Cl and $CF_2ClCFCl_2$, J. Phys. Chem. 81, 256-262.

Weiss, R.F., 1981; The temporal and spacial distribution of tropospheric nitrous oxide, J. Geophys. Res. 86, 7185-7195.

Wiin-Nielsen, A., 1967; On the annual variation and spectral distribution of atmospheric energy, Tellus 29, 540-559.

WMO, 1981; The stratosphere 1981. Theory and measurements, Report No. 11, May 1981.

Yung, Y.L., M.B. McElroy, and S.C. Wofsy, 1975; Atmospheric halocarbons: A discussion with emphasis on chloroform, Geophys. Res. Lett. 2, 397-399.